SPECTRAL-EFFICIENT DESIGN IN MODERN

WIRELESS COMMUNICATIONS NETWORKS

A Dissertation
Presented to
The Academic Faculty

By

LU LU

In Partial Fulfillment
of the Requirements for the Degree
Doctor of Philosophy
in
Electrical and Computer Engineering

School of Electrical and Computer Engineering
Georgia Institute of Technology
August 2015

SPECTRAL-EFFICIENT DESIGN IN MODERN WIRELESS COMMUNICATIONS NETWORKS

Approved by:

Dr. Geoffrey Ye Li, Advisor
Professor, School of Electrical and Computer Engineering
Georgia Institute of Technology

Dr. Xiaoli Ma
Professor, School of Electrical and Computer Engineering
Georgia Institute of Technology

Dr. Gordon L. Stüber
Professor, School of Electrical and Computer Engineering
Georgia Institute of Technology

Dr. Xingxing Yu
Professor, School of Mathematics
Georgia Institute of Technology

Dr. Ian F. Akyildiz
Professor, School of Electrical and Computer Engineering
Georgia Institute of Technology

Date Approved: June 03, 2015

To my dearest family.

ACKNOWLEDGEMENTS

This thesis is mainly the fruit of my hard work during the past four years at Georgia Institute of Technology and it would not have been possible without the generous love and support throughout my past life.

I owe my deepest gratitude to my advisors Prof. Geoffrey Ye Li for serving as friends and mentors during my study at Georgia Tech. His deep insights and continuous encouragements have inspired me in the research and helped me overcome challenges on the way. I would also thank Prof. Gang Wu at UESTC for recommending me to Prof. Li, leading to this great opportunity of studying at Georgia Tech.

I would like to express my thanks to Profs. Gordon L. Stüber, Ian F. Akyildiz, Xiaoli Ma, and Xingxing Yu to be my dissertation committee members. Their broad perspective and suggestions have helped me a lot in refining this dissertation. Besides, working with Prof. Xingxing Yu and his group on graph theory was quite inspiring.

My special thanks also goes to my dearest husband, Cong Xiong. He is always so supportive. Without him, I would never have leaded a so happy life in Atlanta and never have achieved such fruitful results in research.

Moreover, thank you, Daewon Lee, for everything. You are always so kind and helpful, from the moment I met you till now. Thank you, Xiangwei Zhou, Cen Lin, Hao He, Jian Yu, Wei Guo, Xu Bao, Rui Yin, Yinjun Liu, and all other lab members. Dear swimming team members, thank you for helping me become healthier. I would also like to thank my dear friends, Zhen Huang, Chong Han, Yun Wei, Qingsong Wen, and my other friends.

Finally, I would like to dedicate my most special thanks to my dear mom and my dear grandparents. All my academic successes can be traced back to them. Their unconditional love and huge support is always my source of power. I am so glad and lucky to have them as my family.

TABLE OF CONTENTS

LIST OF TABLES

LIST OF FIGURES

SUMMARY

With the tremendously increasing demand on high-speed wireless communications, more and more spectrum resources are required. Since the spectrum bands we can use are limited, the spectral efficiency needs to be improved. However, static allocation and exclusive access in current spectrum assignment policy caused a lot of licensed bands to be underutilized. To address this problem, *cognitive radio* (CR) technology has been developed. With the help of the CR technology, unlicensed users, also called *secondary users* (SUs) are allowed to use the licensed spectrum bands as long as they do not generate unacceptable interference to the licensed users, also called *primary users* (PUs). Through this way, the spectral efficiency can be improved.

There are two essential procedures to fulfil the goals, including spectrum sensing and spectrum access. During the spectrum sensing period, SUs continuously monitor the activities of the PUs to determine the spectrum bands that can be used. One traditional spectrum sensing procedure is to determine the absence or presence of the PU signal. Techniques, such as matched filtering detector, energy detector, and feature detector, are commonly used. Besides determining the status of the PU signal, more detailed information, such as the *channel state information* (CSI) of the interference channel from the SU to the PU, is beneficial for the followed transmission design, which can be obtained through feedback or learning. Based on the sensing results, spectrum access schemes are carefully designed for the SUs to transmit and to protect the transmission of the PUs. According to the access strategies of the SUs, the spectrum access models can be categorized into spectrum overlay and spectrum underlay. In the spectrum overlay system, SUs can transmit only when PUs are not transmitting or SUs create no interference to the PUs by using advanced techniques. In the spectrum underlay system, SUs are allowed to transmit while the PUs are transmitting if the SUs generate only tolerable interference to the PUs. To obtain the benefits of CR networks, efficient spectrum sensing and access schemes are necessary to be developed.

Our research aims at improving spectral efficiency of wireless communications networks by studying both spectrum sensing and spectrum access techniques for CR networks.

We start with the spectrum sensing design. Firstly, we investigate a spectrum sensing strategy by using a variable number of samples for making decisions based on sequential detection. We design a sequential detection to maximize the throughput of the SUs for a given detection probability of the PUs. Then, we investigate the design by taking the status change of the PU signal into account. We develop a joint sensing block length and detection threshold optimization scheme to maximize the throughput of the CR network under an interference constraint and required detection and false-alarm probabilities. The optimal solution for the studied problem is derived.

We then design spectrum overlay transmission schemes. To improve spectral efficiency of the secondary links while protecting primary links, we propose signal alignment based precoding schemes for the SUs to use the leftover spaces of the PUs in both spatial and frequency domains with and without cooperation among the SUs and the PUs. To consider a general interference environment, we then investigate a multiple-cell secondary network where inter- and intra-cell interference within the secondary network will be considered jointly with the interference to the PUs. To support more symbols to be transmitted by each user without being interfered by other users in the secondary network, we develop another signal alignment precoding method, where the dimension at the secondary base station for the intended signals is increased by reducing that of the interference signals from other cells through alignment. Since the dimension of solution space for alignment may not be equal to that of the used signal space, we propose several chordal-distance-based subspace-choosing algorithms to determine the signal space. The proposed schemes improve the spectral efficiency compared to traditional *time-division multiple access* (TDMA).

At last, we focus on the design for the spectrum underlay systems. Firstly, we study a secondary network with both direct- and relay-aided transmissions. For the studied system, we formulate a power allocation problem to maximize the overall data rate of the secondary

network under an interference constraint to the primary network. To take the fairness between SUs into consideration, we then formulate another power allocation problem with an additional sum power constraint. Secondly, we study the resource allocation scheme by taking preferences of all users, including the SUs and the PUs, into account. A stable resource allocation based on the Gale-Shapley algorithm is proposed. The proposed stable resource allocation considers fairness, but is not robust to the system condition variations. To improve robustness, we then propose several edge-cutting algorithms.

In summary, we aims at improving the spectral efficiency of wireless communications networks by focusing on studying the CR networks. Several schemes are proposed for different scenarios. Besides the CR networks, the proposed schemes have potential to be utilized in various application scenarios, such as *device-to-device* (D2D) communications, spectrum trading, and *heterogeneous networks* (HetNets). With these schemes, the spectral efficiency of wireless communications networks can be significantly enhanced.

CHAPTER 1

INTRODUCTION

1.1   Motivation

Due to the rapid growth of wireless communications, more and more spectrum resources are needed. Within the current spectrum framework, most of the spectrum bands are exclusively allocated to specific licensed services. However, a lot of licensed bands, such as those for TV broadcasting, are underutilized, resulting in spectrum wastage [1]. This has promoted *Federal Communications Commission* (FCC) to open the licensed bands to unlicensed users through the use of *cognitive radio* (CR) technology [2, 3, 4, 5, 6, 7]. The IEEE 802.22 working group [8] has been formed to develop the air interference for opportunistic secondary access to TV bands. In recent years, the idea of CR has been studied in more general application scenarios. With CR technology, the spectral efficiency of wireless communications networks can be improved.

In practice, the unlicensed users, also called *secondary users* (SUs), need to continuously monitor the activities of the licensed users, also called *primary users* (PUs), to find the *spectrum holes* (SHs), which is defined as the spectrum bands that can be used by the SUs without generating intolerable interference with the PUs. There are different types of SHs, namely temporal, spatial, and frequency SHs [9], respectively. A temporal SH appears when there is no PU transmission during a certain time period and the SUs can use the spectrum for transmission. A spatial SH appears when the PU transmission is within an area and the SUs can use the spectrum outside that area or SUs can design the transmission to generate orthogonal transmission to the PUs. A frequency SH defines the opportunity on the frequency domain, which is similar as the temporal and spatial SHs.

The procedure of determining SHs is called spectrum sensing [7, 9, 10]. The traditional spectrum sensing procedure only determines the presence or absence of the PU transmission. There are different types of traditional spectrum sensing techniques, such as matched

filtering detection, energy detection, and feature detection [11]. To better utilize the spectrum bands, more detailed information is beneficial, such as the *channel state information* (CSI) of the interference channel from the SU to the PU. The CSI can be obtained by using feedback channels [12] or learning mechanisms [13, 14]. A certain level of cooperation between PUs and SUs helps as well.

Based on the sensing results, SUs obtain information about the channels that they can access. As the PUs have priorities to use the spectrum when the SUs coexist with them, the transmission of the PUs needs to be protected. According to the interference generated by the SUs to the PUs, the spectrum access models of the SUs can be categorized into spectrum overlay and spectrum underlay [6]. In the spectrum overlay system, the SUs can transmit only when the PUs are not transmitting or the SUs create no interference to the PUs by using advanced techniques. For the spectrum overlay, the performance of the PUs keeps the same as there is no transmission of the SUs. In the spectrum underlay system, the SUs are allowed to transmit while the PUs are transmitting if the SUs generate only tolerable interference to the PUs. Efficient spectrum access schemes are necessary to be developed for different types of CR networks [6, 15, 16, 17].

The goal of our research is to improve the spectral efficiency of wireless networks by exploiting efficient spectrum sensing and spectrum access strategies. We start with studying spectrum sensing techniques with more general assumptions, including using a variable number of samples for making sensing decision and taking the status change of the PUs into account. We then emphasize designing transmission schemes of the SUs for both spectrum overlay and spectrum underlay application scenarios, including precoding design of the SUs for *multiple-input multiple-output* (MIMO) *orthogonal frequency-division multiplexing* (OFDM) systems, power control for relay-aided secondary systems, and graph-based robust resource allocation design.

1.2 Literature Review

In this section, we review state-of-the-art techniques for spectrum sensing and spectrum access design of CR networks, respectively.

1.2.1 Spectrum Sensing Design

In practice, the CR users, also called the SUs, need to continuously monitor the activities of the licensed users, also called the PUs, to find the SHs, which are the spectrum bands that can be used by the SUs without interfering with the PUs. This procedure is called spectrum sensing [10].

The traditional spectrum sensing techniques, such as matched filtering detection, energy detection, and feature detection [11], are used to determine the presence or absence of the PU signal. If the SUs know information about the PU signal, the optimal detection method is matched filtering [11], which correlates the known primary signal with the received signal to detect the presence of the PU signal and thus maximizes the *signal-to-noise ratio* (SNR). The matched filtering detector requires short sensing time to achieve good detection performance. However, it needs knowledge of the transmit signal by the PU that may not be known at the SUs. Thus, the matched filtering technique is not applicable when transmit signals by the PUs are unknown to the SUs. *Energy detector* (ED) [11] is the most common spectrum sensing method. The decision statistics of the ED are defined as the average energy of the observed samples. The ED is easy to implement and requires no prior information about the PU signal. However, the uncertainty of noise power imposes fundamental limitations on the performance of the ED [18, 19, 20]. Feature detector, such as cyclostationary detector [21, 22], can distinguish noise from the PU signals and can be used for detecting weak signals at a very low SNR region, where the energy detection and matched filtering detection are not applicable.

Our study mainly focuses on ED. The statistical characteristics of the licensed channel occupancy have been utilized to optimize the SU frame structure in [23, 24, 25, 26], where they all assume the PUs appear at the beginning of a sensing block, which is not a practical

3

assumption. To make it more practical, the case that the PUs appear during a sensing period has been investigated in [27]. However, a more general scenario considering other possibilities of PUs' status should be investigated.

Traditional EDs normally use a fixed number of samples for sensing. Alternatively, *sequential detection* (SD) has been proposed as a new candidate for spectrum sensing. In the literature, there are two types of SDs. The basic idea of the first type is to divide the whole spectrum into multiple sub-channels and sense them successively [28, 29, 30]. The second type is based on the sequential tests introduced by Wald [31], which is to sense one channel to make decision with variable number of samples [32, 33, 34, 35, 36, 37, 38]. We will focus on the second type of SD for CR systems [32, 33, 34, 35, 36, 37, 38]. It has been shown that this SD is useful in several fields, such as signal detection with low SNR or with few samples. Different modifications have been made based on the algorithm introduced by Wald in [31]. In [34], the SD with time-varying threshold has been employed in low SNR regimes. The sensitivity of SD to PU signal variance estimation has been addressed in [32]. A simple sequential spectrum sensing scheme, namely the sequential shifted chi-square test, has been proposed in [35] to get several desirable features for CR networks. To efficiently and accurately evaluate detection performance, the exact expression for the false-alarm probability has also been derived. In [33], the impact of sample correlation on the performance of SD has been investigated. SD has also been used for the cooperative spectrum sensing in [37] and [36]. Distributed algorithms have been proposed to improve the spectrum sensing performance. Moreover, SD can be used for the quick detection of the PU signal [38].

Besides the presence or absence of PUs, more detailed information is beneficial, such as the CSI of the interference channel from the SU to the PU. The CSI can be obtained by using feedback channels [12] or learning mechanisms [13, 14]. A certain level of cooperation between PUs and SUs helps as well.

1.2.2 Spectrum Access Design

After obtaining the information of the spectrum bands through spectrum sensing, how to design the access strategies of SUs on the available spectrum bands without generating untolerable interference to the PUs is essential. Here, existing strategies for two main spectrum access modes, called as spectrum overlay and spectrum underlay, will be reviewed.

1.2.2.1 *Opportunistic transmission for spectrum overlay systems*

Spectrum overlay, also called as opportunistic transmission, is one important spectrum access mode, where the transmission of the SUs are designed to be orthogonal to the PU's transmission and no interference will be generated [39]. In this case, the PU's performance is the same as there is no transmission of the SUs. Opportunistic transmission of the SUs can be generated in both spatial and frequency domains.

Opportunistic transmission in spatial domain:

MIMO techniques have been widely used in wireless networks nowadays. *Single-input multiple-output* (SIMO) and *multiple-input single-output* (MISO) are two special cases of MIMO. Transmission schemes based on MIMO utilize the resources in the spatial domain and have been shown to be effective to improve system capacity, coverage, and spectral efficiency. In this section, we will summarize opportunistic transmission schemes for MIMO systems.

Considering the case with multiple antennas at both the primary and the secondary links first, to generate interference-free transmission to the primary link, one simple way for the secondary transmitter is to project the signal into the nullspace of the interference channel to the primary receiver. Once the interference channel is known, its nullspace can be determined. In general, the dimension of the nullspace is the difference of the numbers of antennas at the secondary transmitter and at the primary receiver. The power allocation information of the primary link can be used by the secondary link to improve its performance, which is called as *opportunistic interference alignment* (OIA) [39]. It aligns the interference from the secondary transmitter to the unused subspaces at the primary receiver

to avoid interference. Comparing OIA and ZF, more spaces are utilized by OIA, leading to higher throughput in general. The performance gap depends on the power allocation scheme of the primary link.

Besides nulling the interference to the primary link, the idea of ZF and OIA can be used to mitigate interference among multiple secondary links. A scheme based on ZF has been discussed in [40]. When the channels of two links are orthogonal, no interference will be generated between them, since the transmit signal on one channel will be in the nullspace of the other. The OIA-based scheme can be used to mitigate interference among secondary links and to the primary link as well. To achieve interference-free transmission, an iterative method has been proposed in [41]. Since the procedure is similar to the classic interference alignment scheme with additional constraint on the primary links, it has been called as constrained interference alignment.

In general, with multiple antennas at each nodes, more opportunities can be explored to improve system performance while guaranteeing interference constraints.

Opportunistic transmission in frequency domain:

OFDM has been extensively studied in the past couple decades and has been widely used in wireless networks and standards, such as 802.11a/g, *Worldwide Interoperability for Microwave Access* (WiMAX), and the *Third Generation Partnership Project* (3GPP) *Long Term Evolution* (LTE). It is able to deal with frequency selectivity of wireless channels successfully. OFDM divides a broadband wireless channel into many orthogonal narrowband subchannels and inserts *cyclic prefix* (CP) in time domain to combat *inter-symbol-interference* (ISI). The length of CP must be at least the delay spread of the channel to completely avoid ISI.

When the PU link is based on the OFDM, CP is removed first at the PU receiver. The effective time-domain channel matrix from the transmitter to the receiver after the CP remover is a Sylvester matrix, which has more columns than rows. That means, the effective time-domain channel matrix has nullspace with the dimension equal to the length

6

of CP. Vandermonde precoder [42], also called *Vandermonde-subspace frequency division multiplexing* (VFDM), has been proposed for the SU link to utilize the nullspace generated by CP. Figure 1.1 shows the system structure. Note that the ZF precoder uses nullspace in the spatial domain while the VFDM precoder uses nullspace in the frequency domain.
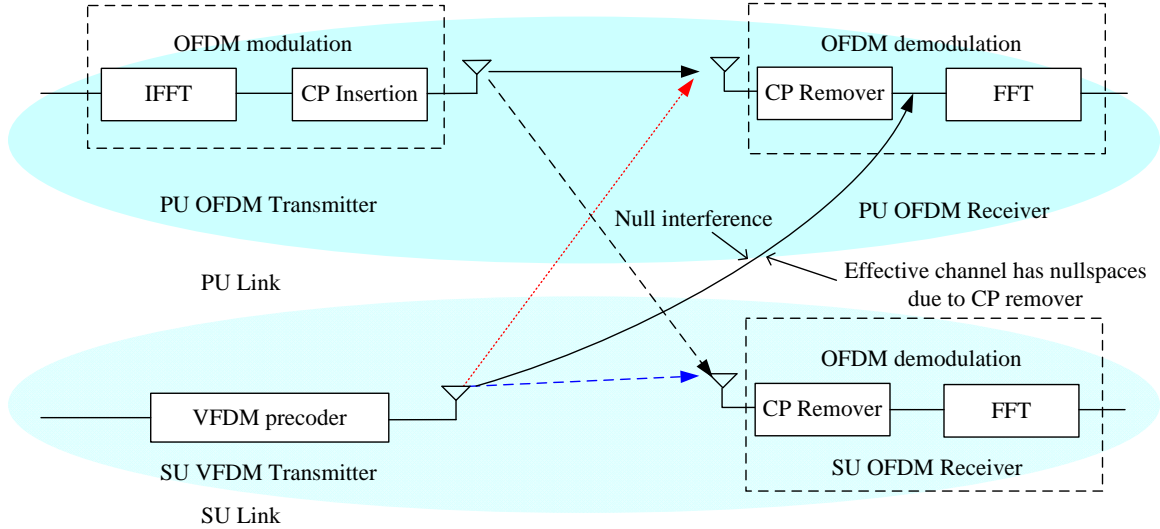
Figure 1.1. Basic concept of the VFDM.

The idea for VFDM can be easily extended to the case where the primary link is based on OFDMA [43]. Due to the orthogonality among users based on OFDMA, the effective interference channel from the secondary transmitter to all primary receivers has similar structure as the case with only one primary receiver. The dimension of the nullspace of the effective interference channel still equals the length of the CP. However, the Vandermonde structure is not applicable. Instead, the standard *singular value decomposition* (SVD) can be used to find out the precoder. Moreover, it can be also used for the single-carrier primary systems with frequency-domain equalization where CP is also used.

Considering a system where multiple secondary links want to transmit simultaneously with the primary one, each secondary transmitter can still have its own precoder to project its signal into the nullspace created by removing CP at the primary receivers as before. The detail has been discussed in [43], which is called *cognitive interference alignment* (CIA). The precoder design for this system is more complicated since the precoder should also

consider mitigating interference to other secondary links besides the primary link. The spectral efficiency of the system increases with the number of secondary links even though the performance of each secondary link decreases due to the increase of interference among them.

In brief, the CP in OFDM transmission creates opportunity for the secondary links to transmit without generating interference to the primary ones, leading to spectral efficiency improvement.

1.2.2.2 *Interference-constrained transmission for spectrum underlay systems*

Spectrum underlay is another spectrum access mode for CR networks. For the spectrum underlay mode, SUs can transmit as long as the interference to the PUs are tolerable. It is suitable for the scenarios that PUs can tolerate a certain level of performance degradation. Different resource allocation and transmission schemes have been studied for the underlay mode.

General resource allocation design:

Given CSI of interference channels from SUs to PUs, interference power at PUs can be guaranteed under a given threshold [44, 45, 46, 47, 48]. In [44], transmit covariance matrices of SUs are designed to maximize their own throughput. To take the fairness of SUs into account, an *signal-to-interference-ratio* (SINR) balancing issue has been studied in [45]. When only the statistics of interference CSI are known or the CSI has error, SUs can be designed to control average interference to the PUs [46] or to guarantee PUs' average [47] or outage performance [48].

To improve the coverage, the rate, and the energy efficiency of wireless networks, cooperative transmissions and relay strategies have been proposed [49]. They have been also widely used in CR networks [50, 51]. Due to practical constraints, full duplex operation is very challenging at the relay [52]. Thus, half-duplex relay is considered, where it cannot transmit and receive simultaneously. In [50], transmit power allocation schemes among relays have been studied, where overall transmit power is minimized under interference

8

constraints as well as the SINR requirement of the targeting SU receiver. Besides power control, a joint power and channel allocation scheme has been studied for a three-node CR network to optimize end-to-end throughput in [51]. With multiple relays, a simplified relay selection and power allocation has been studied in [53].

Besides the design for the direct link or the relay-aided link, hybrid systems with both direct and relay-aided links worth studying as well. Without coexisting PU network, a network with both direct and relay-aided transmissions has been studied in [54, 55, 56]. To manage the interference, a particular overhearing-based scheme has been proposed in [54]. In their studied network, the relay-aided user has priority and another direct user only can transmit without impairing it. Based on the overhearing scheme, coordinated transmissions with an amplify-and-forward relay have been considered in [55]. In [56], the rate regions for both uplink and downlink schemes have been studied based on *decode-and-forward* (DF) relay. Based on the findings in the existing work, designing the direct and relay-aided links jointly can improve the system performance. The extension to the CR network is an interesting direction.

Graph-based resource allocation:

Graph theory is one of the fastest growing areas of mathematics [57]. It is closely connected with such disciplines as communications, computer sciences, and industrial optimization. As a useful and convenient tool, graph theory based schemes have been studied for the resource allocation design in wireless communications networks.

To optimize the sum/average utility of SUs, the maximal weighted matching based on the Hungarian algorithm is commonly used for resource allocation [58]. The basic procedure is as follows. With necessary information, such as CSI, each SU can determine its utility, such as the spectrum efficiency and the energy efficiency, on available resources. This step normally incorporates power allocation and other operations to determine the optimal utility. Then, the Hungarian algorithm can be used to get a one-to-one SU-to-resource mapping to maximize the sum/average utility.

Besides the maximal weighted matching, the stable matching [57], which takes both PUs' and SUs' preferences into account, can be used for resource allocation as well. There are several advantages to use the stable matching. First, it incorporates fairness issues. Second, efficient algorithms, such as the *Gale-Shapley* (GS) algorithm, can be used to find a solution with polynomial complexity. Stable matching based resource allocation has been studied in [59, 60, 61, 62]. In [59], a one-to-many stable matching and its optimality properties have been studied. In [60], stable matching based on queue- and channel-aware lists for cross-layer scheduling has been investigated. In [61], tight lower and upper bounds for stable allocation performance have been derived. Moreover, stable matching with auction has been studied in [62]. Existing schemes on stable matching mainly focus on the design based on a fixed system condition while the robustness to the variation of the system condition is seldom investigated.

1.3 Our Approaches and Thesis Outline

The major goal of this research is to investigate spectrum sensing and spectrum access techniques to improve the spectral efficiency of wireless communications networks. The proposed schemes will be utilized in various application scenarios, such as CR networks, *device-to-device* (D2D) communications, spectrum trading, and *heterogeneous networks* (HetNets). With these schemes, the spectral efficiency of wireless communications networks will be significantly enhanced.

We will first investigate spectrum sensing techniques by taking more general assumptions into account. We start with designing spectrum sensing with a variable number of sensing samples based on sequential detection in Chapter 3 to maximize the throughput of SUs for a given detection probability of the PUs. We then study the scenario that the status of the PU can change at any time within one sensing/transmission frame in Chapter 3. We develop a joint sensing block length and detection threshold optimization scheme to maximize the throughput of the CR network under interference constraint and required

detection and false-alarm probabilities. We optimize sensing block length under a general scenario where the status of the PU may change at any time during a frame, either the sensing block or the transmission/silent block.

Then, we focus on spectrum access strategies design, including both spectrum overlay in Chapters 4 and 5 and spectrum underlay scenarios in Chapters 6 and 7.

For spectrum overlay design in Chapters 4 and 5, we focus on a MIMO-OFDM primary link, which captures the features of both MIMO and OFDM. To improve the performance of the secondary link, we consider a scenario of cooperation among the primary and the secondary links in Chapter 4, where the MIMO-OFDM primary link can reallocate its power and release some freedom to the secondary link when its own *quality-of-service* (QoS) requirement can be satisfied. Since the performance of the secondary link is related to the nullspace generated by the primary link, we formulate a throughput maximization problem to find out the optimal nullspace that can be released from the primary link without violating its own QoS requirement. Three nullspace releasing algorithms, called as *exhaustive-search algorithm* (ESA), *small-eigenvalue algorithm* (SEA), and *best-throughput algorithm* (BTA) are proposed.

We then extend our study to a multi-cell secondary system in Chapter 5, where the inter- and intra-cell interference mitigation within the secondary system needs to be considered together with the interference to the primary system. Based on a two-cell secondary uplink setting, we propose a signal alignment transmission scheme and analyze the number of interference-free symbols can be transmitted by each SU by mitigating both inter- and intra-cell interference within the secondary system together with mitigating interference to the primary system. Due to the system limitation, alignment may not be achieved perfectly. Results for both perfectly- and partially-aligned transmissions are discussed. We then propose precoding matrix for both perfectly- and partially-aligned transmission cases. Two chordal-distance based schemes, called as exhaustive search and heuristic algorithms, are developed for each case.

After discussing the spectrum overlay systems, we continue on studying the spectrum underlay systems. A secondary system with both direct- and relay-aided links is studied first in Chapter 6. We first formulate a power allocation problem to maximize the overall data rate of the CR network under an interference constraint to the primary network. To take the fairness between CR users into consideration, we then formulate another power allocation problem with an additional sum power constraint. In Chapter 7, we study the resource allocation design by taking all users' preferences into account. A stable resource allocation based on graph theory is proposed as a solution. We then focus on improving robustness of the stable resource allocation. A truncated scheme generating almost stable matchings is first investigated. Based on the properties of the truncated scheme, two types of edge-cutting algorithms, called *direct edge-cutting* (DEC) and *Gale-Shapley based edge-cutting* (GSEC), are developed to improve resource allocation robustness to the CSI variation. To mitigate the problem that certain SUs may not be able to find suitable resources after edge-cutting, *multi-stage* (MS) algorithms are then proposed.

CHAPTER 2

OPTIMAL SEQUENTIAL DETECTION IN COGNITIVE RADIO NETWORKS

CR can successfully deal with the growing demand and the scarcity of the wireless spectrum. To increase the spectrum usage, CR technology allows SUs to access licensed spectrum bands. Since licensed users, also called as PUs, have priorities to use the bands, the SUs need to continuously monitor the activities of the PUs to avoid interference and collisions.

In this chapter, we will focus on the *sequential detection* (SD) design to maximize the throughput of the SU system for a given detection probability. Since the thresholds of SD are determined by the required detection and false-alarm probabilities, we design the false-alarm probability instead of considering the thresholds of SD directly. Moreover, we limit the interference from SUs to PUs. Theoretical analysis is presented to solve the problem and a unique optimal solution is found.

The rest of this chapter is organized as follows. In Section 2.1, we present the system model and introduce the idea of SD. In Section 2.2, we formulate the throughput optimization problem for SD. In Section 2.3, we theoretically analyze the problem and find a unique optimal solution. Then, we provide asymptotic analysis in Section 2.4 and present numerical results in Section 2.5. Finally, we conclude this chapter in Section 2.6.

2.1   System Model

The CR network is assumed to operate on a frame-by-frame basis. We consider the frame structure with a fixed frame length, which consists of T samples. The frame consists of a sensing block of the few samples and a data transmission or a silent block of the rest samples depending on the sensing result, as shown in Fig. 2.1.

Spectrum sensing in CR is to detect the status (presence or absence) of PU signals. The

13

Sensing block	Transmission/ silent block
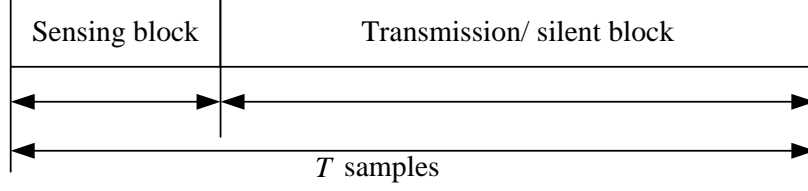
T samples

Figure 2.1. Frame structure for CR networks.

i-th received sample at a SU, r_i, can be expressed as

$$r_i = \begin{cases} n_i, & \mathcal{H}_0 \\ s_i + n_i, & \mathcal{H}_1 \end{cases}, \tag{2.1}$$

where s_i and n_i denote the received PU signal sample and white noise sample, respectively. In (2.1), $\mathcal{H}_0$ and $\mathcal{H}_1$ denote the hypotheses corresponding to the absence and presence of the PU signal, respectively. We assume s_i's are *independent and identically distributed* (i.i.d) complex Gaussian random variables with zero mean and variance γ as in [27]. Such a Gaussian PU signal assumption is reasonable when there is no *line-of-sight* (LOS) path between the SU and the PU, where the received signal is a combination of several *non-line-of-sight* (NLOS) signals and can be approximated as a Gaussian signal based on the central limit theorem. We also assume n_i's are i.i.d complex Gaussian random variables with zero mean and unit variance. As a result, *gamma* is the singal-to-noise ratio. Then, the *probability density functions* (pdf) for r_i under hypotheses $\mathcal{H}_1$ and $\mathcal{H}_0$ can be expressed as

$$p(r_i|\mathcal{H}_1) = \frac{1}{\pi(1+\gamma)}e^{-\frac{|r_i|^2}{1+\gamma}}, \quad p(r_i|\mathcal{H}_0) = \frac{1}{\pi}e^{-|r_i|^2}, \tag{2.2}$$

respectively.

Moreover, it is assumed that the statistics of the PU traffic, $P(\mathcal{H}_0)$ and $P(\mathcal{H}_1)$, are known as a priori through long-term channel measurements and the status of the PU signal will not change within one frame.

SD requires a variable number of samples to make decisions. To implement SD, we need to calculate the *log-likelihood ratios* (LLRs) of the samples. The LLR for the i-th

14

sample is

$$
\begin{aligned}
LLR_i &= \log \frac{p(r_i|\mathcal{H}_1)}{p(r_i|\mathcal{H}_0)} = \log \frac{\frac{1}{\pi(1+\gamma)} e^{-\frac{|r_i|^2}{1+\gamma}}}{\frac{1}{\pi} e^{-|r_i|^2}} \\
&= -\log(1+\gamma) + \frac{\gamma}{1+\gamma}|r_i|^2.
\end{aligned}
\tag{2.3}
$$

Since r_i's are i.i.d random variables, the cumulative LLR after N samples can be written as

$$
\begin{aligned}
L_N &= \log \frac{p(r_1, r_2, ..., r_N|\mathcal{H}_1)}{p(r_1, r_2, ..., r_N|\mathcal{H}_0)} = \log \frac{\prod_{i=1}^{N} p(r_i|\mathcal{H}_1)}{\prod_{i=1}^{N} p(r_i|\mathcal{H}_0)} \\
&= \sum_{i=1}^{N} \log \frac{p(r_i|\mathcal{H}_1)}{p(r_i|\mathcal{H}_0)} = \sum_{i=1}^{N} LLR_i \\
&= -N \log(1+\gamma) + \frac{\gamma}{1+\gamma} \sum_{i=1}^{N} |r_i|^2,
\end{aligned}
\tag{2.4}
$$

which is the test statistic of SD. Using SD, the SU makes decisions according to the following rule: $\mathcal{H}_1$, if $L_N \geq a_L$; $\mathcal{H}_0$, if $L_N \leq b_L$; more samples are needed if $b_L < L_N < a_L$. Instead of using one threshold as the conventional energy detection [11], SD has two thresholds to make decisions.

From [31], the thresholds of the SD are designed as

$$
a_L = \log \frac{P_d}{P_f}, \quad b_L = \log \frac{1 - P_d}{1 - P_f},
\tag{2.5}
$$

where P_d and P_f are the required detection probability and false-alarm probability, respectively.

2.2 Problem Formulation

In order to improve the performance of SD, we need to carefully design a_L and b_L. In this section, we will focus on this issue.

Here, we assume the number of samples, T, is large enough to meet the spectrum sensing requirement. Then, for a given P_d and P_f, the average number of samples required

for spectrum sensing under $\mathcal{H}_0$ and $\mathcal{H}_1$ can be expressed as [31]

$$
\begin{aligned}
E_{\mathcal{H}_0}[N] &= \frac{L(\mathcal{H}_0)b_L + (1 - L(\mathcal{H}_0))a_L}{E_{\mathcal{H}_0}(LLR_i)}, \\
E_{\mathcal{H}_1}[N] &= \frac{L(\mathcal{H}_1)b_L + (1 - L(\mathcal{H}_1))a_L}{E_{\mathcal{H}_1}(LLR_i)},
\end{aligned}
\tag{2.6}
$$

where

$$
L(\mathcal{H}_0) = \frac{e^{a_L} - 1}{e^{a_L} - e^{b_L}}, \quad L(\mathcal{H}_1) = \frac{e^{-a_L} - 1}{e^{-a_L} - e^{-b_L}},
$$

$$
\begin{aligned}
E_{\mathcal{H}_0}(LLR_i) &= -\log(1 + \gamma) + \frac{\gamma}{1 + \gamma}, \\
E_{\mathcal{H}_1}(LLR_i) &= -\log(1 + \gamma) + \gamma.
\end{aligned}
\tag{2.7}
$$

Substitute (2.5) into (2.6), we can get

$$
E_{\mathcal{H}_0}[N] = \frac{(1 - P_f)\log\frac{1 - P_d}{1 - P_f} + P_f \log\frac{P_d}{P_f}}{E_{\mathcal{H}_0}(LLR_i)},
\tag{2.8}
$$

$$
E_{\mathcal{H}_1}[N] = \frac{(1 - P_d)\log\frac{1 - P_d}{1 - P_f} + P_d \log\frac{P_d}{P_f}}{E_{\mathcal{H}_1}(LLR_i)}.
\tag{2.9}
$$

Then, the average number of samples for data transmission is,

$$
n_T = \begin{cases} T - E_{\mathcal{H}_0}[N], & \mathcal{H}_0 \\ T - E_{\mathcal{H}_1}[N], & \mathcal{H}_1 \end{cases}.
\tag{2.10}
$$

The transmitted data samples after the sensing procedure will be considered lost if misdetection occurs. Therefore, the number of data samples transmitted effectively can be written as

$$
\bar{n}_T = P(\mathcal{H}_0)(1 - P_f)(T - E_{\mathcal{H}_0}[N]),
\tag{2.11}
$$

where $P(\mathcal{H}_0)$ is the probability that hypothesis $\mathcal{H}_0$ occurs.

Normally, the SU system has a target detection probability, P_d, enforced by the PU system to protect the PU transmission. On the other hand, the false-alarm probability, P_f,

can be designed by the SU system to optimize its own performance. Here, we use the throughput of the SU system as a performance metric. Maximizing the throughput of the SU is equivalent to maximizing the number of data samples transmitted effectively, which is $\bar{n}_T$. Meanwhile, we need to limit the interference generated to the PU system. If misdetection occurs, the average number of samples that are interfered by the SU, $\bar{n}_I$, is,

$$\bar{n}_I = P(\mathcal{H}_1)(1 - P_d)(T - E_{\mathcal{H}_1}[N]). \tag{2.12}$$

Thus, our problem turns out finding an optimal false-alarm probability, P_f, with a given target detection probability, P_d, to maximize the number of data samples transmitted effectively of the SU with limited interference introduced to PU. This problem can be mathematically formulated as

$$\max_{P_f} \quad \bar{n}_T \tag{2.13}$$

subject to

$$\bar{n}_I \leq I, \tag{2.14}$$

where I denotes the threshold for the interference level that the PU can tolerate.

Note that the thresholds, a_L and b_L, for SD are determined by P_d and P_f as shown in (2.5). Thus, we can design the thresholds, a_L and b_L, for SD by the target P_d and the optimal P_f that is from the formulated problem.

2.3 Theoretical Analysis

In this section, we prove that there exists a unique optimal false-alarm probability, P_f, for our problem.

From (2.12), we have the following Property 2.1, which is proved in Appendix A.1.

Property 2.1 *The average number of samples that are interfered by the SU, $\bar{n}_I$, is a monotonically increasing function of the false-alarm probability, P_f.*

17

From Property 2.1, we can easily find the range of the false-alarm probability satisfying (2.14). We denote the false-alarm probability that makes $\bar{n}_I = I$ as P_f^u. Since the average number of samples interfered by the SU is a monotonically increasing function of the false-alarm probability, we can find a unique point P_f^u. In practice, $P_f \leq 0.5$. Thus, $P_f \in (0, P_f^u]$ when $P_f^u < 0.5$; otherwise, $P_f \in (0, 0.5]$ under practical consideration.

The property of the objective function (2.10) is summarized in Property 2.2, which is proved in Appendix A.2.

Property 2.2 *The number of data samples transmitted effectively, $\bar{n}_T$, is a concave function of the false-alarm probability, P_f.*

From Property 2.2, there exists a unique globally maximal throughput.

Next, we analyze the property of the optimal false-alarm probability, P_f^*. Without considering the constraint, the point maximizing $\bar{n}_T$ satisfies

$$\frac{\mathrm{d}\bar{n}_T}{\mathrm{d}P_f} = 0. \tag{2.15}$$

Since the number of data samples transmitted efficiently is a concave function of the false-alarm probability, we can find one optimizing unique point. We denote the point satisfying (2.15) as P_f^c. Thus, we can conclude that

$$P_f^* = \begin{cases} P_f^c, & \text{if } P_f^c \leq \min\{P_f^u, 0.5\} \\ P_f^u, & \text{if } P_f^u \leq \min\{P_f^c, 0.5\} \\ 0.5, & \text{otherwise} \end{cases} \tag{2.16}$$

where P_f^u and P_f^c are from

$$\bar{n}_I|_{P_f = P_f^u} = I, \quad \frac{\mathrm{d}\bar{n}_T}{\mathrm{d}P_f}|_{P_f = P_f^c} = 0. \tag{2.17}$$

Then, the optimal throughput is

$$\bar{n}_T^* = P(\mathcal{H}_0)(1 - P_f^*)(T - E_{\mathcal{H}_0}[N]). \tag{2.18}$$

Again, after P_f^* is derived, the thresholds, a_L and b_L, for SD are straightforwardly determined by (2.5).

2.4 Asymptotic Analysis

In this section, we consider SD performance under two extreme cases: (1) the PU signal is strong, i.e, $\gamma \to +\infty$; (2) the PU signal is weak, i.e. $\gamma \to 0$.

2.4.1 Large SNR

Consider the constraint function, we have

$$\lim_{\gamma \to +\infty} E_{\mathcal{H}_1}(LLR_i) = \lim_{\gamma \to +\infty} (-\log(1 + \gamma) + \gamma) = +\infty. \tag{2.19}$$

Then,

$$\lim_{\gamma \to +\infty} E_{\mathcal{H}_1}[N] = 0. \tag{2.20}$$

That means, the number of samples needed to achieve small P_f is small. Thus, we can choose $P_f \to 0$. Then, we have

$$\lim_{\gamma \to +\infty} \bar{n}_I = P(\mathcal{H}_1)(1 - P_d)T. \tag{2.21}$$

Similarly, we can get

$$\lim_{\gamma \to +\infty} E_{\mathcal{H}_0}[N] = 0. \tag{2.22}$$

Then,

$$\lim_{\gamma \to +\infty} \bar{n}_T = P(\mathcal{H}_0)T. \tag{2.23}$$

In this case, a_L can be chosen as a very large number to guarantee good performance of the detection while b_L is only related to P_d, i.e. $b_L = \log(1 - P_d)$.

2.4.2 Small SNR

When $\gamma \to 0$, we have

$$\lim_{\gamma \to 0} E_{\mathcal{H}_1}(LLR_i) = 0. \tag{2.24}$$

That means,

$$\lim_{\gamma \to 0} E_{\mathcal{H}_1}[N] = +\infty. \tag{2.25}$$

Unless $I \to +\infty$, the constraint cannot be fulfilled. In practice, this cannot be achieved. Thus, the whole block will be used for sensing without transmission to protect the PU when γ is small.

2.5 Numerical Results

In this section, we present numerical results to demonstrate the properties of the aforementioned problem. It is assumed that $P(\mathcal{H}_0) = 0.35$ and $P(\mathcal{H}_1) = 0.65$, which are consistent with the PUs under *voice over Internet Protocol* (VoIP) service [26] .

The evaluation of the objective and the constraint functions for different γ and P_f values are illustrated in Fig. 2.2(a) and Fig. 2.2(b), respectively. From Fig. 2.2(a), the concavity of the objective function with the false-alarm probability, P_f. The optimal throughput increases with γ. On the other hand, P_f^c, the optimal P_f providing maximal value of the objective function, decreases with γ. For large γ, small P_f can be achieved by small $E_{\mathcal{H}_1}[N]$ and $E_{\mathcal{H}_0}[N]$. When P_f and $E_{\mathcal{H}_1}[N]$ approach zeros, $\bar{n}_T/T \approx P(\mathcal{H}_0) = 0.65$, which equals the upper bound obtained by (2.23). As shown in the figure, $\gamma = 1$ and $\gamma = 2$ can lead to the upper bound. Figure 2.2(b) evaluates the constraint function. The figure confirms that the constraint function is monotonically increasing with P_f. For a given P_f, the interference increases with γ. The reason is that the number of samples needed to meet P_f decreases with γ, and thus more samples will be used for transmission, which results in higher levels of interference. To solve this problem, a larger detection probability, P_d, can be chosen for the system with large γ.

The impact of P_d on the system performance is shown in Fig. 2.3. Here, we investigate the system with $\gamma = 1$. The maximal interference generated by the SU system is plotted in the upper subfigure for $P_f \in (0, 0.5)$. In the lower subfigure, the maximal throughput for different P_d is given. We can see that the interference decreases with P_d while the maximal

20
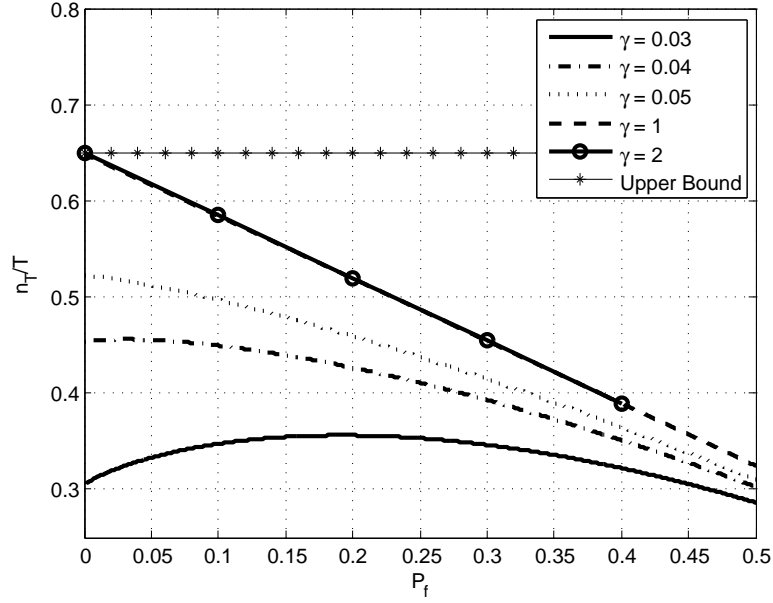
(a) Evaluation of the objective function.
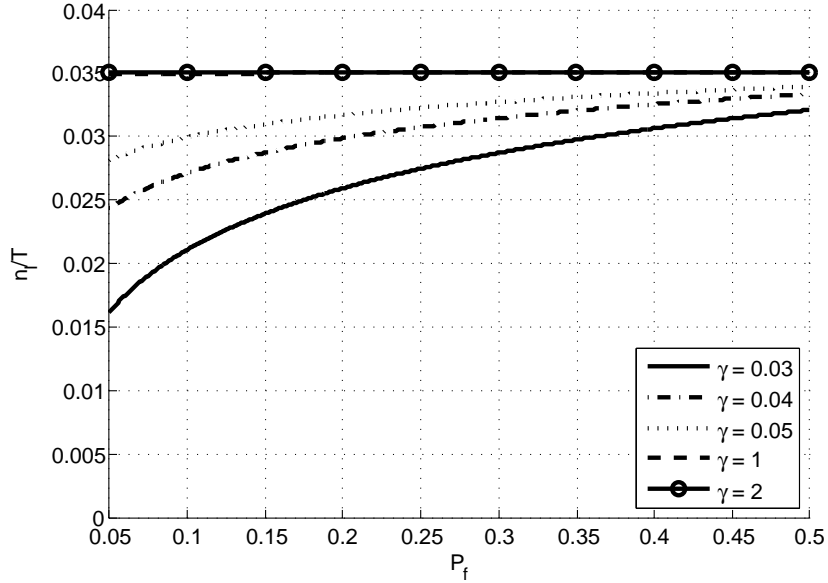
(b) Evaluation of the constraint function, where $P_d = 0.9$.

Figure 2.2. Performance evaluation of the objective and constraint functions, where $P_d = 0.9$.

throughput remains almost the same. Moreover, when γ is large, interference is dominated by P_d and the maximal throughput can only be achieved with small P_f as shown by the curves for $\gamma = 1$ and $\gamma = 2$ in Fig. 2.2(b). Thus, we can conclude that when γ is large, the target P_d can be increased to protect the PU system and to enhance the throughput of
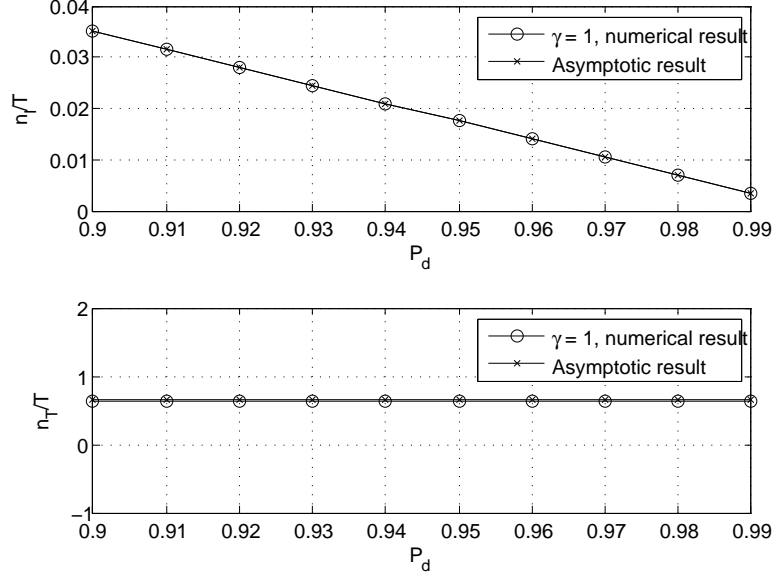
Figure 2.3. The impact of P_d, where $\gamma = 1$.

the SU system. Moreover, the asymptotic results for $\gamma \to +\infty$ are also plotted in Fig. 2.3. The asymptotic curves in the upper and the lower subfigures are from (2.21) and (2.23), respectively. From the figure, the asymptotic curves and the numerical curves match well.

As shown in Section 2.3, the optimal value P_f^* depends not only on the optimal value P_f^c maximizing the objective function, but also on P_f^u. In Figs. 2.4(a) and 2.4(b), the optimal throughput and P_f^* are shown for the system with $\gamma = 0.04$, respectively. From Fig. 2.4(a), the throughput increases with the interference threshold, I, when it is small. When I is large enough, i.e., $\gamma \geq 0.022$, the optimal throughput remains same. From Fig. 2.4(b), similar behavior of P_f^* with I can be observed. We can conclude that when I is small, the corresponding P_f^u is small. Thus, when $P_f^u < P_f^c$, P_f^* is determined by P_f^u while P_f^u increases with I. When $P_f^c < P_f^u$, P_f^* is determined by P_f^c, which will not change with I. Similarly, when I is small, the maximal throughput is determined by P_f^u, which increases with I. And when $P_f^c > P_f^u$, the maximal throughput is determined by P_f^c, which will not change with I. That is why the curves are flat when $\gamma \geq 0.022$ in both figures. The optimal false-alarm probability, P_f, in the flat region is obtained when (2.17) holds. And the corresponding maximal throughput is derived by (2.18).

22
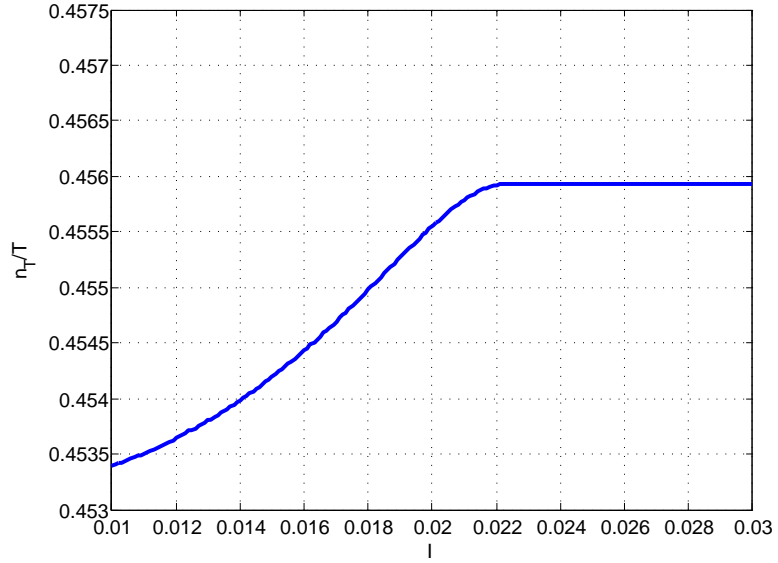
(a) Optimal throughput versus interference threshold, where $\gamma = 0.04$ and $P_d = 0.9$.
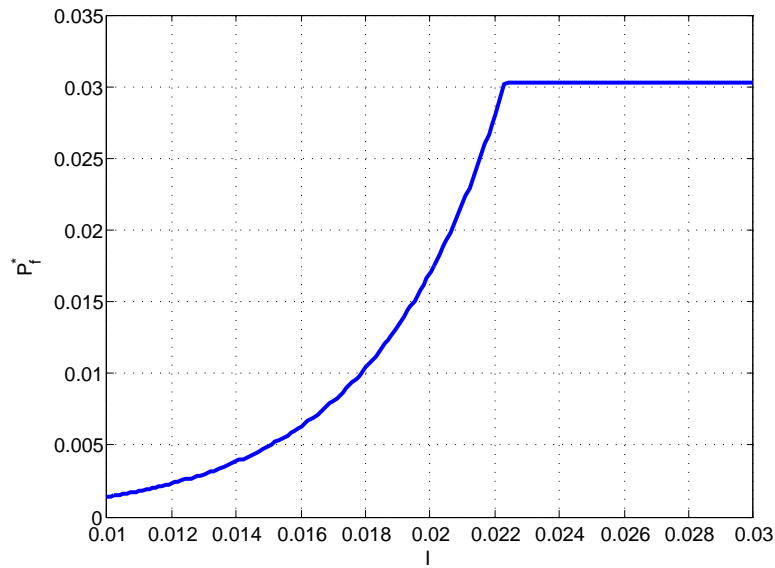
(b) P_f^* versus I, where $\gamma = 0.04$ and $P_d = 0.9$.

Figure 2.4. Performance evaluation for different interference thresholds.

2.6 Conclusions

In this chapter, we have investigated the optimal design of SD for CR networks. Our design is formulated as a throughput optimization problem of the SU system given the target detection probability and interference constraint to the PU system. Theoretical analysis is provided to show that the objective function is concave and the constraint function is

23

monotonically increasing with the false-alarm probability. Based on these properties, a u-nique optimal false-alarm probability is found and thus the throughput of the SU system is accordingly maximized. Numerical results have been presented to verify the analysis. The results show that when the interference constraint is strict, the optimal throughput is dominated by the interference constraint while it is determined by the objective function itself when the interference constraint is loose.

CHAPTER 3

OPTIMUM PERIODIC SPECTRUM SENSING FOR COGNITIVE RADIO NETWORKS

In this chapter, we continue our study on spectrum sensing. We focus on the scenario that the PU can change its status at any time within one frame. We develop a joint sensing block length and detection threshold optimization scheme to maximize the throughput of the CR network under interference constraint and required detection and false-alarm probabilities. We optimize the sensing block length under the general scenario where the status of the PU may change at any time during a frame, either the sensing block or the transmission/silent block. Numerical results are provided to demonstrate the impact of different system parameters on the system performance.

The rest of this chapter is organized as follows. In Section 3.1, we introduce the system model. In Section 3.2, we analyze the performance of the system. In Section 3.3, a joint sensing block length and detection threshold optimization problem is formulated to maximize the throughput of the CR network. The solution to the problem is addressed in Section 3.3. Numerical results are provided in Section 3.4. Finally, Section 3.5 concludes the chapter.

3.1   System Model

As in Chapter 2, the SU is assumed to operate on a frame-by-frame basis. One frame has a fixed length with T samples, consisting of a sensing block of M samples and a data transmission or a silent block of the rest L samples depending on the sensing result. Again, the received primary signal power to noise ratio at the SU is denoted as γ.

We use ED for spectrum sensing, which is easy to implement and also commonly used [10]. Based on ED, the test statistics will be $\Gamma = \sum_{i=1}^{M} |r_i|^2$.

The behavior of the PU is modeled as an alternating renewal source between busy and

25

idle states [63], where busy and idle denote the present or absent of the PU on the spectrum band. We assume the busy and idle periods are exponentially distritbuted random variables with *probability density functions* (PDFs) $f_B(t) = \alpha e^{-\alpha t}$ and $f_I(t) = \beta e^{-\beta t}$, where α and β denote the transition rate from busy to idle and from idle to busy, respectively. Accordingly, the stationary probabilities for the present and absent of the PU are $P_B = \frac{\beta}{\alpha+\beta}$ and $P_I = \frac{\alpha}{\alpha+\beta}$. Since α and β can be estimated with statistical methods, we assume they are known at the SU. We consider the scenario that the status of the PU can change at anytime within one frame. However, it is intractable and unnecessary to consider all possibilities. As shown in Fig. 3.1, the probability of changing at most once during one frame for practical cases is large. To make the analysis tractable as well as catch the main feature of the problem, we make an assumption to limit changes to at most once, which is reasonable for the practical case when $T\tau \ll \min\left\{\frac{1}{\alpha}, \frac{1}{\beta}\right\}$, where τ is the sampling rate.
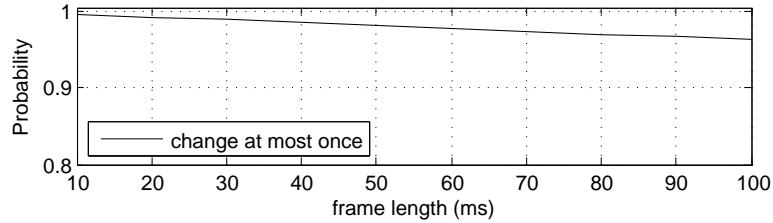
Figure 3.1. Probability of changing at most once where $\alpha = 0.3$ sec^{-1} and $\beta = 0.5$ sec^{-1}.

3.2   Throughput and Interference Analysis

In this section, we will analyze the behavior of the system. According to the status of the PU, we consider the following four cases.

Case I: The PU is absent at the beginning of the frame and changes the status during the sensing block.

Case II: The PU keeps absent during the sensing block while may change during the transmission/silent block.

Case III: The PU is present at the beginning of the frame and changes the status during the sensing block.

Case IV: The PU is present during the whole sensing block, while may change during the transmission/silent block.

We assume that if SU and PU are transmitting simultaneously, they will both lose the packets. The throughput of the SU is measured by the number of samples transmitting successfully while the interference to the PU is measured as the number of its lost samples.

3.2.1 Case I

If the licensed band is idle at the beginning of the frame, the conditional probability that it is still idle at the l-th sample while busy at the $(l + 1)$-th sample is

$$P_{1,l} = e^{-\beta l \tau} \left(1 - e^{-\beta \tau} \right). \tag{3.1}$$

The probability that Case I occurs is

$$P_1 = P_I \sum_{l=1}^{M} P_{1,l} = \frac{\alpha}{\alpha + \beta} \left(1 - e^{-\beta M \tau} \right). \tag{3.2}$$

The observed energy during the sensing period is $\Gamma_{1,l} = \sum_{i=1}^{l} |n_i|^2 + \sum_{i=l+1}^{M} |s_i + n_i|^2$. From the Appendix B.1, $\Gamma_{1,l}$ follows a Gaussian distribution, i.e.,

$$\Gamma_{1,l} \sim N \left(2M (\gamma + 1) - 2l\gamma, 4l + 4 (M - l) (\gamma + 1)^2 \right). \tag{3.3}$$

Given the condition that the band is still idle at the l-th sample while busy at the $(l+1)$-th sample, the detection probability can be expressed as

$$D_{1,l} = \Pr \left\{ \frac{1}{M} \Gamma_{1,l} > \lambda \right\} = Q \left(\frac{\lambda - \frac{2M(\gamma+1)-2l\gamma}{M}}{\sqrt{\frac{4l+4(M-l)(\gamma+1)^2}{M^2}}} \right), \tag{3.4}$$

where λ is the detection threshold, and $Q(\cdot)$ is the Q-function of the standard Gaussian, i.e., $Q(x) = 1/\sqrt{2\pi} \int_x^\infty \exp\left(-t^2/2\right) dt$.

Given the condition that the band is idle at the beginning of the frame and busy at the end of the sensing period, the detection probability is $D_1 = \sum_{l=1}^{M} D_{1,l} P_{1,l}$.

In this case, the SU will transmit if mis-detection occurs and all the transmitting samples will cause interference to the PU. Thus, the throughput of the SU in this case is 0, while all

the L packets from the PU will be interfered as well. If the SU detects the presence of the PU, it keeps silent. The throughput of the SU is 0 while no interference happens. Thus, the average throughput and interference in this case are

$$R_1 \;=\; 0 \text{ and } I_1 = P_I[(1 - e^{-\beta M\tau}) - D_1]L,$$

respectively.

3.2.2 Case II

The probability that the band is idle for the whole sensing block is

$$P_2 = \frac{\alpha}{\alpha + \beta} e^{-\beta M\tau}. \tag{3.5}$$

In this case, the observed energy during the sensing period is $\Gamma_2 = \sum_{i=1}^{M} |n_i|^2$. Similarly to Case I, Γ_2 follows a Gaussian distribution, i.e., $\Gamma_2 \sim N(2M, 4M)$. The false-alarm probability is

$$F_2 = \Pr\left\{\frac{1}{M}\Gamma_2 \geq \lambda\right\} = Q\left(\frac{\sqrt{M}(\lambda - 2)}{2}\right). \tag{3.6}$$

In this case, the SU keeps silent if false-alarm occurs, where the SU's throughput is 0 and the interference to the PU is 0 as well. On the other hand, the SU will transmit if it detects the absence of the PU. However, it is possible that the PU will appear during the transmission period, leading to the packet loss of both users. Given the PU is absent at the beginning of the transmission period, the probability that it appears at the $(l + 1)$-th transmission sample is

$$P_{a,l,2} = e^{-\beta l\tau}\left(1 - e^{-\beta\tau}\right). \tag{3.7}$$

The corresponding throughput of the SU and interference to the PU are $R_{2,l} = l$ and $I_{2,l} = L - l$, respectively.

If Case II happens, the average throughput and interference will be

$$R_{2,a} = \sum_{l=1}^{L} R_{2,l}P_{a,l,2} = \frac{1 - e^{-L\beta\tau}}{1 - e^{-\beta\tau}} - Le^{-(L+1)\beta\tau} \tag{3.8}$$

and

$$I_{2,a} = \sum_{l=1}^{L} I_{2,l} P_{a,l,2} = L\left(1 - e^{-\beta L\tau}\right) - R_{2,a}.$$ (3.9)

The average throughput and interference for this case are

$$R_2 = P_2(1 - F_2)R_{2,a} \text{ and } I_2 = P_2(1 - F_2)I_{2,a},$$ (3.10)

respectively.

3.2.3 Case III

If the band is busy at the beginning of the frame, the conditional probability that it is still busy at the l-th sample while becoming idle at the $(l + 1)$-th sample is

$$P_{3,l} = e^{-\alpha l\tau}\left(1 - e^{-\alpha\tau}\right).$$ (3.11)

The probability of Case III happens is $P_3 = \sum_{l=1}^{M} P_{3,l}$. During the sensing period, the observed energy is $\Gamma_{3,l} = \sum_{i=1}^{l} |s_i + n_i|^2 + \sum_{i=l+1}^{M} |n_i|^2$. Then, $\Gamma_{3,l}$ follows a Gaussian distribution, i.e., $\Gamma_{3,l} \sim N\left(2l\gamma + 2M, 4l(1 + \gamma)^2 + 4(M - l)\right)$.

Given the condition that the band is busy at the l-th sample while idle at the $(l + 1)$-th sample, the false-alarm probability is

$$F_{3,l} = \Pr\left\{\frac{1}{M}\Gamma_{3,l} \geq \lambda\right\} = Q\left(\frac{\lambda - \frac{2l\gamma + 2M}{M}}{\sqrt{\frac{4l(1+\gamma)^2 + 4(M-l)}{M^2}}}\right).$$ (3.12)

Then, the false-alarm probability of this case is $F_3 = \sum_{l=1}^{M} F_{3,l} P_{3,l}$.

If the SU decides the absence of the PU, it will transmit. The throughput of the SU is L and no interference will occur. On the other hand, if false-alarm occurs, the SU keeps silent. The corresponding throughput of the SU is 0 while no interference occurs as well. Then, the average throughput and interference for this case are

$$R_3 = P_B(1 - F_3)L \text{ and } I_3 = 0,$$ (3.13)

respectively.

3.2.4 Case IV

The probability that the band is busy for the whole sensing block is

$$P_4 = \frac{\beta}{\alpha + \beta} e^{-\alpha M \tau}. \tag{3.14}$$

The observed energy during the sensing period is $\Gamma_4 = \sum_{i=1}^{M} |r_i|^2 = \sum_{i=1}^{M} |s_i + n_i|^2$. Similarly, Γ_4 follows a Gaussian distribution, i.e., $\Gamma_4 \sim N\left(2M(\gamma + 1), 4M(\gamma + 1)^2\right)$.

Based on it, the detection probability is

$$D_4 = \Pr\left\{\frac{1}{M}\Gamma_4 \geq \lambda\right\} = Q\left(\frac{\lambda - 2(\gamma + 1)}{2(\gamma + 1)}\sqrt{M}\right), \tag{3.15}$$

and the mis-detection probability is $M_4 = 1 - D_4$.

In this case, the SU keeps silent if it detects the presence of the PU, where its throughput and the interference are both 0. When mis-detection occurs, the SU will transmit. Since the PU may leave the band during the transmission, we need to take this probability into account. If the PU is present at the beginning of the transmission period, the probability that it disappears at the $(l + 1)$-th transmission sample will be

$$P_{d,l,4} = e^{-\alpha l \tau}\left(1 - e^{-\alpha \tau}\right). \tag{3.16}$$

In this situation, the throughput of the SU and the interference to the PU are $R_{4,l} = L - l$ and $I_{4,l} = l$, respectively.

If Case IV occurs, the average throughput will be

$$R_{4,d} = \sum_{l=1}^{L} R_{4,l} P_{d,l,4} = L\left(1 - e^{-\alpha L \tau}\right) - I_{4,d}, \tag{3.17}$$

where $I_{4,d}$ is the average interference in case of mis-detection for Case IV, which can be expressed as

$$I_{4,d} = \frac{1 - e^{-L\alpha\tau}}{1 - e^{-\alpha\tau}} - Le^{-(L+1)\alpha\tau}. \tag{3.18}$$

The average throughput and interference for this case are

$$R_4 = P_4 M_4 R_{4,d} \text{ and } I_4 = P_4 M_4 I_{4,d}, \tag{3.19}$$

respectively.

Based on the results for all four cases, the average overall throughput and interference are

$$R(\lambda, M) = \sum_{i=1}^{4} R_i \text{ and } I(\lambda, M) = \sum_{i=1}^{4} I_i, \qquad (3.20)$$

respectively. The detection and false-alarm probabilities are

$$P_d(\lambda, M) = \frac{D_1 + D_4}{P_1 + P_4} \text{ and } P_f(\lambda, M) = \frac{F_2 + F_3}{P_2 + P_3}, \qquad (3.21)$$

respectively.

3.3 Throughput Optimization

From the previous discussion, the sensing block length and the detection threshold determine the system performance. To protect the PU, there are required detection and false-alarm probabilities, denoted as P_d^t and P_f^t. Moreover, the average interference generated by the SU cannot exceed a given interference threshold, I_{th}. Under these constraints, the throughput of the CR network is considered to be maximized by designing the sensing block length and the detection threshold. The problem is formulated as follows,

$$\max_{M, \lambda} \quad R(\lambda, M), \qquad (3.22)$$

$$s.t. \quad I(\lambda, M) \leq I_{th}, \ P_d(\lambda, M) \geq P_d^t, \ P_f(\lambda, M) \leq P_f^t.$$

For a given sensing block length, M, it is easy to show that $R(\lambda, M)$ and $I(\lambda, M)$ are monotonically increasing functions of λ while $P_d(\lambda, M)$ and $P_f(\lambda, M)$ are monotonically decreasing functions of it.

Thus, if $\min\{P_d^{-1}(P_d^t), I^{-1}(I_{th})\} < P_f^{-1}(P_f^t)$, the optimal threshold, $\lambda(M)$, for a given M, is

$$\lambda(M) = \min\{P_d^{-1}(P_d^t), I^{-1}(I_{th})\}. \qquad (3.23)$$

Otherwise, no solution exists for fulfilling all constraints.

Substituting (3.23) into (3.22), the problem is equivalent to

$$\max_{M} \quad R\left(\lambda\left(M\right), M\right), \tag{3.24}$$

which is an optimization problem without constraint.

$R\left(\lambda\left(M\right), M\right)$ is a complicated expression of M, which is hard to solve. However, since M has finite values, we can use exhaustive search to find out the optimal sensing block length, denoted as M^{*}. The worst case computational complexity is around $O(T^2/2)$. Since the calculation is done based on the statistical system parameters, which will not change frequently, the computational complexity is not a burden to the system.

3.4   Numerical Results

In this section, we provide numerical results to demonstrate the system performance. We set the length of one frame to be 200 ms, and sampling interval to be 0.01 ms. Thus, the length of one frame is $T = 20,000$ samples. We set $\alpha = 0.3\text{sec}^{-1}$, $\beta = 0.5\text{sec}^{-1}$, $P_d^t = 0.9$, and $P_f^t = 0.1$. For comparison, the optimum solutions based on the assumption that the status of the PU keeps same within one frame will be given.

The optimum solutions on the number of samples used for spectrum sensing with different interference thresholds are shown in Fig. 3.2. From the figure, the optimal sensing length decreases with the increase of SNR for each case. For a specific SNR, the sensing length decreases with the increase of interference thresholds. Based on the assumption that the PU status keeps same during the whole frame, the optimal sensing length decreases with the increase of the SNR while the impact of different interference thresholds is negligible. Compared to the proposed algorithm, the optimum sensing length is larger than the corresponding results without considering PU status change. That means that much samples are needed for decision by introducing uncertainty about the PU status.

The corresponding maximal throughput is shown in Fig. 3.3. From the figure, higher average throughput can be obtained by considering the PU status change than the case without considering it. With the increase of SNR, better throughput can be obtained. Moreover,
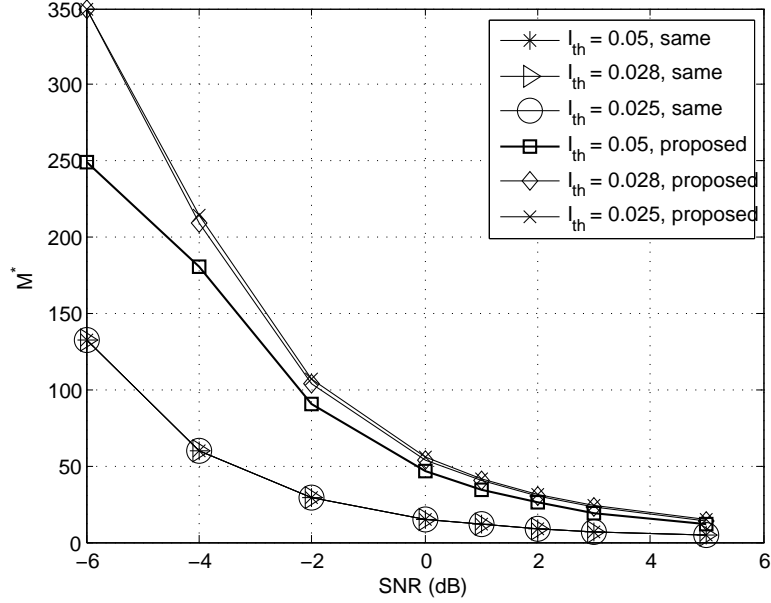
Figure 3.2. Optimum sensing block length for different γ.

the impact of the interference threshold is negligible for the proposed algorithm while the increase of interference threshold leads to better throughput for the case without considering PU status change.

3.5 Conclusions

In this chapter, we have investigated the optimal spectrum sensing length design for a general PU on-off model. We consider four scenarios where the status of the PU can change during the sensing block or the transmission/silent block. Then, we formulate a throughput optimization problem of the CR network given the target interference constraint to the PU system, the detection and false-alarm probabilities. Based on the properties of the objective and constraint functions, the original problem has been simplified to a one-parameter optimization problem without constraint. Exhaustive search is used to find out the optimal sensing block length. Numerical results show that higher throughput can be obtained by considering the PU status change compared to the case without considering it.
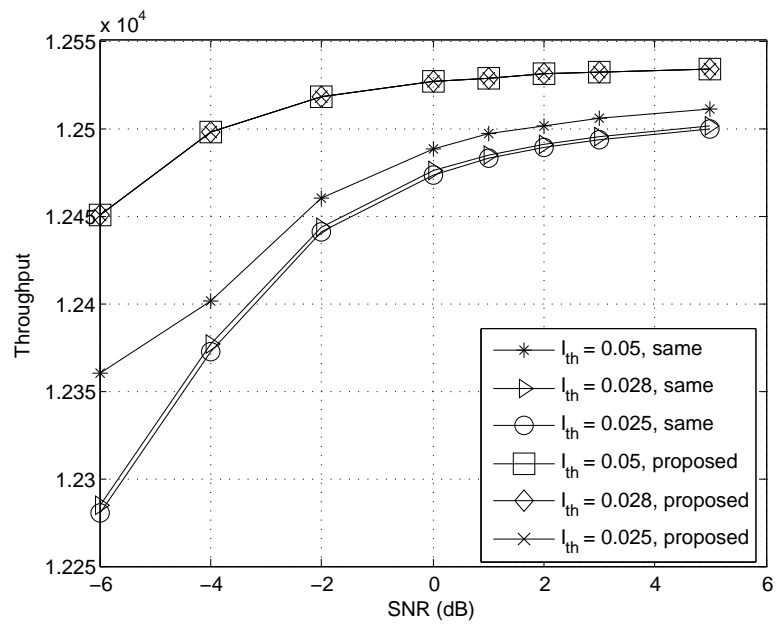
Figure 3.3. Maximum throughput for different γ**.**

CHAPTER 4

NULLSPACE RELEASING FOR SPATIAL-FREQUENCY OPPORTUNISTIC TRANSMISSION

From this chapter, we begin to summarize our findings on spectrum access strategies. We start with the spectrum overlay systems. In this chapter, we investigate spatial-frequency opportunistic transmission in MIMO-OFDM systems, whereby a secondary link uses a nullspace of the primary link to opportunistically transmit its own data without generating interference to the primary link. To further improve the performance of the secondary link, we consider a scenario of cooperation among the primary and the secondary links, where the primary link is based on MIMO-OFDM and can reallocate its power and release some freedom to the secondary link when its own QoS requirement can be satisfied. Three nullspace releasing algorithms are proposed, called as *exhaustive-search* (ESA), *small-eigenvalue* (SEA), and *best-throughput* (BTA) algorithms. From the numerical results, the BTA has lower computational complexity than the ESA and provides higher throughput than the SEA, thus offering a good compromise between implementation complexity and achievable throughput.

The rest of this chapter is organized as follows. In Section 4.1, we introduce the basic system setup. In Section 4.2, we present the nullspace releasing design. Numerical results are provided in Section 4.3. Finally, Section 4.4 concludes this chapter.

4.1 Basic System

As in Fig. 4.1, we consider a scenario that an $N_t^{(1)}$ input and $N_r^{(1)}$ output secondary link coexists with a $N_t^{(0)}$ input and $N_r^{(0)}$ output primary link, where the primary and secondary transmitters/receivers are denoted as transmit/receive nodes 0 and 1, respectively. The primary link transmission is based on OFDM with K subcarriers and L points of CP. The proposed algorithms in the following sections are also suitable for the primary link with
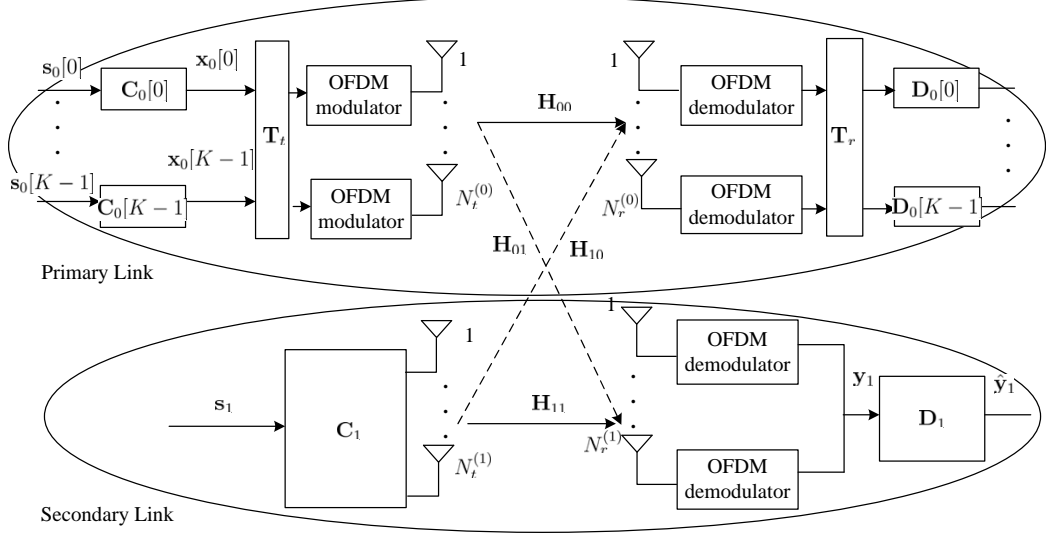
Figure 4.1. System model for spatial-frequency opportunistic transmission.

multiple primary pairs based on *orthogonal frequency division multiple access* (OFDMA). Here, we focus on a single primary pair for simplicity. The secondary link will generate interference-free transmission to the primary one. Channel between any link of transmit and receive antenna is assumed to be frequency-selective and with at most $L + 1$ taps. Denote $\mathbf{\Gamma}_{i,j}^{(k,n)}$ as a circulant time-domain channel matrix from the k-th transmit antenna of the i-th transmit node to the n-th receive antenna of the j-th receive node, which is,

$$
\mathbf{\Gamma}_{i,j}^{(k,n)} =
\begin{pmatrix}
h_{i,j}^{(k,n)}[0] & 0 & \cdots & \cdots & \cdots\cdots & h_{i,j}^{(k,n)}[1] \\
\vdots & \ddots\ddots & \ddots & \ddots\ddots & \vdots \\
h_{i,j}^{(k,n)}[L] & \ddots\ddots & \ddots & \ddots\ddots & \vdots \\
0 & \ddots\ddots & h_{i,j}^{(k,n)}[0] & \ddots\ddots & \vdots \\
\vdots & \ddots\ddots & \vdots & \ddots\ddots & \vdots \\
0 & \cdots\cdots & \cdots & \cdots\cdots & h_{i,j}^{(k,n)}[0]
\end{pmatrix}
\tag{4.1}
$$

where $h_{i,j}^{(k,n)}[l]$ is the l-th tap channel impulse response from the k-th transmit antenna of the i-th transmit node to the n-th receive antenna of the j-th receive node. All channel coefficients are assumed to be i.i.d. following Rayleigh distribution.

4.1.1 Primary System

At the primary receiver, the signal after OFDM demodulation can be expressed as

$$\mathbf{y}_0 = \mathbf{H}_{00}\mathbf{x}_0 + \mathbf{H}_{10}\mathbf{x}_1 + \mathbf{n}_0, \tag{4.2}$$

where $\mathbf{H}_{00} \in C^{N_r^{(0)}K \times N_t^{(0)}K}$ and $\mathbf{H}_{10} \in C^{N_r^{(0)}K \times N_t^{(1)}(K+L)}$ are the effective channel matrices from the primary and secondary transmitters to the primary receiver, respectively. $\mathbf{x}_0 \in C^{N_t^{(0)}K \times 1}$ and $\mathbf{x}_1 \in C^{N_t^{(1)}(K+L) \times 1}$ are the transmit vectors from the primary and the secondary transmitters, respectively. $\mathbf{n}_0 \sim CN(0, \sigma^2\mathbf{I}_K)$ is an additive white Gaussian noise vector. The effective channel matrices in (4.2) can be expressed as

$$\mathbf{H}_{00} = \begin{pmatrix} \mathbf{FB\Gamma}_{0,0}^{(1,1)}\mathbf{AF}^H & \cdots & \mathbf{FB\Gamma}_{0,0}^{(N_t^{(0)},1)}\mathbf{AF}^H \\ \vdots & \ddots & \vdots \\ \mathbf{FB\Gamma}_{0,0}^{(1,N_r^{(0)})}\mathbf{AF}^H & \cdots & \mathbf{FB\Gamma}_{0,0}^{(N_t^{(0)},N_r^{(0)})}\mathbf{AF}^H \end{pmatrix}, \tag{4.3}$$

and

$$\mathbf{H}_{10} = \begin{pmatrix} \mathbf{FB\Gamma}_{1,0}^{(1,1)} & \cdots & \mathbf{FB\Gamma}_{1,0}^{(N_t^{(1)},1)} \\ \vdots & \ddots & \vdots \\ \mathbf{FB\Gamma}_{1,0}^{(1,N_r^{(1)})} & \cdots & \mathbf{FB\Gamma}_{1,0}^{(N_t^{(1)},N_r^{(1)})} \end{pmatrix}, \tag{4.4}$$

where $\mathbf{A} \in C^{(K+L) \times K}$ and $\mathbf{B} \in C^{K \times (K+L)}$ are the CP insertion and removal matrices, respectively, $\mathbf{F} = \frac{1}{\sqrt{K}} \left(e^{-j2\pi\frac{nk}{K}}\right)_{k,n=0}^{K-1}$ is a normalized DFT matrix.

For the primary link, the precoding and postcoding are conducted on each subcarrier as there is no secondary link [64]. Based on the property of OFDM, the system on the k-th subcarrier is an equivalent MIMO system with channel matrix $\mathbf{H}_{00}[k] \in C^{N_r^{(0)} \times N_t^{(0)}}$. To maximize the achievable rate, the precoding matrix, $\mathbf{C}_0[k] \in C^{N_t^{(0)} \times d_0}$, and the postcoding matrix, $\mathbf{D}_0[k] \in C^{d_0 \times N_r^{(0)}}$, on the k-th subcarrier are designed based on the *singular-value decomposition* (SVD) of $\mathbf{H}_{00}[k]$, where $d_0 \leq \min\{N_t^{(0)}, N_r^{(0)}\}$ is the number of symbols transmitted on each subcarrier of the primary link. The m-th singular values of $\mathbf{H}_{00}[k]$ is denoted as $\lambda_m^0[k]$. The operation is based on standard SVD method.

To make the representation compact, the transmit signal vector for the primary link can

be expressed as

$$\mathbf{x}_0 = \mathbf{T}_t \mathbf{C}_0 \mathbf{s}_0, \tag{4.5}$$

where $\mathbf{C}_0 = \text{diag}\,(\mathbf{C}_0[0], ..., \mathbf{C}_0[K-1])$ and $\mathbf{s}_0 = \left((\mathbf{s}_0[0])^{\mathrm{T}}, \cdots, (\mathbf{s}_0[K-1])^{\mathrm{T}}\right)^{\mathrm{T}}$ with $\mathbf{s}_0[k] \in C^{d_0 \times 1}$ being the source signal vector on the k-th subcarrier, and $\mathbf{T}_t \in C^{N_t^{(0)}K \times N_t^{(0)}K}$ is to rearrange symbols on each subcarrier to a transmit stream one each antenna, with its (i, j) entry as

$$\mathbf{T}_t[i, j] = \begin{cases} 1, & j = \lfloor \frac{i-1}{K} \rfloor + ((i-1)_{modK})N_t^{(0)}+1, \\ 0, & \text{else.} \end{cases} \tag{4.6}$$

The post-processed signal vector at the primary receiver can be expressed as

$$\hat{\mathbf{y}}_{00} = \mathbf{D}_0 \mathbf{T}_r \mathbf{y}_{00}, \tag{4.7}$$

where $\mathbf{D}_0 = \text{diag}\,(\mathbf{D}_0[0], ..., \mathbf{D}_0[K-1])$ and $\mathbf{T}_r$ is to rearrange the receive signal stream on each antenna to symbols on each subcarrier with its (i, j)-entry as

$$\mathbf{T}_r[i, j] = \begin{cases} 1, & j = \lfloor \frac{i-1}{N_r^{(0)}} \rfloor + ((i-1)_{modN_r^{(0)}})K+1, \\ 0, & \text{else.} \end{cases} \tag{4.8}$$

If power allocation is used at the primary transmitter, the power allocation matrix of the source signal from the primary transmitter, $\mathbf{P}_0 = E\{\mathbf{s}_0(\mathbf{s}_0)^{\mathrm{H}}\}$, is a diagonal matrix with diagonal elements $(P_1^0[0], ..., P_{d_0}^0[0], ..., P_1^0[K-1], ..., P_{d_0}^0[K-1])$, where $P_m^0[k] = \left(\mu - \frac{\sigma^2}{(\lambda_m^0[k])^2}\right)^+$, where $(x)^+ = \max\{0, x\}$ and μ is chosen to satisfy the total power constraint $\sum_{k=0}^{K-1} \sum_{m=1}^{\min\{N_t^{(0)}, N_r^{(0)}\}} P_m^0[k] = P_{th}^{(0)}$, $P_{th}^{(0)}$ is the total power constraint at the primary transmitter.

4.1.2 Secondary System

Similar to the primary link, the received signal vector at the secondary receiver, $\mathbf{y}_1 \in C^{N_r^{(1)}K \times 1}$, can be expressed as

$$\mathbf{y}_1 = \mathbf{H}_{11}\mathbf{x}_1 + \mathbf{H}_{01}\mathbf{x}_0 + \mathbf{n}_1, \tag{4.9}$$

where $\mathbf{H}_{11} \in C^{N_r^{(1)}K \times N_t^{(1)}(K+L)}$ and $\mathbf{H}_{01} \in C^{N_r^{(1)}K \times N_t^{(0)}K}$ are effective channel matrices from the secondary and the primary transmitters to the secondary receiver, respectively, and can be

38

defined as in (5.3) and (5.2), respectively. $\mathbf{n}_1 \in C^{N_r^{(1)}K \times 1}$ is the additive noise. The transmit signal vector $\mathbf{x}_1$ can be expressed as $\mathbf{x}_1 = \mathbf{C}_1\mathbf{s}_1$, where $\mathbf{C}_1$ and $\mathbf{s}_1$ are the precoding matrix and the source information vector at the secondary transmitter, respectively. To completely eliminate the interference to the primary link, the precoding matrix is designed as in [65],

$$\mathbf{C}_1 = \text{null}\left(\widetilde{\mathbf{H}}_{10}\right), \tag{4.10}$$

where $\widetilde{\mathbf{H}}_{10}$ contains the rows of $\mathbf{D}_0\mathbf{T}_r\mathbf{H}_{10}$ with $P_m^0[k] \neq 0$. The required channel information can be obtained through different ways, such as using channel reciprocity, feedback or learning mechanisms [39]. For some application scenarios, it is also possible for a central node who has all required information to coordinate the process.

To minimize the impact of the interference from the primary link, a postcoding matrix $\mathbf{D}_1$ is designed as in [65] as $\mathbf{D}_1 = \mathbf{Q}^{-\frac{1}{2}}$, where $\mathbf{Q} = E\left\{(\mathbf{H}_{01}\mathbf{x}_0 + \mathbf{n}_1)(\mathbf{H}_{01}\mathbf{x}_0 + \mathbf{n}_1)^{\mathrm{H}}\right\}$ is the covariance matrix of the interference signal and the noise. The power allocation matrix of the secondary link $\mathbf{P}_1 = E\{\mathbf{s}_1(\mathbf{s}_1)^{\mathrm{H}}\}$ can be designed to maximize the overall data transmission rate. As in [66, 65], the optimal power allocation matrix of the SU can be expressed as

$$\mathbf{P}_1 = \left((\mathbf{C}_1)^{\mathrm{H}}\mathbf{C}_1\right)^{-\frac{1}{2}} \mathbf{V}\widehat{\mathbf{P}}_1^*\mathbf{V}^{\mathrm{H}}\left((\mathbf{C}_1)^{\mathrm{H}}\mathbf{C}_1\right)^{-\frac{1}{2}}, \tag{4.11}$$

where $\widehat{\mathbf{P}}_1^*(n, n) = \left(\rho - \frac{1}{\lambda_n^2}\right)^+$, λ_i are the singular values of $\widetilde{\mathbf{Q}} = \mathbf{Q}^{-\frac{1}{2}}\mathbf{H}_{11}\mathbf{C}_1\left((\mathbf{C}_1)^{\mathrm{H}}\mathbf{C}_1\right)^{-\frac{1}{2}}$, whose SVD is denoted as $\widetilde{\mathbf{Q}} = \mathbf{U}\mathbf{\Lambda}\mathbf{V}^{\mathrm{H}}$, and ρ is determined to satisfy total power constraint $P_{th}^{(1)}$.

4.2 NullSpace Releasing

To generalize the analysis in the previous section and further improve the performance of the secondary link, we consider the scenario that the primary link can release more nullspace for the secondary link as long as its QoS requirement is maintained if there is some cooperation between the primary and the secondary links.

The objective here is to maximize the data rate of the secondary link while guaranteeing that of the primary one. As before, we still design interference-free transmission from the

secondary transmitter to the primary receiver. To fulfill the goal, the primary link should assign no power to those channels with very bad conditions and assign more power for the ones with good conditions. Then, the rank of the nullspace is increased and the secondary link can transmit more symbols.

Denote $R_{th}^{(0)}$ as the minimum rate requirement of the primary link. Mathematically, the problem can be formulated as

$$\max_{P_m^0[k], \mathbf{C}_1, \mathbf{P}_1} R_1 = \frac{1}{K+L} \log_2 |\mathbf{I} + \mathbf{D}_1 \mathbf{H}_{11} \mathbf{C}_1 \mathbf{P}_1 (\mathbf{C}_1)^H (\mathbf{H}_{11})^H \mathbf{D}_1|, \qquad (4.12a)$$

subject to

$$R_0 = \frac{1}{K+L} \sum_{k=0}^{K-1} \sum_{m=1}^{\min\{N_t^{(0)}, N_r^{(0)}\}} \log_2 \left(1 + \frac{P_m^0[k](\lambda_m^0[k])^2}{\sigma^2}\right) \geq R_{th}^{(0)}, \qquad (4.12b)$$

$$\sum_{k=0}^{K-1} \sum_{m=1}^{\min\{N_t^{(0)}, N_r^{(0)}\}} P_m^0[k] \leq P_{th}^{(0)}, \text{Trace}\left\{\mathbf{C}_1 \mathbf{P}_1 (\mathbf{C}_1)^H\right\} \leq P_{th}^{(1)}. \qquad (4.12c)$$

The first constraint is the rate requirement of the primary link, represents its QoS requirement. Eq. (4.12c) is the total power constraint at the primary and the secondary link, respectively.

The problem can be solved in two steps. First, we determine the power allocation of the primary link, i.e., $P_m^0[k]$. After the power allocation of the primary link is determined, the nullspace for the secondary link is determined. Then, the precoding and postcoding operations for the secondary link are the same as we have provided in the Section 4.1. Therefore, we will focus on the first step and develop three algorithms to release nullspace.

4.2.1 Exhaustive-Search Algorithm (ESA)

The optimal nullspace releasing can be found through exhaustive search. Denote

$$\Omega = \{(1, 0), ..., (1, K - 1), ...(\min\{N_t^{(0)}, N_r^{(0)}\}, K - 1)\}$$

40

to be the set to represent all positions of source symbols of the primary link. For a subset of Ω that $\mathcal{Z}_g \subset \Omega$, let

$$P_m^0[k] = \begin{cases} 0, & (m,k) \in \mathcal{Z}_g, \\ \left(\mu - \sigma^2/(\lambda_m^0[k])^2\right)^+, & \text{else,} \end{cases} \tag{4.13}$$

where μ is chosen to satisfy the total power constraint. Based on the power allocation result, if the rate requirement of the primary link is satisfied, it is called one candidate. We then calculate the rate of the secondary link for all candidates. The optimal solution will be the one providing largest rate for the secondary link. Note that, the above problem belongs to integer programming and is NP-hard. There is no efficient algorithm for the optimal solution in general, but we can conduct the search smartly to reduce the complexity.

With the increase of the number of subcarriers, K, and the number of antennas of the primary link, the complexity will increase dramatically. To reduce the computational complexity while maintaining reasonable performance, we will develop two suboptimal algorithms.

4.2.2 Small-Eigenvalue Algorithm (SEA)

Intuitively, a simple idea is to ask the primary link to release the subspaces with small eigenvalues to the secondary link. The idea is similar as in [67, 68], but the procedure for power allocation is different. In [68], the power on one direction is set to be zero without recalculation if the power allocated on it is less than a threshold based on the traditional power allocation results. In our algorithm, power allocation matrix will be recalculated after subspace releasing. The detailed procedure is as follows.

4.2.2.1 Initialization

$P_m^0[k]$ is calculated as if without the secondary link. If the QoS requirement of the primary link can not be satisfied, the operation at the secondary link is the same as without releasing. Otherwise, the primary link can release additional subspaces. This is the first iteration.

For the *n*-th iteration, rearrange $\lambda_m^0[k]$ in an increasing order. Find the smallest eigenvalue, $\lambda_j^0[l]$, that has $P_j^0[l] \neq 0$. Recalculate the power allocation as

$$P_m^0[k] = \begin{cases} 0, & \lambda_m^0[k] \leq \lambda_j^0[l], \\ \left(\mu - \sigma^2/(\lambda_m^0[k])^2\right)^+, & \text{else,} \end{cases} \tag{4.14}$$

The QoS of the primary link can be guaranteed and the procedure is simple. However, we only consider the QoS of the primary link during the nullspace releasing procedure. It is expected to be improved by taking the secondary link's rate into account, which motivates the BTA, next.

4.2.3 Best-Throughput Algorithm (BTA)

We take both the QoS requirement of the primary link and the rate of the secondary link into account. Again, the primary link releases one-dimensional subspace in one iteration as the SEA. Instead of using the subspace with smallest eigenvalue, it releases the subspace that can provide the most rate improvement of the secondary link. The procedure is as follows.

4.2.3.1 *Initialization*

Same as the SEA in Section 4.2.2.

4.2.3.2 *Updating*

Find all the subspaces that $P_m^0[k] \neq 0$ and let $\mathcal{Z}_b = \{(m, k)|P_m^0[k] \neq 0\}$. For each component in $\mathcal{Z}_b$, calculate

$$P_m^0[k] = \begin{cases} \left(\mu - \sigma^2/(\lambda_m^0[k])^2\right)^+, & (m, k) \in \mathcal{Z}_b, \\ 0, & \text{else,} \end{cases} \tag{4.15}$$

where μ is chosen to satisfy the total power constraint. The resulting power allocation is denoted as $\mathbf{P}_0[m, k]$ for each component and then, calculate the corresponding rate of the primary link, denoted as $R_0[m, k]$. Find out all the possibilities that the QoS of the primary link can be satisfied and let $\widetilde{\mathcal{Z}}_b = \{(\widetilde{m}, \widetilde{k})|R_0[\widetilde{m}, \widetilde{k}] \geq R_{th}^{(0)}\}$.

If $\widetilde{\mathcal{Z}}_b = \emptyset$, stop updating. Otherwise, we calculate the rate of the secondary link for each component in $\widetilde{\mathcal{Z}}_b$ based on its corresponding power allocation result $\mathbf{P}_0[\widetilde{m}, \widetilde{k}]$, denoted as $R_1[\widetilde{m}, \widetilde{k}]$. Let $(m^*, k^*) = \arg\max R_1[\widetilde{m}, \widetilde{k}]$. Set $P^0_{m^*}[k^*] = 0$ and repeat updating.

4.2.4 Complexity

Here, we analyze the complexity of all three algorithms. The dominated computational complexity is the SVD operation. The rough complexities for the ESA, the SEA, and the BTA are $O(K \times K^3)$, $O(K^3)$, and $O(K \times K^3)$, respectively. For example, when the number of subcarriers is $K = 4$ and the length of CP is $L = 1$, the rough complexities for the E-SA, the SEA, and the BTA are $O(1536)$, $O(64)$, and $O(256)$. However, when $K = 64$ and $L = 16$, the rough complexities for the ESA, the SEA, and the BTA become $O(3.3 \times 10^{94})$, $O(2.6 \times 10^5)$, and $O(2.6 \times 10^7)$. It is obvious that the computational complexity of the three algorithms from high to low is the ESA, the BTA, and the SEA. For the ESA, the complexity increases dramatically with the number of subcarriers, which makes it impractical for the system with a large number of subcarriers. However, the ESA is still useful for theoretical analysis and comparison.

4.3 Numerical Results

In this section, numerical results will be provided to demonstrate the performance of the proposed algorithms. To limit the number of variables, we set the SNRs from the secondary(primary) transmitter to the primary(secondary) receiver to be -15 dB and we assume the SNRs of the primary and the secondary links are same. Without loss of generality, we assume $R^{(0)}_{th} = 3$ bps/Hz.

Fig. 4.2 shows the data rate of the secondary link with different algorithms for $N^{(0)}_t = N^{(0)}_r = 2$ and $N^{(1)}_t = N^{(1)}_r = M$. Since the computational complexity is high for the ESA with large subcarrier number, we only show ESA's results with $K = 4$ subcarriers and $L = 1$ point CP. When SNR is small, the QoS requirement of the primary link can not be satisfied, and thus, it will not release additional subspaces to the secondary link. The
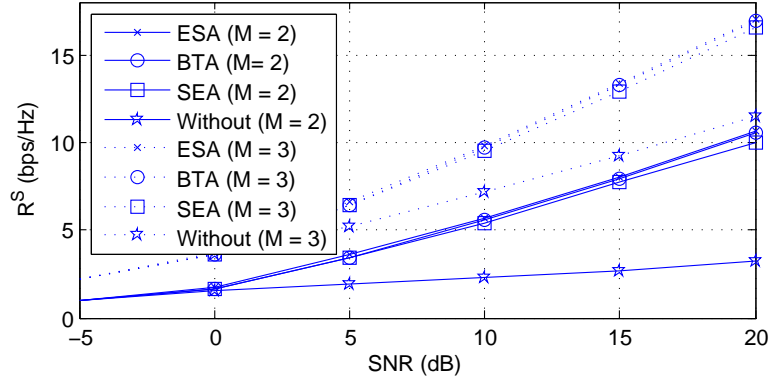
Figure 4.2. Data rate of the secondary link for $K = 4$**,** $L = 1$**.**

results for the algorithms with and without nullspace releasing are the same. After the QoS requirement of the primary link can be satisfied, the secondary link has higher data rate based on the algorithms with nullspace releasing. Comparing the three nullspace releasing algorithms, the ESA has the best performance and the SEA has the worst performance. With the increase of SNR, the performance of the BTA converges to the ESA and there exists a small gap between the performance of the SEA and the ESA. Thus, the BTA is a good tradeoff since it has lower computational complexity than the ESA while providing better performance than the SEA.

Fig. 4.3 shows the results for a system with $K = 64$ and $L = 16$, which is similar to the case with $K = 4$ and $L = 1$.
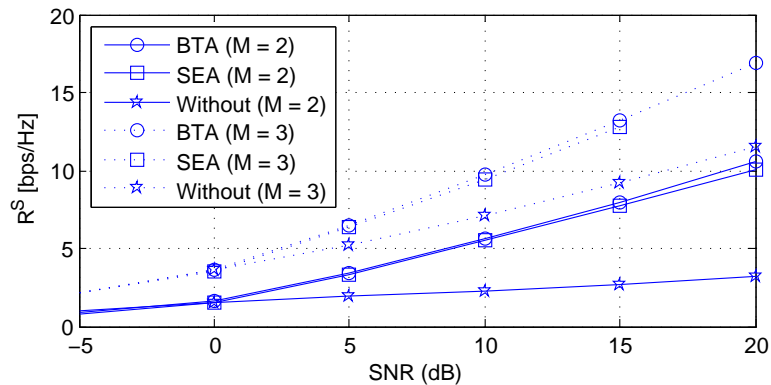
Figure 4.3. Data rate of the secondary link for $K = 64$ **and** $L = 16$**.**

44

4.4 Conclusions

In this article, we discuss a scenario allowing the primary link to release some of its own freedom to the secondary link without violating its own QoS requirement to improve the performance of the secondary link. A throughput maximization problem is formulated to find out optimal subspace that can be released by the primary link to the secondary link. Three novel subspace releasing algorithms, the ESA, the SEA, and, the BTA, are proposed. The nullspace releasing algorithms improve the performance of the secondary link when the primary link is good enough to satisfy its own QoS requirement. From our numerical results, the BTA is a good tradeoff between computational complexity and performance. The proposed algorithms can be extended to a more general scenario, which will be our future topic.

CHAPTER 5

SPATIAL-FREQUENCY SIGNAL ALIGNMENT FOR OPPORTUNISTIC TRANSMISSION

In this chapter, we extend our study of the opportunistic transmission design for MIMO-OFDM systems to a scenario with multiple secondary cells. Besides the interference to the PUs, the inter- and intra-interference among the SUs are considered as well. The number of symbols that can be transmitted by each SU satisfying all interference-free constraints is obtained. Precoding matrix design will be discussed for perfectly- and partially-aligned transmission. Two chordal-distance based schemes, called as exhaustive search algorithm and heuristic algorithm, will be developed for each case. Compared to the traditional *time-division multiple access* (TDMA) scheme, the proposed scheme can support more interference-free symbols to be transmitted by SUs simultaneously.

The rest of this chapter is organized as follows. After introducing the basic system model in Section 5.1, we propose a signal alignment scheme in Section 5.2. In Section 5.3, precoding matrix design for perfectly- and partially-aligned transmission is discussed. Numerical results are presented in Section 5.4. Some related issues and potential extensions will be discussed in Section 5.5. Finally, Section 5.6 concludes the chapter.

5.1 Basic System

Figure 5.1 shows a scenario that a two-cell secondary uplink system coexists with a primary system. We will investigate transmission schemes for the secondary system to generate interference-free transmission to the primary system. One primary link uses N_t input and N_r output OFDM system with K subcarriers and L points of CP. For the secondary system, each cell consists of one SBS with M_r antennas and M SUs, each with M_t antennas. We denote the primary transmitter as node 0, the i-th SU in cell 1 as node i ($i = 1, 2, ..., M$) and the j-th SU in cell 2 as node $j + M$ ($j = 1, 2, ..., M$). The primary receiver is denoted as
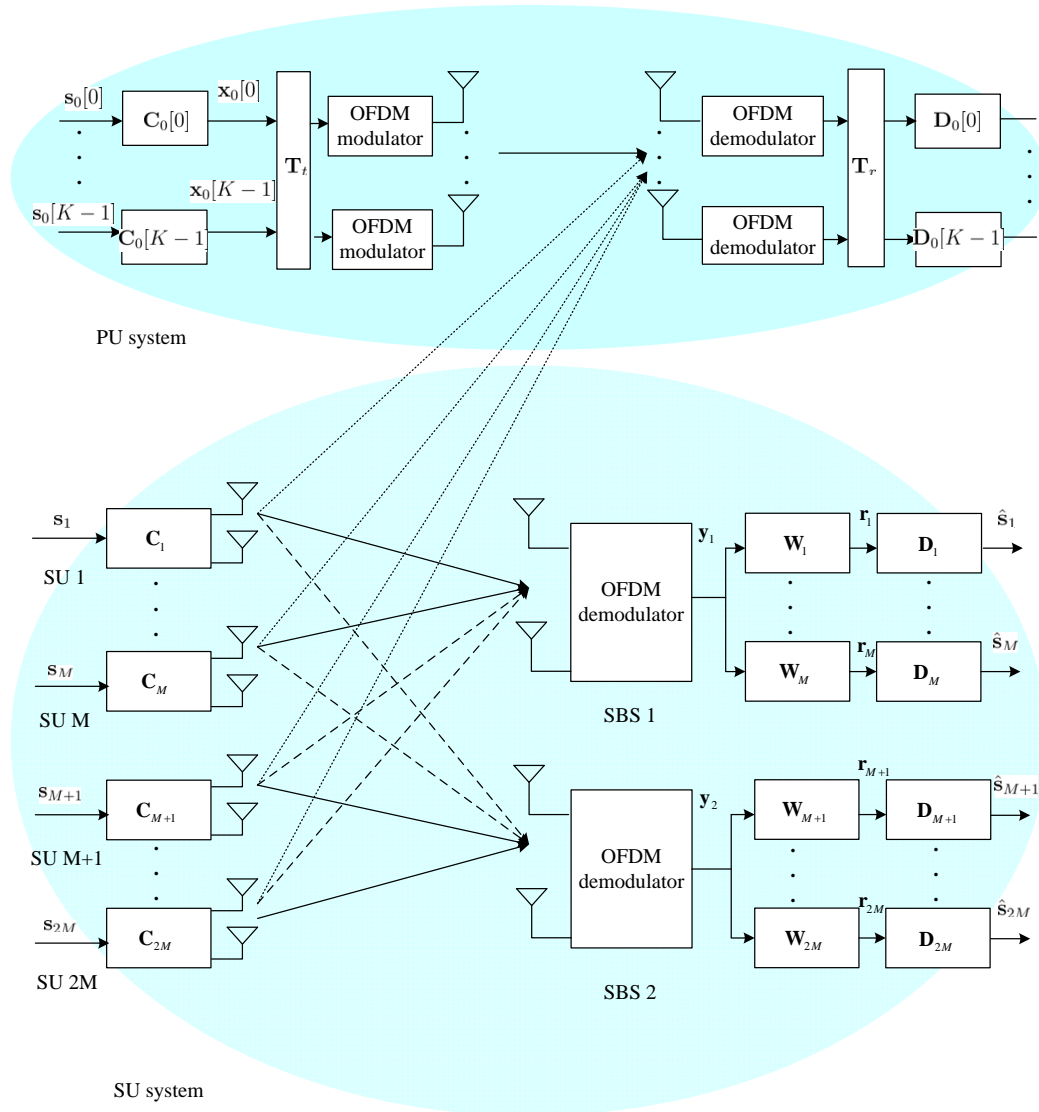
Figure 5.1. System model of a two-cell secondary network where solid lines and dashed lines denote the intended signals and interference signals, respectively.

node 0 while the i-th SBS is denoted as node i ($i = 1, 2$).

Channel between any link of transmit and receive antenna is assumed to be frequency-selective and with no more than $L+1$ taps. Denote $\mathbf{\Gamma}_{i,j}^{(k,n)}$ as a circulant time-domain channel matrix from the k-th transmit antenna of the i-th transmit node to the n-th receive antenna of the j-th receive node, which is defined the same as (4.1) in Chapter 4.

5.1.1 Primary System

The received signal vector at the primary receiver after OFDM demodulation can be represented as

$$\mathbf{y}_0 = \mathbf{H}_{0,0}\mathbf{x}_0 + \sum_{i=1}^{2M} \mathbf{H}_{i,0}\mathbf{x}_i + \mathbf{FB}\mathbf{n}_0, \tag{5.1}$$

where $\mathbf{H}_{0,0} \in C^{N_rK \times N_tK}$ is the effective channel matrix from the primary transmitter, $\mathbf{H}_{i,0} \in C^{N_rK \times M_t(K+L)}$ is the effective channel matrix from the i-th SU, $\mathbf{x}_0 \in C^{N_tK \times 1}$ is the transmit vector from the primary transmitter, $\mathbf{x}_i \in C^{M_t(K+L) \times 1}$ is the transmit signal vector from the i-th SU, and $\mathbf{n}_0 \sim CN(0, \sigma^2\mathbf{I}_K)$ is an additive white Gaussian noise vector. The effective channel matrices in (5.1) can be expressed as

$$\mathbf{H}_{0,0} = \begin{pmatrix} \mathbf{FB\Gamma}_{0,0}^{(1,1)}\mathbf{AF}^H & \cdots & \cdots & \mathbf{FB\Gamma}_{0,0}^{(N_t,1)}\mathbf{AF}^H \\ \mathbf{FB\Gamma}_{0,0}^{(1,2)}\mathbf{AF}^H & \cdots & \cdots & \mathbf{FB\Gamma}_{0,0}^{(N_t,2)}\mathbf{AF}^H \\ \vdots & \vdots & \ddots & \vdots \\ \mathbf{FB\Gamma}_{0,0}^{(1,N_r)}\mathbf{AF}^H & \cdots & \cdots & \mathbf{FB\Gamma}_{0,0}^{(N_t,N_r)}\mathbf{AF}^H \end{pmatrix}, \tag{5.2}$$

and

$$\mathbf{H}_{i,0} = \begin{pmatrix} \mathbf{FB\Gamma}_{i,0}^{(1,1)} & \mathbf{FB\Gamma}_{i,0}^{(2,1)} & \cdots & \mathbf{FB\Gamma}_{i,0}^{(M_t,1)} \\ \mathbf{FB\Gamma}_{i,0}^{(1,2)} & \ddots & \ddots & \mathbf{FB\Gamma}_{i,0}^{(M_t,2)} \\ \vdots & \ddots & \ddots & \vdots \\ \mathbf{FB\Gamma}_{i,0}^{(1,M_r)} & \cdots & \cdots & \mathbf{FB\Gamma}_{i,0}^{(M_t,M_r)} \end{pmatrix}, \tag{5.3}$$

where $\mathbf{A} \in C^{(K+L) \times K}$ and $\mathbf{B} \in C^{K \times (K+L)}$ are the CP insertion and removal matrices, respectively, $\mathbf{F} = \frac{1}{\sqrt{K}}\left(e^{-j2\pi\frac{nk}{K}}\right)_{k,n=0}^{K-1}$ is a normalized DFT matrix, and $\otimes$ is the Kronecker product.

For the primary link, the operation is the same as the scenario that the secondary link does not exist and the precoding and postcoding are conducted on each subcarrier [64]. Denote $\mathbf{s}_0[k] \in C^{d_0 \times 1}$ and $\mathbf{C}_0[k] \in C^{N_t \times d_0}$ as the source signal and the precoding matrix at the primary transmitter on the k-th subcarrier, respectively, where $d_0 \le \min\{N_t, N_r\}$ is the number of symbols transmitted on each subcarrier of the primary link. Then, the transmit signal vector at the primary transmitter on the k-th subcarrier, $\mathbf{x}_0[k] \in C^{N_t \times 1}$, after precoding

can be expressed as

$$\mathbf{x}_0[k] = \mathbf{C}_0[k]\mathbf{s}_0[k]. \tag{5.4}$$

Denote $\mathbf{H}_{0,0}[k] \in C^{N_r \times N_t}$ as the equivalent MIMO channel of the primary link on the k-th subcarrier, which can be expressed as

$$\mathbf{H}_{0,0}[k] = \begin{pmatrix} H_{0,0}^{(1,1)}[k] & \cdots & \cdots & H_{0,0}^{(N_t,1)}[k] \\ H_{0,0}^{(1,2)}[k] & \cdots & \cdots & H_{0,0}^{(N_t,2)}[k] \\ \vdots & \vdots & \ddots & \vdots \\ H_{0,0}^{(1,N_t)}[k] & \cdots & \cdots & H_{0,0}^{(N_t,N_r)}[k] \end{pmatrix}, \tag{5.5}$$

where $H_{0,0}^{(i,j)}[k]$ is the channel frequency response on the k-th subcarrier from the i-th transmit antenna to the j-th receive antenna of the primary link. Based on the property of OFDM transmission, $H_{0,0}^{(i,j)}[k] = \sum_{l=0}^{L} h_{0,0}^{(i,j)}[l]e^{\frac{-i2\pi kl}{K}}$. Denote SVD of $\mathbf{H}_{0,0}[k]$ as

$$\mathbf{H}_{0,0}[k] = \mathbf{U}_{0,0}[k]\mathbf{\Lambda}_{0,0}[k](\mathbf{V}_{0,0}[k])^{\mathrm{H}}, \tag{5.6}$$

where $\mathbf{U}_{0,0}[k] \in C^{N_r \times N_r}$ and $\mathbf{V}_{0,0}[k] \in C^{N_t \times N_t}$ are unitary matrices, and $\mathbf{\Lambda}_{0,0}[k] \in C^{N_r \times N_t}$ is a diagonal matrix with diagonal elements $(\lambda_{0,0,(1)}[k], \cdots, \lambda_{0,0,(\min\{N_t,N_r\})}[k])$ such that $|\lambda_{0,0,(1)}[k]|^2 \geq \cdots \geq |\lambda_{0,0,(\min\{N_t,N_r\})}[k]|^2$, where $\lambda_{0,0,(h)}[k]$ is the h-th singular values of $\mathbf{H}_{0,0}[k]$.

To maximize the data rate of the primary link, the precoding and postcoding matrices on the k-th subcarrier are used and can be expressed as

$$\mathbf{C}_0[k] = \mathbf{V}_{0,0}[k], \tag{5.7}$$

and

$$\mathbf{D}_0[k] = (\mathbf{U}_{0,0}[k])^{\mathrm{H}}, \tag{5.8}$$

respectively.

The precoding at the primary transmitter is done on each subcarrier while the transmit signal, $\mathbf{x}_0$ in (5.1), is constructed by the signal vectors on each transmit antenna. Denote $\mathbf{T}_t \in C^{N_t K \times N_t K}$ as a matrix to rearrange symbols on each subcarrier to a transmit stream one

each antenna, where its (i, j) entry is

$$
t_{i,j} = \begin{cases} 1 & j = \lfloor \frac{i-1}{K} \rfloor + ((i-1)_{modK})N_t + 1 \\ 0 & \text{others} \end{cases}.
$$
(5.9)

Then, we have

$$
\mathbf{x}_0 = \mathbf{T}_t \begin{pmatrix} \mathbf{x}_0[0] \\ \vdots \\ \mathbf{x}_0[K-1] \end{pmatrix}.
$$
(5.10)

Define the effective precoding matrix $\mathbf{C}_0 \in C^{N_t K \times K d_0}$ and the overall source symbol vector $\mathbf{s}_0 \in C^{K d_0 \times 1}$ at the primary transmitter as

$$
\mathbf{C}_0 = \begin{pmatrix} \mathbf{C}_0[0] & 0 & 0 & 0 \\ 0 & \mathbf{C}_0[1] & \cdots & 0 \\ \vdots & \vdots & \ddots & \vdots \\ 0 & \cdots & \cdots & \mathbf{C}_0[K-1] \end{pmatrix},
$$
(5.11)

and $\mathbf{s}_0 = \left((\mathbf{s}_0[0])^{\mathrm{T}} \quad (\mathbf{s}_0[1])^{\mathrm{T}} \quad \cdots \quad (\mathbf{s}_0[K-1])^{\mathrm{T}} \right)^{\mathrm{T}}$. Then, we have the transmit vector from the primary transmitter in (5.1) as

$$
\mathbf{x}_0 = \mathbf{T}_t \mathbf{C}_0 \mathbf{s}_0.
$$
(5.12)

At the primary receiver, the received signal $\mathbf{y}_0$ in (5.1) is first mapped from signal stream on each antenna to symbols on each subcarrier. The mapping matrix is denoted as $\mathbf{T}_r \in C^{N_r K \times N_r K}$, where its (i, j) entry is

$$
r_{i,j} = \begin{cases} 1 & j = \lfloor \frac{i-1}{N_r} \rfloor + ((i-1)_{modN_r})K + 1 \\ 0 & \text{others} \end{cases}.
$$
(5.13)

Then, the post-processed signal vector $\widehat{\mathbf{y}}_0 \in C^{K d_0 \times 1}$, can be expressed as

$$
\begin{aligned} \widehat{\mathbf{y}}_0 &= \mathbf{D}_0 \mathbf{T}_r \mathbf{y}_0 \\ &= \mathbf{D}_0 \mathbf{T}_r \left(\mathbf{H}_{0,0} \mathbf{x}_0 + \sum_{i=1}^{2M} \mathbf{H}_{i,0} \mathbf{x}_i + \mathbf{F} \mathbf{B} \mathbf{n}_0 \right), \end{aligned}
$$
(5.14)

50

where

$$\mathbf{D}_0 = \begin{pmatrix} \mathbf{D}_0[0] & 0 & 0 \\ \vdots & \ddots & \vdots \\ 0 & \cdots & \mathbf{D}_0[K-1] \end{pmatrix}. \tag{5.15}$$

Moreover, if water-filling power allocation is used at the primary transmitter, the power allocation matrix of the source signal from the primary transmitter, $\mathbf{P}_0 = E\{\mathbf{s}_0(\mathbf{s}_0)^H\}$, is a diagonal matrix with diagonal elements $(P_{0,(1)}[0], ..., P_{0,(d_0)}[0], ..., P_{0,(1)}[K-1], ..., P_{0,(d_0)}[K-1])$, where

$$P_{0,(h)}[k] = \left(\mu - \frac{\sigma^2}{(\lambda_{0,0,(h)}[k])^2}\right)^+, \tag{5.16}$$

where $(x)^+ = \max\{0, x\}$ and μ is chosen to satisfy the total power constraint $\sum_{k=0}^{K-1} \sum_{h=1}^{\min\{N_t, N_r\}} P_{0,(h)}[k] = P_{0,th}$, $P_{0,th}$ is the total power constraint at the primary transmitter.

5.1.2 Secondary System

As in Fig. 5.1, the transmit signal vector from the i-th SU is

$$\mathbf{x}_i = \mathbf{C}_i \mathbf{s}_i, \tag{5.17}$$

where $\mathbf{s}_i \in C^{d_i \times 1}$ is the information vector, $\mathbf{C}_i \in C^{M_t(K+L) \times d_i}$ is the precoding matrix and d_i is the number of symbols transmitted by the i-th SU to be determined later.

Like the primary receiver, SBSs discard L points and perform DFT. Then, the received signals after DFT at the SBS 1 and SBS 2 are

$$\mathbf{y}_1 = \sum_{i=1}^{M} \mathbf{H}_{i,1}\mathbf{x}_i + \sum_{i=M+1}^{2M} \mathbf{H}_{i,1}\mathbf{x}_i + \mathbf{H}_{0,1}\mathbf{x}_0 + (\mathbf{FB}) \otimes \mathbf{n}_1, \tag{5.18}$$

and

$$\mathbf{y}_2 = \sum_{i=M+1}^{2M} \mathbf{H}_{i,2}\mathbf{x}_i + \sum_{i=1}^{M} \mathbf{H}_{i,2}\mathbf{x}_i + \mathbf{H}_{0,2}\mathbf{x}_0 + (\mathbf{FB}) \otimes \mathbf{n}_2, \tag{5.19}$$

respectively. $\mathbf{H}_{i,j} \in C^{M_r K \times M_t(K+L)}$, for $i = 1, ..., 2M$, $j = 1, 2$, is the channel matrix from the i-th SU to the j-th SBS, which has the similar form as $\mathbf{H}_{i,0}$ in (5.3). The channel matrix from the primary transmitter, $\mathbf{H}_{0,j} \in C^{M_r K \times N_t K}$, has similar form as $\mathbf{H}_{0,0}$ in (5.2). In (5.18) and (5.19), the first term is the summation of the desired signals for the SBS, the second

term is the summation of the interference signals from the other cell, the third term is the interference from the PU, and the last term is the noise vector.

At each SBS, a receive beamforming matrix $\mathbf{W}_i \in C^{M_r K \times d_i}$ is conducted to decode the desired signals for the i-th SU. Then, the decoded signal vector for the i-th SU, $\mathbf{r}_i \in C^{d_i \times 1}$, can be expressed as

$$\mathbf{r}_i = \mathbf{W}_i^H \left(\sum_{i=1}^{2M} \mathbf{H}_{i,1} \mathbf{x}_i + \mathbf{H}_{0,1} \mathbf{x}_0 + (\mathbf{FB}) \otimes \mathbf{n}_1 \right), \tag{5.20}$$

for $i = 1, ..., M$, and

$$\mathbf{r}_i = \mathbf{W}_i^H \left(\sum_{i=1}^{2M} \mathbf{H}_{i,2} \mathbf{x}_i + \mathbf{H}_{0,2} \mathbf{x}_0 + (\mathbf{FB}) \otimes \mathbf{n}_2 \right), \tag{5.21}$$

for $i = M + 1, ..., 2M$.

We assume each SBS has accurate CSI about its own cell, interference channels to the other cell, interference channels to the primary receiver and primary power allocation results. As stated in [39], the required CSI can be obtained by using feedback channels [12] or learning mechanisms [13, 14]. Note that the PU power allocation results are not necessary here. Without it, our proposed algorithms still work, but the freedom available to the secondary system will decrease. Based on the CSI, SBSs determine precoding matrices for its served SUs. Once precoding matrices are determined, each SBS sends the effective interference channel information from its served SUs to the other SBS, to the other SBS. At last, SBSs determine receive beamforming and power allocation matrix for its served SUs. Each SU will get information about its own precoding and power allocation matrices from its SBS. In our study, we assume that each SBS requires no CSI for the channels in the other SU cell to reduce the amount of information exchange between two SBSs.

5.2   Signal Alignment

In this section, we will discuss the dimensions for SUs to generate interference-free transmission to the PU and to mitigate inter- and intra-cell interference within the secondary

system. Then, we will develop signal alignment schemes for the perfectly- and partially-aligned transmissions.

5.2.1 Dimension of Interference-Free Symbols

We will design the precoding matrices of the SUs to generate interference-free transmission to the PU. Based on the operations at the primary link, the interference signal at the primary receiver after the post-processing from the secondary transmitters from (5.1) and (5.17) will be

$$\widehat{\mathbf{I}} = \mathbf{D}_0\mathbf{T}_r \sum_{i=1}^{2M} \mathbf{H}_{i,0}\mathbf{x}_i = \mathbf{D}_0\mathbf{T}_r \sum_{i=1}^{2M} \mathbf{H}_{i,0}\mathbf{C}_i\mathbf{s}_i. \tag{5.22}$$

To guarantee interference-free transmission to the primary link for any information vector, $\mathbf{s}_i$, the transmitted signal of the i-th SU uses the nullspace of the the primary link as in [69]. The precoding matrix $\mathbf{C}_i$ should satisfy

$$\widetilde{\mathbf{H}}_{i,0}\mathbf{C}_i = \mathbf{0}, \tag{5.23}$$

where $\widetilde{\mathbf{H}}_{i,0}$ contains the rows of $\mathbf{D}_0\mathbf{T}_r\mathbf{H}_{i,0}$ with $P_{0,(h)}[k] \neq 0$ as in [39]. The dimension of the nullspace of $\widetilde{\mathbf{H}}_{i,0}$ is

$$\dim\left[\mathrm{null}(\widetilde{\mathbf{H}}_{i,0})\right] = M_t(K + L) - \bar{d}_0, \tag{5.24}$$

where

$$\bar{d}_0 = \sum_{k=0}^{K-1} \sum_{h=1}^{\min\{N_t,N_r\}} \mathbf{1}_{P_{0,(h)}[k]}, \tag{5.25}$$

and

$$\mathbf{1}_{\{P_{0,(h)}[k]\neq 0\}} = \begin{cases} 1 & P_{0,(h)}[k] \neq 0 \\ 0 & \text{else} \end{cases}. \tag{5.26}$$

Thus, we can always find a precoding matrix, $\mathbf{C}_i \in C^{M_t(K+L)\times d_i}$, to fulfill the interference-free constraint in (5.23) if the number of transmitted symbols from the i-th SU satisfies

$$d_i \leq M_t(K + L) - \bar{d}_0. \tag{5.27}$$

When the primary link has only one transmit and one receive antenna, and the SU has only one transmit antenna, i.e., $N_t = N_r = M_t = 1$, the number of symbols can be transmitted by each SU is $d_i = L$, which is the same as in [70].

Based on (5.23), the interference at the PU is eliminated after post-processing instead of eliminating interference directly in the received signal. To realize it, secondary link needs the information of the PU power allocation [39]. If the PU power allocation information is not accessible at the secondary link, interference-free transmission can only be achieved by satisfying

$$\mathbf{H}_{i,0}\mathbf{C}_i = \mathbf{0}, \tag{5.28}$$

where the dimension of the nullspace of $\mathbf{H}_{i,0}$ is $M_t(K + L) - M_rK$, which is smaller than the dimension in (5.24). Correspondingly, the nullspace for secondary link transmission is smaller. In the rest of this chapter, we focus on the scenario that the power allocation information of the PU is known at the secondary system. Similar procedure can be extended to the scenario when the PU power allocation information is unknown.

Besides interference to the PU, there exists interference within the secondary system. Next, we aim at mitigating interference within the secondary system while satisfying the interference-free constraint to the PU.

We start with the decoding capability of each SBS. From (5.3), the receive dimension of the channel matrix to SBSs is M_rK. Then, at each SBS, there are M_rK-dimensional subspace for signals from all SUs, including the desired and interference signals, as the traditional MIMO case [71]. Then, the total number of symbols can be decoded at each SBS is

$$d_r = M_rK, \tag{5.29}$$

which is called as the decoding capability of each SBS. To maximize the number of transmit symbols within the secondary system, inter-cell interference signals are aligned into lower dimensions, and thus, more dimensions are allowed for the desired signals [72]. Denote $\overline{d}_j$

as the dimension of the inter-cell interference signals at the j-th SBS. Then, the j-th SBS leaves $(M_r K - \bar{d}_j)$-dimensional space for the signals of SUs.

Due to interference-free constraint to the primary system and dimension constraints at all SUs and SBSs, interference signals can be perfectly- or partially-aligned or cannot be aligned at all.

5.2.1.1 Feasibility Condition

For the i-th SU, its precoding matrix, $\mathbf{C}_i \in C^{M_t(K+L) \times d_i}$, are divided into two submatrices: $\hat{\mathbf{C}}_i \in C^{M_t(K+L) \times \hat{d}_i}$ for aligned signals and $\check{\mathbf{C}} \in C^{M_t(K+L) \times \check{d}_i}$ for unaligned signals, where $\check{d}_i + \hat{d}_i = d_i$. Then, the precoding matrix can be expressed as

$$\mathbf{C}_i = \left(\hat{\mathbf{C}}_i, \check{\mathbf{C}}_i \right). \tag{5.30}$$

The interference signals at SBS 1 are from SUs in cell 2. From [73], to align these interference signals from cell 2, we must have

$$\text{span}(\mathbf{H}_{M+1,1} \hat{\mathbf{C}}_{M+1}) = ... = \text{span}(\mathbf{H}_{2M,1} \hat{\mathbf{C}}_{2M}), \tag{5.31}$$

where span($\cdot$) denotes the space spanned by the column vectors of a matrix. Denote $\bar{\mathbf{H}}_1$ as a aligned interference matrix at SBS 1, which implies the space spanned by the column vectors of $\bar{\mathbf{H}}_1$ is the aligned interference subspace at SBS 1. Therefore,

$$\text{span}(\bar{\mathbf{H}}_1) = \text{span}(\mathbf{H}_{i,1} \hat{\mathbf{C}}_i), \ i = M + 1, ..., 2M. \tag{5.32}$$

Based on Lemma 1 in [73], the aligned interference matrix satisfying (5.32) can be found through solving

$$\begin{pmatrix} -\mathbf{I} & \mathbf{H}_{(M+1),1} & \mathbf{0} & \cdots & \mathbf{0} \\ -\mathbf{I} & \mathbf{0} & \mathbf{H}_{(M+2),1} & \cdots & \mathbf{0} \\ \vdots & \vdots & \ddots & \ddots & \vdots \\ -\mathbf{I} & \mathbf{0} & \cdots & \cdots & \mathbf{H}_{(2M),1} \end{pmatrix} \begin{pmatrix} \bar{\mathbf{H}}_1 \\ \tilde{\mathbf{C}}_{M+1} \\ \vdots \\ \tilde{\mathbf{C}}_{2M} \end{pmatrix} = \mathbf{0}, \tag{5.33}$$

55

where the space spanned by the column vectors of $\tilde{\mathbf{C}}_i$ is the same as the space spanned by the corresponding aligned precoding submatrix, $\hat{\mathbf{C}}_i$.

Besides the alignment requirement, the interference-free constraint in (5.23) should be also satisfied. Then, the aligned interference matrix satisfying both the interference-free constraint in (5.23) and the alignment requirement in (5.32) can be found by

$$
\begin{pmatrix}
-\mathbf{I} & \mathbf{H}_{(M+1),1} & \mathbf{0} & \cdots & \mathbf{0} \\
-\mathbf{I} & \mathbf{0} & \mathbf{H}_{(M+2),1} & \cdots & \mathbf{0} \\
\vdots & \vdots & \ddots & \ddots & \vdots \\
-\mathbf{I} & \mathbf{0} & \cdots & \cdots & \mathbf{H}_{(2M),1} \\
\mathbf{0} & \widetilde{\mathbf{H}}_{(M+1),0} & \mathbf{0} & \cdots & \mathbf{0} \\
\mathbf{0} & \mathbf{0} & \widetilde{\mathbf{H}}_{(M+2),0} & \cdots & \mathbf{0} \\
\vdots & \ddots & \ddots & \ddots & \vdots \\
\mathbf{0} & \cdots & \cdots & \cdots & \widetilde{\mathbf{H}}_{(2M),0}
\end{pmatrix}
\begin{pmatrix}
\bar{\mathbf{H}}_1 \\
\tilde{\mathbf{C}}_{M+1} \\
\tilde{\mathbf{C}}_{M+2} \\
\vdots \\
\tilde{\mathbf{C}}_{2M}
\end{pmatrix} = \mathbf{0},
\tag{5.34}
$$

or $\mathbf{M}_1 \mathbf{T}_1 = \mathbf{0}$, where

$$
\mathbf{M}_1 =
\begin{pmatrix}
-\mathbf{I} & \mathbf{H}_{(M+1),1} & \mathbf{0} & \cdots & \mathbf{0} \\
-\mathbf{I} & \mathbf{0} & \mathbf{H}_{(M+2),1} & \cdots & \mathbf{0} \\
\vdots & \vdots & \ddots & \ddots & \vdots \\
-\mathbf{I} & \mathbf{0} & \cdots & \cdots & \mathbf{H}_{(2M),1} \\
\mathbf{0} & \widetilde{\mathbf{H}}_{(M+1),0} & \mathbf{0} & \cdots & \mathbf{0} \\
\mathbf{0} & \mathbf{0} & \widetilde{\mathbf{H}}_{(M+2),0} & \cdots & \mathbf{0} \\
\vdots & \ddots & \ddots & \ddots & \vdots \\
\mathbf{0} & \cdots & \cdots & \cdots & \widetilde{\mathbf{H}}_{(2M),0}
\end{pmatrix}
\tag{5.35}
$$

and

$$\mathbf{T}_1 = \begin{pmatrix} \bar{\mathbf{H}}_1 \\ \tilde{\mathbf{C}}_{M+1} \\ \tilde{\mathbf{C}}_{M+2} \\ \vdots \\ \tilde{\mathbf{C}}_{2M} \end{pmatrix}. \tag{5.36}$$

Then, the aligned precoding submatrices, $\hat{\mathbf{C}}_i$ ($i = M + 1, ..., 2M$), can be determined based on $\tilde{\mathbf{C}}_i$. The detail will be provided in the precoding matrix design part. In (5.35), $\mathbf{M}_1$ is a $(MM_rK + M\bar{d}_0) \times (MM_t(K + L) + M_rK)$ matrix. For (5.34) to have solution, we must have $MM_rK + M\bar{d}_0 < (MM_t(K + L) + M_rK)$ or

$$m = MM_t(K + L) + M_rK(1 - M) - M\bar{d}_0 > 0, \tag{5.37}$$

which is called as the feasibility condition for SUs in cell 2. It is also the feasibility condition for SUs in cell 1, where $\bar{\mathbf{H}}_2$, $\tilde{\mathbf{C}}_i$ ($i = 1, ..., M$) are similarly defined and their constraints can be found similar to (5.34).

When the feasibility condition in (5.37) is satisfied, perfect- and partially-aligned transmissions will be discussed separately. Otherwise, it is unaligned transmission.

5.2.1.2 Unaligned Transmission ($m = MM_t(K + L) + M_rK(1 - M) - M\bar{d}_0 \leq 0$)

If the feasibility condition in (5.37) is violated, signal alignment cannot be achieved, which corresponds to the unaligned transmission. If the transmitted signals from each SU are all spatially independent, the dimension of the interference signals at SBS 1 will be $\bar{d}_1 = \sum_{i=M+1}^{2M} d_i$. The dimension of the desired and interference signals at SBS 1 is $\sum_{i=1}^{2M} d_i$. Similarly, the dimension of the interference signals at SBS 2 will be $\bar{d}_2 = \sum_{i=1}^{M} d_i$ and the total dimension of the desired and interference signals is $\sum_{i=1}^{2M} d_i$. Then, based on the decoding capacity of each SBS in (5.29), the total dimension of the desired and interference signals at each SBS should have

$$\sum_{i=1}^{2M} d_i \leq M_rK. \tag{5.38}$$

57

When the numbers of symbols transmitted by SUs are the same, i.e., $d = d_i$, we have

$$d \leq \frac{M_r K}{2M}. \tag{5.39}$$

If the interference-free constraint in (5.27), i.e., $d_i \leq M_t(K + L) - \bar{d}_0$, is also considered, the maximal number of symbols can be transmitted by each SU for the unaligned transmission will be

$$d = \left(\min\left\{ \frac{M_r K}{2M}, M_t(K + L) - \bar{d}_0 \right\} \right)^+. \tag{5.40}$$

Without loss of generality, we will focus on the scenario that the number of symbols transmitted by each SUs is the same, i.e., $d_1 = d_2 = d_3 = d_4 = d$, in the rest of the chapter.

5.2.1.3 *Perfectly-Aligned Transmission ($m = MM_t(K + L) + M_r K(1 - M) - M\bar{d}_0 \geq d > 0$)*

If the number of symbols transmitted by each SU, d, is less than the dimension of the nullspace of $\mathbf{M}_1$ in (5.35), m, i.e., $d \leq m$ we can find a d-dimensional solution for the aligned precoding submatrix, $\hat{\mathbf{C}}_i$, satisfying both interference-free constraint in (5.23) and the alignment requirement in (5.32) through solving (5.34) and set the precoding matrix for the i-th SU as

$$\mathbf{C}_i = \hat{\mathbf{C}}_i \tag{5.41}$$

to minimize the dimension of the interference subspace at each SBS. In this case, if the transmitted signals from SUs are all spatially independent, there will be d-dimensional interference signals and $2d$-dimensional desired signals at each SBS. Based on the decoding capability at each SBS in (5.29), the total dimension of the desired and interference signals should have

$$(M + 1)d \leq M_r K. \tag{5.42}$$

Thus, maximal number of symbols can be transmitted by each SU is

$$d = \frac{M_r K}{M + 1}. \tag{5.43}$$

Since the condition for this perfectly-aligned transmission is the number of symbols transmitted by each SU, d, is less than the dimension of the nullspace of $\mathbf{M}_i$, m, we should have

$$d = \frac{M_r K}{M + 1} \le m = MM_t(K + L) + M_r K(1 - M) - M\bar{d}_0, \tag{5.44}$$

which is equivalent to

$$KMM_r + (1 + M)\bar{d}_0 \le (M + 1)(K + L)M_t, \tag{5.45}$$

5.2.1.4 Partially-Aligned Transmission ($0 < m = MM_t(K + L) + M_r K(1 - M) - M\bar{d}_0 < d$)

By the interference-free constraint and the alignment constraint, it is possible that the number of symbols transmitted by each SU, d, is larger than the dimension of the nullspace of $\mathbf{M}_i$ in (5.35), m, i.e., $d > m$. In this case, the precoding matrix for each SU is constructed by a m-dimensional aligned submatrix $\hat{\mathbf{C}}_i$ and a $(d - m)$-dimensional unaligned submatrix, $\check{\mathbf{C}}_i$. In this case, there will be $[Md - (M - 1)m]$-dimensional interference signals at each SBSs, which contains m-dimensional aligned interference signals from the other cell and $(d - m)$-dimensional unaligned interference signals from each SU in the other cell. Moreover, there are Md-dimensional desired signals from SUs of its own cell. Then, based on the decoding capability of each SBS in (5.29), we should have

$$2Md - (M - 1)m \le M_r K. \tag{5.46}$$

Substitute (5.37) into (5.46), the maximal number of symbols that can be transmitted will be

$$d = \frac{(M - 1)(K + L)M_t + K(2 - M)M_r - (M - 1)\bar{d}_0}{2}. \tag{5.47}$$

Since the condition that this partially-aligned transmission occurs is the number of symbols transmitted by each SU, d, is larger than the dimension of the nullspace of $\mathbf{M}_i$ in (5.35), m, we should have

$$KMM_r + (1 + M)\bar{d}_0 > (M + 1)(K + L)M_t, \tag{5.48}$$

$$d = \begin{cases} \min\left\{\frac{M_r K}{2M}, M_t(K+L) - \bar{d}_0\right\}, & \text{if } MM_t(K+L) + M_r K(1-M) - M\bar{d}_0 < 0 \\ \frac{M_r K}{M+1}, & \text{if } KMM_r + (1+M)\bar{d}_0 \leq (M+1)(K+L)M_t \\ \frac{(M-1)(K+L)M_t + K(2-M)M_r - (M-1)\bar{d}_0}{2}, & \text{otherwise} \end{cases}$$

$$(5.49)$$

which is the opposite condition of (5.45).

In brief, the maximal number of interference-free symbols can be transmitted by each SU is in (5.49) at the top of next page, where the first, the second, and the third lines correspond to the unaligned, the perfectly- and the partially-aligned transmission, respectively.

Till now, we have discussed the number of interference-free symbols that can be transmitted by each SU. Before we discuss the precoding matrix design in detail in Section IV, the receive beamforming matrix design will be briefly discussed here.

5.2.2 Signal Detection at SBSs

At SBSs, the receive beamforming matrix for SU i, $\mathbf{W}_i \in C^{M_r K \times d}$, is used to decode the desired signals from the i-th SU while eliminating interference signals from other SUs, including intra- and inter-cell interference signals. We use *zero-forcing* (ZF) receive beamforming for simplicity even through the other types of beamforming, such as *minimum mean-square error* (MMSE) one can be similarly designed. From (5.20), for the ZF beamforming for SU i in cell 1, we require

$$\mathbf{W}_i^H \sum_{j=1, j \neq i}^{2M} \mathbf{H}_{j,1}\mathbf{C}_j\mathbf{x}_j = \mathbf{0}. \tag{5.50}$$

Denote $\hat{\mathbf{I}}_i$ and $\check{\mathbf{I}}_i$ as the intra- and inter-cell interference matrices, defined as

$$\hat{\mathbf{I}}_i = (\mathbf{H}_{i,1}\mathbf{C}_1,.., \mathbf{H}_{i-1,1}\mathbf{C}_{i-1}, \mathbf{H}_{i+1,1}\mathbf{C}_{i+1}, ..., \mathbf{H}_{M,1}\mathbf{C}_M), \tag{5.51}$$

and

$$\check{\mathbf{I}}_i = (\mathbf{H}_{M+1,1}\mathbf{C}_{M+1}, ..., \mathbf{H}_{2M,1}\mathbf{C}_{2M}), \tag{5.52}$$

respectively. Then, we require

$$\mathbf{W}_i \subseteq \text{null}\left(\hat{\mathbf{I}}_i^H, \check{\mathbf{I}}_i^H\right). \tag{5.53}$$

For the perfectly-aligned transmission, the precoding matrix is $\mathbf{C}_i = \hat{\mathbf{C}}_i$ from (5.41) and it satisfies the alignment requirement $\text{span}(\bar{\mathbf{H}}_1) = \text{span}(\mathbf{H}_{j,1}\hat{\mathbf{C}}_j)$ ($j = M + 1, ..., 2M$) from (5.32). Then, we have

$$\begin{aligned}
\mathbf{W}_i &\subseteq \text{null}\left(\hat{\mathbf{I}}_i^H, \check{\mathbf{I}}_i^H\right) \\
&= \text{null}\left((\mathbf{H}_{1,1}, ..., \mathbf{H}_{i-1,1}, \mathbf{H}_{i+1,1}, ..., \mathbf{H}_{M,1}, \bar{\mathbf{H}}_1)^H\right).
\end{aligned} \tag{5.54}$$

The size of the combined intra- and inter-cell interference matrix $(\mathbf{H}_{M+1,1}, ..., \mathbf{H}_{2M,1}, \bar{\mathbf{H}}_1)$ is $M_r K \times Md$. Based on (5.49), we can always find a d-dimensional solution for $\mathbf{W}_i$.

For the partially-aligned transmission, we have

$$\begin{aligned}
\mathbf{W}_i \quad \subseteq \quad & \text{null}\left(\hat{\mathbf{I}}_i^H, \check{\mathbf{I}}_i^H\right) \\
= \quad & \text{null}\left((\mathbf{H}_{1,1}, ..., \mathbf{H}_{i-1,1}, \mathbf{H}_{i+1,1}, ..., \mathbf{H}_{M,1}, \right. \\
& \left. \mathbf{H}_{M+1,1}\check{\mathbf{C}}_{M+1}, ..., \mathbf{H}_{2M,1}\check{\mathbf{C}}_{2M}, \bar{\mathbf{H}}_1)^H\right),
\end{aligned} \tag{5.55}$$

where (5.32) is used for the second equality. The sizes of the intra-cell interference matrix, $(\mathbf{H}_{1,1}, ..., \mathbf{H}_{i-1,1}, \mathbf{H}_{i+1,1}, ..., \mathbf{H}_{M,1})$, the unaligned inter-cell interference matrices, $(\mathbf{H}_{M+1,1}\check{\mathbf{C}}_{M+1}, ..., \mathbf{H}_{2M,1}\check{\mathbf{C}}_{2M})$, and the aligned inter-cell interference matrix, $\bar{\mathbf{H}}_1$, are $M_r K \times (M - 1)d$, $M_r K \times M(d - m)$, and $M_r K \times m$, respectively. Based on (5.49), we can always find a d-dimensional solution for $\mathbf{W}_i$.

Thus, the receive beamforming matrix, $\mathbf{W}_i$ for SU i, can be designed for both perfectly- and partially-aligned transmissions. Similarly, we can determine the receive beamforming matrices for other SUs. Moreover, similar design can be used for the unaligned transmission and we skip the detail here.

5.3 Precoding Matrix Design

In this section, we will first focus on the precoding matrix design for the perfectly- and partially-aligned transmission, respectively, and then briefly discuss power allocation.

5.3.1 Perfectly-Aligned Transmission

For the perfectly-aligned transmission, the precoding matrix is constructed by the aligned submatrix only, i.e., $\mathbf{C}_i = \hat{\mathbf{C}}_i$ from (5.41). To determine the precoding matrix $\mathbf{C}_i$, we denote SVD of $\mathbf{M}_i$ from (5.35) as $\mathbf{M}_i = \mathbf{U}_i\mathbf{D}_i\mathbf{V}_i^H$, where $\mathbf{U}_i$ and $\mathbf{V}_i$ are unitary matrices, $\mathbf{D}_i$ is a diagonal matrix with $\mathbf{M}_i$'s singular values as its diagonal elements as $\left(\lambda_1^{(i)}, ..., \lambda_{MM_rK+M\bar{d}_0}^{(i)}\right)$ such that $(|\lambda_1^{(i)}|)^2 \geq ... \geq (|\lambda_{MM_rK+M\bar{d}_0}^{(i)}|)^2$. Then, the nullspace of $\mathbf{M}_i$ from (5.35) can be expressed as

$$\mathbf{N}_i = \left(\begin{array}{ccc} \mathbf{v}_{MM_rK+M\bar{d}_0+1}^{(i)} & \cdots & \mathbf{v}_{MM_t(K+L)+M_rK}^{(i)} \end{array} \right), \tag{5.56}$$

where $\mathbf{v}_k^{(i)}$ is the k-th column of $\mathbf{V}_i$.

Next, we discuss the precoding matrix design for two cases: (1) the number of symbols transmitted by each SU equals to the dimension of the nullspace of $\mathbf{M}_i$ in (5.35), i.e., $d = m$; (2) the number of symbols transmitted by each SU is fewer than to the dimension of the nullspace of $\mathbf{M}_i$, i.e., $d < m$.

5.3.1.1 $m = d$

When the dimension of the nullspace of $\mathbf{M}_i$ from (5.35) equals to the number of symbols that transmitted by each SU, i.e., $d = m$, all the columns of $\mathbf{N}_i$ from (5.56) will be used to construct precoding matrices.

Let the solution for (5.34) be

$$\tilde{\mathbf{C}}_i = \left(\begin{array}{c} \mathbf{n}_{M_rK+(i-M-1)M_t(K+L)+1}^{(1)} \\ \vdots \\ \mathbf{n}_{M_rK+(i-M)M_t(K+L)}^{(1)} \end{array} \right), \tag{5.57}$$

where $\mathbf{n}_k^{(i)} \in C^{1\times d}$ is the k-th row of $\mathbf{N}_i$. Then, the precoding matrices for SUs i ($i = M + 1, ..., 2M$) can be set as

$$\mathbf{C}_i = \text{orth}(\tilde{\mathbf{C}}_i), \tag{5.58}$$

where $\text{orth}(\mathbf{X})$ denotes the orthonomal subspace of $\mathbf{X}$. Similarly, we can find $\mathbf{C}_i$ ($i = 1, ..., M$) based on $\mathbf{N}_2$.

5.3.1.2 $m > d$

When the dimension of the nullspace of $\mathbf{M}_i$ from (5.35) is larger than the number of symbols transmitted by each SU, i.e., $m > d$, we need to choose d-dimensional subspace from m-dimensional subspace spanned by the column vectors of $\mathbf{N}_i$ from (5.56) to construct precoding matrices. Since $\mathbf{N}_i$ is constructed by uncorrelated unitary vectors $\mathbf{v}_k^{(i)}$, we can decide the subspace by choosing d vectors from all column vectors of $\mathbf{N}_i$.

Based on the assumption in Section 5.1 that the information about the inter-cell interference signals is unknown at the precoding matrix design stage, we choose the vectors that can minimize intra-cell interference among SUs in the same cell. Intra-cell and inter-cell interference can be considered jointly to determine precoding matrices, which requires global CSI at SBSs or iterative operations as in [74] and is beyond the scope of this chapter.

For the i-th SU, since the ZF beamforming is used at the receiver, maximizing the distance of the signal subspace spanned by the column vector of signal matrices from other SUs in the same cell is beneficial for minimizing the intra-cell interference based on the similar idea in [75, 74]. Here, chordal distance is used as a metric to measure the distance between two subspaces spanned by the corresponding signal matrices. The chordal distance between matrices $\mathbf{A}$ and $\mathbf{B}$ is defined as [75]

$$d_c(\mathbf{A}, \mathbf{B}) = \|\text{orth}(\mathbf{A})\text{orth}(\mathbf{A})^H - \text{orth}(\mathbf{B})\text{orth}(\mathbf{B})^H\|_F. \tag{5.59}$$

Based on the chordal distance, we can determine a d-dimensional subspace that maximizes the distance of the signal subspaces from different SUs at the intended SBS, where the subspace is spanned by the column vectors of the corresponding signal matrix.

Exhaustive Search Algorithm: One way to determine a d-dimensional subspace that maximizes the distance of the signal subspaces from different SUs at the intended SBS is exhaustive search. The detailed procedure is as follows. We take the precoding matrix design for SUs in cell 1 as example. Each time, we choose d vectors from m column vectors of $\mathbf{N}_2$ from (5.56). There are $N = \binom{d}{m}$ combinations. Denote a length d vector $\mathbf{p}_k$ as the positions of column vectors from $\mathbf{N}_2$ for the k-th combination. Denote $\widetilde{\mathbf{N}}_{k,2}$ as a matrix

constructed by the column vectors of $\mathbf{N}_2$ defined by $\mathbf{p}_k$. For instance, if $d = 2$, $m = 3$, then $N = \binom{2}{3} = 3$, and $\mathbf{p}_1 = (1, 2)$, $\mathbf{p}_2 = (1, 3)$ and $\mathbf{p}_3 = (2, 3)$, $\widetilde{\mathbf{N}}_{1,2}$, $\widetilde{\mathbf{N}}_{2,2}$, and $\widetilde{\mathbf{N}}_{3,2}$ consist of the first and second columns, the first and third columns, and the second and third columns of $\mathbf{N}_2$, respectively.

Then, using $\widetilde{\mathbf{N}}_{k,2}$ instead of $\mathbf{N}_2$, we define $\mathbf{C}_{i,k}$ following (5.57) for the case with $m = d$. Then, the corresponding distance between the signal matrices corresponding to SU i and j in cell 1 is

$$d_1^g(k, i, j) = d_c\left(\mathbf{H}_{e,i}(k), \mathbf{H}_{e,j}(k)\right), \tag{5.60}$$

where $\mathbf{H}_{e,i}(k)$ and $\mathbf{H}_{e,j}(k)$ are effective channel matrices for SUs i and j, respectively, defined as

$$\mathbf{H}_{e,i}(k) = \mathbf{H}_{i,1}\mathbf{C}_{i,k}, \tag{5.61}$$

for $i = 1, ..., M$.

Then, the distance between the signal matrices corresponding to SUs in cell 1 is the minimal chordal distance among any two SUs in cell 1, which can be expressed as

$$d_1^g(k) = \min_{i,j} d_1^g(k, i, j). \tag{5.62}$$

To maximize the distance between signal matrices, we choose the k_1^*-th combination for cell 1 as

$$k_1^* = \arg\max_k d_1^g(k). \tag{5.63}$$

Then, the precoding matrices for SUs in cell 1 are determined as

$$\mathbf{C}_i = \mathbf{C}_{i,k_1^*}. \tag{5.64}$$

The complexity of the exhaustive search algorithm will increase quickly with the number of antennas at SUs and SBS, the number of subcarriers, K, and the length of CP, L. To decrease the computational complexity, we develop a heuristic algorithm.

Heuristic Algorithm: Instead of considering all possible combinations of columns of $\mathbf{N}_i$ from (5.56) as for the exhaustive search algorithm, the heuristic algorithm considers one column of $\mathbf{N}_i$ each time. For each column of $\mathbf{N}_i$, one-dimensional precoding vector is determined. Then, the distance between the effective signal vectors at the intended SBS from SUs in the same cell is calculated. At last, we choose d vectors that provide the largest d distance values.

The detailed procedure is summarized in Table 5.1 and the main calculation is as follows. From (5.56), the k-th column vector of $\mathbf{N}_2$ is $\mathbf{v}^{(2)}_{MM_rK+M\bar{d}_0+k}$. Using $\mathbf{v}^{(2)}_{MM_rK+M\bar{d}_0+k}$ instead of $\mathbf{N}_2$, we define $\mathbf{c}_{i,k} \in C^{M_t(K+L)\times 1}$ following (5.57) for the case with $m = d$. Then, the distance of the effective signal vectors at SBS 1 is the minimal distance between any two SUs as

$$d_1^h(k) = \min_{i,j}(d_1^h(k, i, j)), \ k = 1, ..., m. \tag{5.65}$$

where

$$d_1^h(k, i, j) = d_c(\mathbf{H}_{i,1}\mathbf{c}_{i,k}, \mathbf{H}_{j,1}\mathbf{c}_{j,k}). \tag{5.66}$$

At last, we choose d positions that provide the largest d values of $d_1^h(k)$.

For the exhaustive search algorithm, we need to calculate all $\binom{2}{M}\binom{d}{m}$ distance values while only $\binom{2}{M}m$ distance values are calculated for the heuristic algorithm. The computational complexity decreases dramatically.

5.3.2 Partially-Aligned Transmission

For the partially-aligned transmission, we have $d > m$ from Section 5.2.1.4. Then, the precoding matrix, $\mathbf{C}_i$, will be constructed by two submatrices, the aligned submatrix, $\hat{\mathbf{C}}_i$, and the unaligned submatrix, $\check{\mathbf{C}}_i$, as defined in (5.30). The design for the aligned submatrix, $\hat{\mathbf{C}}_i$, is the same as the case with $m = d$ in the perfectly-aligned transmission. We will focus on the unaligned submatrix design here.

The unaligned submatrix, $\check{\mathbf{C}}_i$, should satisfies two constraints: the interference-free constraint in (5.23), $\widetilde{\mathbf{H}}_{i,0}\check{\mathbf{C}}_i = \mathbf{0}$, and orthogonal to the aligned submatrix $\hat{\mathbf{C}}_i$. From [76], the

Table 5.1. Heuristic Algorithm for the Perfectly-Aligned Transmission

1: Find the null space of $\mathbf{M}_1$, denoted as $\mathbf{N}_1 = \text{null}(\mathbf{M}_1)$.

2: **for** $k = 1 : m$ **do**

3:    **for** $i = 1 : M - 1$ **do**

4:       **for** $j = i + 1 : M$ **do**

5:          Calculate
$$d_1^h(k, i, j) = d_c(\mathbf{H}_{i,1}\mathbf{c}_{i,k}, \mathbf{H}_{j,1}\mathbf{c}_{j,k}),$$
         where $\mathbf{c}_{i,k}$ and $\mathbf{c}_{j,k}$ are defined by the k-th column of $\mathbf{N}_1$.

6:       **end for**

7:    **end for**

8:    Define the distance of the k-th column, $d_1^h(k)$, is the minimal value of $d_1^h(k, i, j)$, expressed as
$$d_1^h(k) = \min_{i,j}(d_1^h(k, i, j))$$

9: **end for**

10: Find d largest values of $d_1^h(k)$, record the corresponding column positions in $\mathcal{K}$.

11: Use the columns of $\mathbf{N}_1$ defined in $\mathcal{K}$ to construct precoding matrices.

---

orthogonal complement subspace of the subspace spanned by the column vectors of the aligned precoding submatrix, $\hat{\mathbf{C}}_i$, in the nullspace of the interference channel from the i-th SU to the primary receiver, $\widetilde{\mathbf{H}}_{i,0}$, satisfies both constraints. Denote the orthonomal bases of the nullspace of $\widetilde{\mathbf{H}}_{i,0}$ as $\mathbf{A}_i = \text{orth}(\text{null}(\widetilde{\mathbf{H}}_{i,0}))$. Since the subspace spanned by the column vectors of the aligned precoding submatrix, $\hat{\mathbf{C}}_i$, is a subspace of $\mathbf{A}_i$, the former one can be expressed as the linear combination of the latter one, expressed as $\hat{\mathbf{C}}_i = \mathbf{A}_i\mathbf{U}_1$, where $\mathbf{U}_1$ is the linear transformation matrix from $\mathbf{A}_i$ to $\hat{\mathbf{C}}_i$. Then, $\mathbf{U}_1 = \mathbf{A}_i^H\hat{\mathbf{C}}_i$. The orthogonal complement of the aligned precoding submatrix, $\hat{\mathbf{C}}_i$, in $\mathbf{A}_i$ can be found as

$$\hat{\mathbf{C}}_i^{\perp} = \mathbf{A}_i\mathbf{U}_1^{\perp}, \tag{5.67}$$

where $\mathbf{U}_1^{\perp}$ spans the orthogonal complement subspace of $\mathbf{U}_1$, found as $\mathbf{U}_1^{\perp} = \text{null}(\mathbf{U}_1^T)$.

By the construction, the size of the orthogonal complement subspace of the aligned precoding submatrix, $\hat{\mathbf{C}}_i^{\perp}$, is $M_t(K + L) \times (M_t(K + L) - \bar{d}_0 - m)$ and its column vectors are linearly independent [76]. It is obvious that $d - m < M_t(K + L) - \bar{d}_0 - m$ from (5.27), and thus, we need to choose $(d - m)$-dimensional subspace from the subspace spanned by the column vectors of $\hat{\mathbf{C}}_i^{\perp}$ to construct precoding matrices as similar as the perfectly-aligned

transmission. We still choose the subspace that maximizes the chordal distance between signals from SUs in the same cell at the intended SBS. Similar to perfectly-aligned case, we can have an exhaustive search and a heuristic algorithm.

5.3.2.1 Exhaustive Search Algorithm

Again, the first method is exhaustive search. For the partially-aligned transmission, the orthogonal complement subspace of the aligned precoding submatrix, $\hat{\mathbf{C}}_i^\perp$, are independent for each SU since the nullspace of the interference channel from the i-th SU to the primary receiver, $\mathbf{A}_i$, are independent [73]. This is different from the case for determining $\hat{\mathbf{C}}_i$, where $\hat{\mathbf{C}}_i$ are under alignment constraints. Since $\hat{\mathbf{C}}_i^\perp$ for different SUs are independent, the i-th SU can choose $(d-m)$ columns from $\hat{\mathbf{C}}_i^\perp$ independently. For the i-th SU, there are $N_i = \binom{d-m}{M_t(K+L)-\bar{d}_0-m}$ combinations. Since there are M SUs, we need to compare $N = N_i^M$ distance values. Similar to the perfectly-aligned transmission, denote $\mathbf{p}_{k,i}$ and $\mathbf{p}_{k,j}$ to be the position vectors for the i-th and j-th SU in the k-th combination, respectively. Then, the distance for the k-th combination, d_1^g, is defined as in (5.62), where the precoding matrix for SU i for the k-th combination are expressed as $\mathbf{C}_i = (\hat{\mathbf{C}}_i, \hat{\mathbf{C}}_{i,k}^\perp)$, where $\hat{\mathbf{C}}_{i,k}^\perp$ is constructed by the column vectors of $\hat{\mathbf{C}}_i^\perp$ defined by $\mathbf{p}_{k,i}$. At last, the k^*-th combination with the largest chordal distance will be chosen and the precoding matrices are defined accordingly.

5.3.2.2 Heuristic Algorithm

The heuristic algorithm for the perfectly-aligned transmission can be also extended here. For this algorithm, each SU will determine its precoding matrix independently by choosing $(d-m)$-dimensional subspace that has maximal minimum distance to the others. Denote the k-th column of $\hat{\mathbf{C}}_i^\perp$ as $\hat{\mathbf{c}}_{i,k}^\perp$. For the k-th column, the distance of the i-th SU is defined as the minimal distance from the i-th SU's signal space to other SU's signal spaces in the same cell. At last, we choose $(d-m)$ columns that provide $(d-m)$ largest values of distance. The detailed procedure of the heuristic algorithm is shown in Table 5.2.

Table 5.2. Heuristic Algorithm for the Partially-Aligned Transmission

1: Calculate $\hat{\mathbf{C}}_i$ for each SU based on the null space of $\mathbf{M}_1$.

2: Determine the orthogonal complement subspaces of $\hat{\mathbf{C}}_i$ in the nullspace of $\widetilde{\mathbf{H}}_{i,0}$, denoted as $\hat{\mathbf{C}}_i^{\perp}$.

3: **for** $i = 1 : M$ **do**

4:     **for** $k = 1 : M_t(K + L) - \bar{d}_0 - m$ **do**

5:       **for** $j \neq i$ **do**

6:         **for** $t = 1 : M_t(K + L) - K - m$ **do**

7:           Calculate the distance between the signal from the i-th SU and the j-th SU based on the k-th column of $\hat{\mathbf{C}}_i^{\perp}$ and the t-th column of $\hat{\mathbf{C}}_j^{\perp}$, expressed as

$$d_1^h(i, k, j, t) = d_c(\mathbf{H}_{i,1}\hat{\mathbf{c}}_{i,k}^{\perp}, \mathbf{H}_{j,1}\hat{\mathbf{c}}_{j,t}^{\perp}) \qquad (5.68)$$

8:         **end for**

9:       **end for**

10:     Define the distance of the i-th SU to other SUs based on the k-th column of $\hat{\mathbf{C}}_i^{\perp}$ as the minimal distance from the i-th SU to other SUs, expressed as

$$d_1^h(i, k) = \min_{j,t} d_1^h(i, k, j, t). \qquad (5.69)$$

11:     **end for**

12:     Find $(d - m)$ largest values of $d_1^h(i, k)$, record the corresponding column positions in $\mathcal{K}_i$.

13:     Use the columns of $\hat{\mathbf{C}}_i^{\perp}$ defined in $\mathcal{K}_i$ and $\hat{\mathbf{C}}_i$ to construct precoding matrices.

14: **end for**

5.3.3 Power Allocation

In this part, we will discuss the power allocation for each SU. For the i-th SU, the power allocation matrix is expressed as

$$\mathbf{P}_i = E[\mathbf{s}_i \mathbf{s}_i^H]. \tag{5.70}$$

We focus on cell 1 here for simplicity. Based on the ZF receive beamforming in (5.50), the intra- and inter-cell interference within the secondary system will be eliminated, the decoded signal vector in (5.20) can be expressed as

$$\mathbf{r}_i = \mathbf{W}_i^H \left(\mathbf{H}_{i,1} \mathbf{x}_i + \mathbf{H}_{0,1} \mathbf{x}_0 + (\mathbf{FB}) \otimes \mathbf{n}_1 \right). \tag{5.71}$$

That means, after receive beamforming, the transmission is equivalent to a point-to-point transmission from the i-th SU to the SBS with interference from the primary transmitter and additive noise. The interference-plus-noise at the i-th SU as

$$\mathbf{I}_i = \mathbf{W}_i^H (\mathbf{H}_{0,1} \mathbf{x}_0 + (\mathbf{FB}) \otimes \mathbf{n}_1). \tag{5.72}$$

Denote $\mathbf{D}_i$ as the post-processing matrix for the i-th SU after receive beamforming. To maximize the transmission rate, a whitening post-processing matrix is used [39], expressed as $\mathbf{D}_i = \mathbf{Q}_i^{-\frac{1}{2}}$, where $\mathbf{Q}_i$ is the covariance matrix of the interference-plus-noise signal, expressed as $\mathbf{Q}_i = E\left[\mathbf{I}_i \mathbf{I}_i^H \right]$. Then, the achievable transmission rate for the i-th SU given power allocation matrix $\mathbf{P}_i$ will be

$$
\begin{aligned}
&R_i(\mathbf{P}_i) \\
&= \frac{1}{K+L} \log_2 |\mathbf{I} + \mathbf{Q}_i^{-\frac{1}{2}} \mathbf{W}_i^H \mathbf{H}_{i,1} \mathbf{C}_i \mathbf{P}_i \left(\mathbf{D}_i \mathbf{W}_i^H \mathbf{H}_{i,1} \mathbf{C}_i \right)^H \mathbf{Q}_i^{-\frac{1}{2}}|.
\end{aligned}
\tag{5.73}
$$

Note that, to get the rate in (5.73), another post-processing matrix based on the SVD of the effective channel matrix $\mathbf{Q}_i^{-\frac{1}{2}} \mathbf{W}_i^H \mathbf{H}_{i,1} \mathbf{C}_i$ is needed followed by the whitening matrix $\mathbf{D}_i$. Next, we discuss two different power allocation schemes.

$$\max_{\mathbf{P}_i} \ R_i(\mathbf{P}_i) = \frac{1}{K+L} \log_2 |\mathbf{I} + \mathbf{Q}_i^{-\frac{1}{2}} \mathbf{W}_i^H \mathbf{H}_{i,1} \mathbf{C}_i \mathbf{P}_i \left(\mathbf{D}_i \mathbf{W}_i^H \mathbf{H}_{i,1} \mathbf{C}_i \right)^H \mathbf{Q}_i^{-\frac{1}{2}}| \tag{5.75a}$$

$$s.t. \ \text{Trace} \left\{ \mathbf{C}_i \mathbf{P}_i (\mathbf{C}_i)^H \right\} \leq (K+L) p_{max}. \tag{5.75b}$$

5.3.3.1 Equal Power Allocation

When equal power allocation scheme is used, the SUs uniformly allocate its total power on each transmit symbols. Then, the power allocation matrix $\mathbf{P}_i$ can be expressed as

$$\mathbf{P}_i = \frac{p_{max}(K+L)}{\text{Trace}\left(\mathbf{C}_i \mathbf{C}_i^H\right)} \mathbf{I} = \frac{p_{max}(K+L)}{d} \mathbf{I}, \tag{5.74}$$

where p_{max} is the peak power constraint for each SU.

5.3.3.2 Optimal Power Allocation

The optimal power allocation scheme for the i-th SU is designed to maximize its transmission rate given the total power constraint. Then, the problem can be formulated as in (5.75) at the top of the next page. Followed by the power allocation scheme in [66], the optimal power allocation matrix $\mathbf{P}_i$ is

$$\mathbf{P}_i = \left((\mathbf{C}_i)^H \mathbf{C}_i\right)^{-\frac{1}{2}} \mathbf{V}_{\widetilde{\mathbf{Q}}_i} \widehat{\mathbf{P}}_i^* \mathbf{V}_{\widetilde{\mathbf{Q}}_i}^H \left((\mathbf{C}_i)^H \mathbf{C}_i\right)^{-\frac{1}{2}}, \tag{5.76}$$

where

$$\widehat{\mathbf{P}}_i^*(n,n) = \left(\rho - \frac{1}{\lambda_{n,\widetilde{\mathbf{Q}}_i}^2} \right)^+, \tag{5.77}$$

where $\widetilde{\mathbf{Q}}_i = \mathbf{Q}_i^{-\frac{1}{2}} \mathbf{W}_i^H \mathbf{H}_{i,1} \mathbf{C}_i \left((\mathbf{C}_i)^H \mathbf{C}_i\right)^{-\frac{1}{2}}$ and its SVD of is $\widetilde{\mathbf{Q}}_i = \mathbf{U}_{\widetilde{\mathbf{Q}}_i} \mathbf{\Lambda}_{\widetilde{\mathbf{Q}}_i} \mathbf{V}_{\widetilde{\mathbf{Q}}_i}^H$ with $\mathbf{U}_{\widetilde{\mathbf{Q}}_i}$ and $\mathbf{V}_{\widetilde{\mathbf{Q}}_i}^H$ being unitary matrices and $\mathbf{\Lambda}_{\widetilde{\mathbf{Q}}_i}$ being a diagonal matrix with the singular values of $\widetilde{\mathbf{Q}}_i$, $\lambda_{n,\widetilde{\mathbf{Q}}_i}$, as the diagonal elements, and ρ is determined to satisfy $\sum \widehat{\mathbf{P}}_i^*(n,n) = (K+L) p_{max}$.

5.4 Numerical Results

In this section, we will demonstrate the performance of the proposed schemes through numerical results. For comparison, we also provide results based on a scheme that chooses

column positions randomly, called as the random algorithm. Moreover, we also include the results based on traditional TDMA as a benchmark. When TDMA is used, only one SBS is assumed to be active to avoid interference. Without loss of generality, we assume the number of symbols that transmitted by each SU as $d = d_1 = d_2 = ... = d_{2M}$. To show the effects of main system parameters on the system performance and limit the number of changing parameters, we set the SNRs of the received interference signals between the secondary system to the primary system, including signals from the SU to the PU receiver and from the PU transmitter to SBSs, to be -15dB. The change of the SNR value will change the rate value, but the performance trend we will show will be similar. Moreover, we set the numbers of transmit and receive antennas of the PU link to be 1 and 2, respectively. For this setting, the dimension can be used by the secondary system based on signal alignment is different from the value based on traditional ZF techniques and our results will include the benefits of exploiting it.

5.4.1 Impact of Channel Condition

To start with, we present the results for the two-SU cell and each SU and SBS is equiped with two antennas, i.e., $M_t = M_r = 2$. The results for perfectly- and partially-aligned transmissions are in Fig. 5.2 and Fig. 5.3, respectively. We assume the number of subcarriers, $K = 16$, here since the computational complexity is high for the exhaustive search algorithm with a large K. Based on the extended mode and the normal mode from LTE, the ratio of the length of the CP, L, and the number of subcarriers, K, is set as $\frac{L}{K} = 25\%$ and $\frac{L}{K} = 7\%$, respectively. The extended mode corresponds to the perfectly-aligned transmission while the normal mode corresponds to the partially-aligned transmission.

From Fig. 5.2, the exhaustive search algorithm performs best and the random algorithm is the worst. The performance gap from the chordal-distance based algorithms to the random algorithm is larger under equal power allocation than the optimal power allocation. That means, the performance loss coming from choosing signal directions can be compensated through power allocation. This is reasonable since more power will be allocated to

the direction that has larger distance to other SUs' signals to increase the throughput performance. Moreover, for any of the algorithms, the performance gain due to power allocation decreases with SNR.

Comparing the performance of the signal alignment schemes and TDMA, we can see the performance gap increases with SNR. When SNR is small, i.e, less than −3dB with equal power allocation, it is even possible that the transmission based on TDMA can provide better throughput performance. This is due to the fact that less symbols are transmitted based on TDMA, which also causes less interference. The performance gain comes from transmitting more symbols is less than the performance loss by introducing more interference when SNR is small. With the increase of SNR, the system performance is dominated by the number of transmitted symbols, and thus, the proposed schemes perform better than TDMA. Note that, even the throughput based on TDMA is larger than the signal alignment schemes, the number of interference-free symbols transmitted simultaneously based on TDMA is smaller than the latter schemes.

Fig. 5.3 demonstrates the results for the partially-aligned transmission. From the figure, the exhaustive search algorithm performs best and the random algorithm is the worst, similar to the perfectly-aligned transmission. For the partially-aligned transmission, the performance gap between the exhaustive search algorithm and the heuristic algorithm is negligible since the dominated unaligned signals are independent for different SUs. Comparing the signal alignment schemes with TDMA, similar results are obtained as the perfectly-aligned transmission.

Figs. 5.4 show the results for the case with the number of subcarriers $K = 64$. Again, the perfectly-aligned transmission corresponds to the setting based on the ratio for extended mode of LTE and the partially-aligned transmission corresponds to the normal mode. Results show similar trends as the case with $K = 16$.
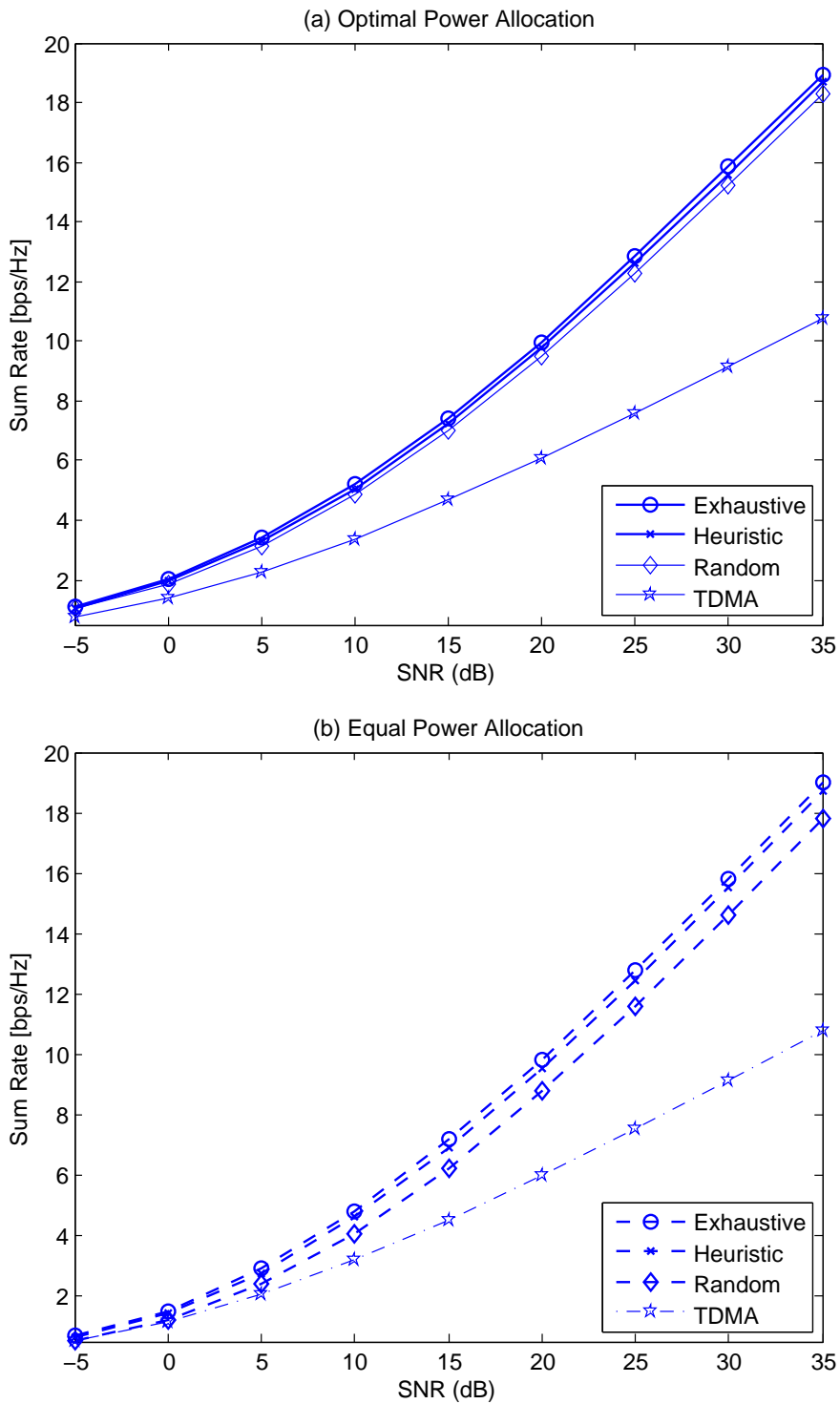
Figure 5.2. Sum rate of two cells for the perfectly-aligned transmission with $K = 16$, $L = 4$, $M = 2$ **and** $M_t = M_r = 2$**.**
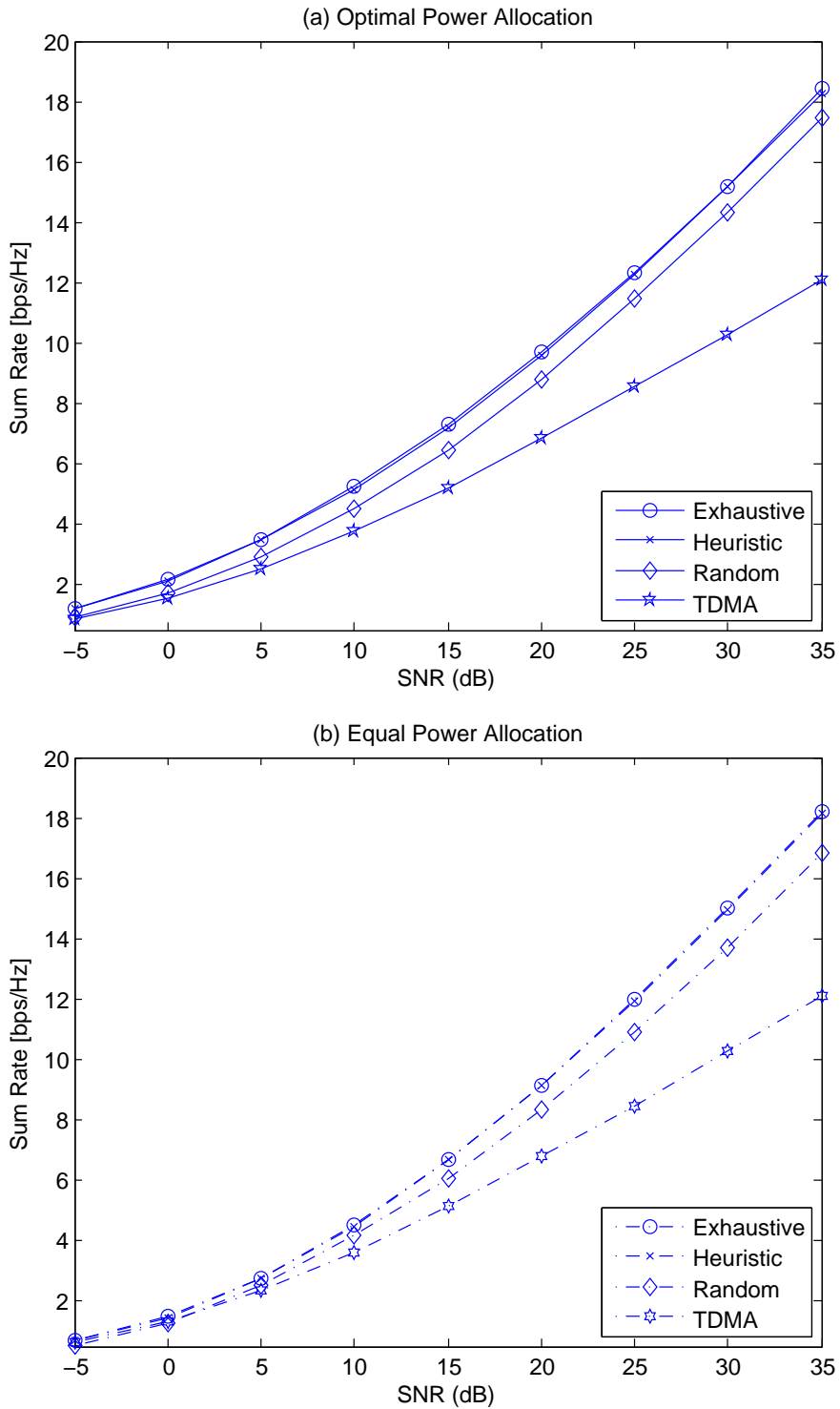
Figure 5.3. Sum rate of two cells for the partially-aligned transmission with $K = 16$, $L = 2$, $M = 2$ **and** $M_t = M_r = 2$**.**
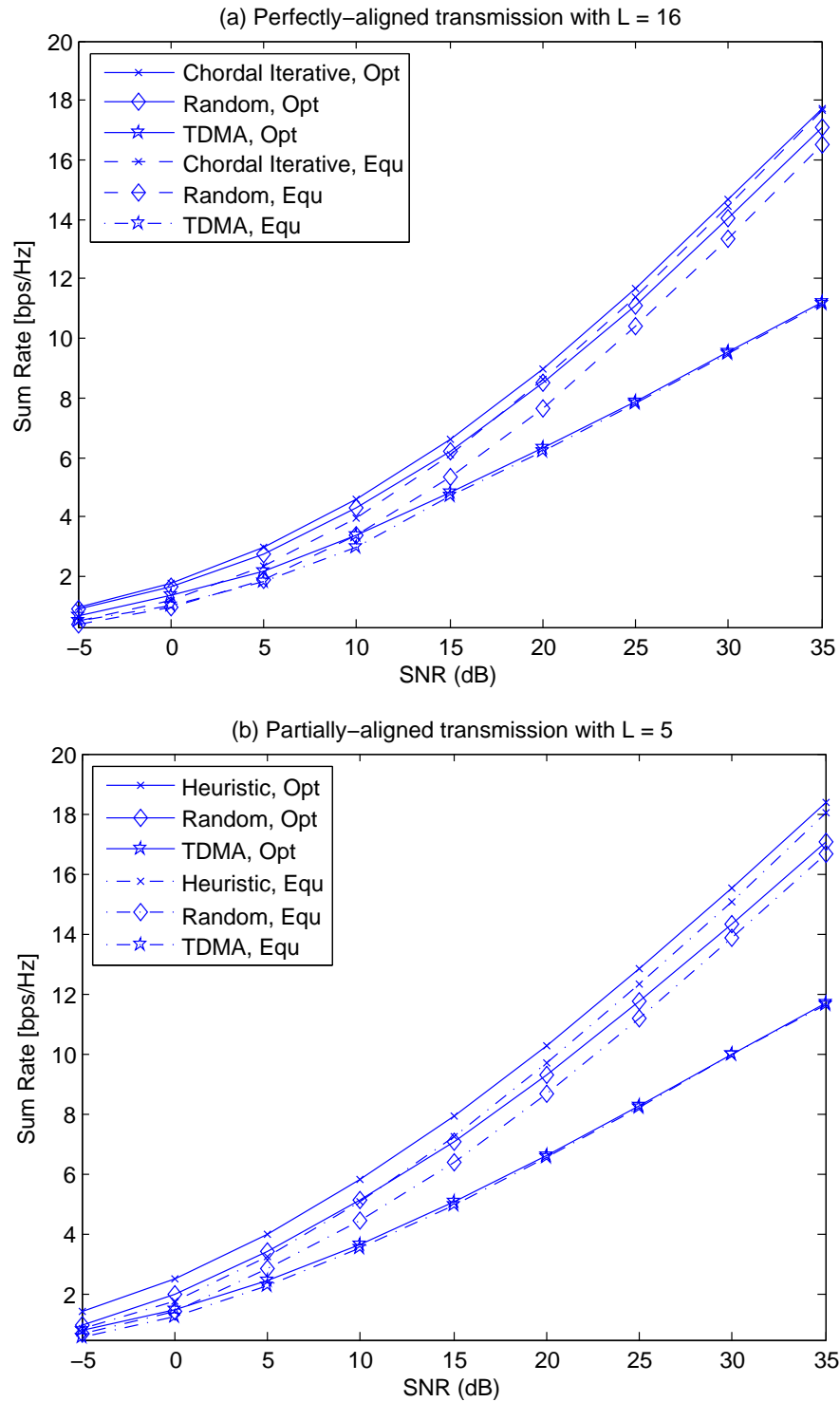
Figure 5.4. Sum rate of two cells for the perfectly- and partially-aligned transmission with $K = 64$**,** $M = 2$ **and** $M_t = M_r = 2$**.**

5.4.2 Impact of SU Numbers

Next, we show the impact of the number of SUs in each cell, M, on the system performance. We focus on the case that signal alignment is feasible, the numbers of transmit and receive antennas are four, $M_t = M_r = 4$, and SNR = 15dB.

The results based on the extended mode in LTE are shown in Fig. 5.5. Significant performance gain can be obtained by using signal alignment schemes over TDMA. For the signal alignment schemes, the throughput increases with the number of SUs in each cell, M, first and then decreases with M. With the increase of M, more SUs are transmitting and thus, more interference signals occur. When M is small, the throughput improvement by introducing more SUs is larger than the performance loss due to interference. Thus, the system throughput increases with M first. With further increase of M, freedom loss due to mitigating interference becomes larger than the performance gain by introducing more SUs. Thus, the system throughput declines.
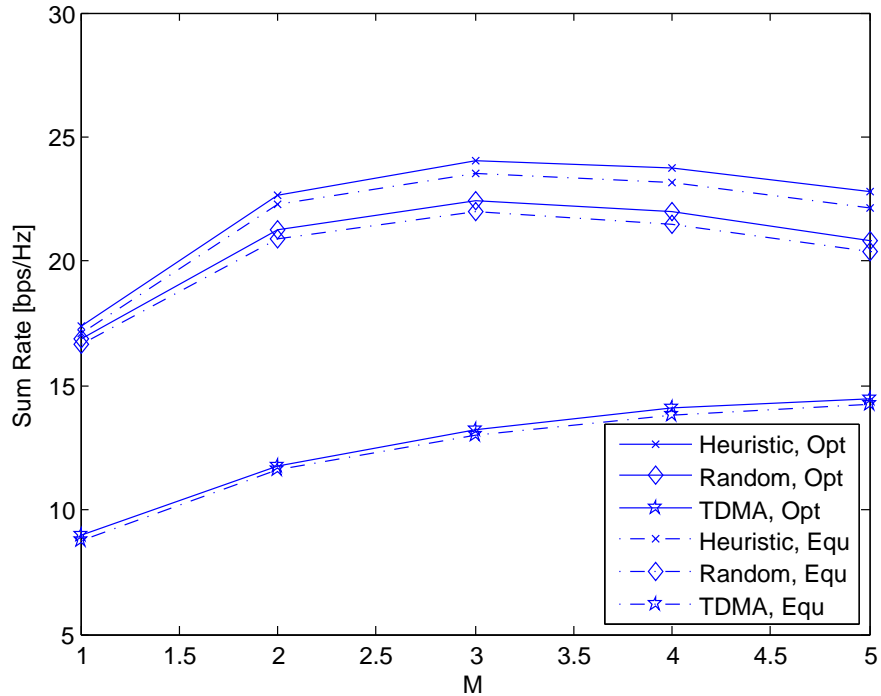
Figure 5.5. Sum rate of two cells for different number of SUs in each cell, M, with $K = 64$ and $L = 16$.

The results based on the normal mode are shown in Fig. 5.6. When the number of

SUs in each cell is smaller than 3, i.e., $M \leq 3$, the performance increases with M, which has the same trend as the extended case. However, when $M > 3$, the performance drops quickly here since the length of CP, L, is small for this case. To achieve signal alignment within the secondary system and interference-free constraint to the primary system, we put constraint on the precoding matrices of the SUs. With small L, the constraint is tight and thus, the throughput performance is sacrificed by allowing transmitting more symbols simultaneously. With a large L, the constraint is loose, and thus, we can get good system performance with large number of simultaneous transmitted symbols. Our scheme can always support more symbols to transmit than TDMA and the performance gain is larger in a higher SNR region.
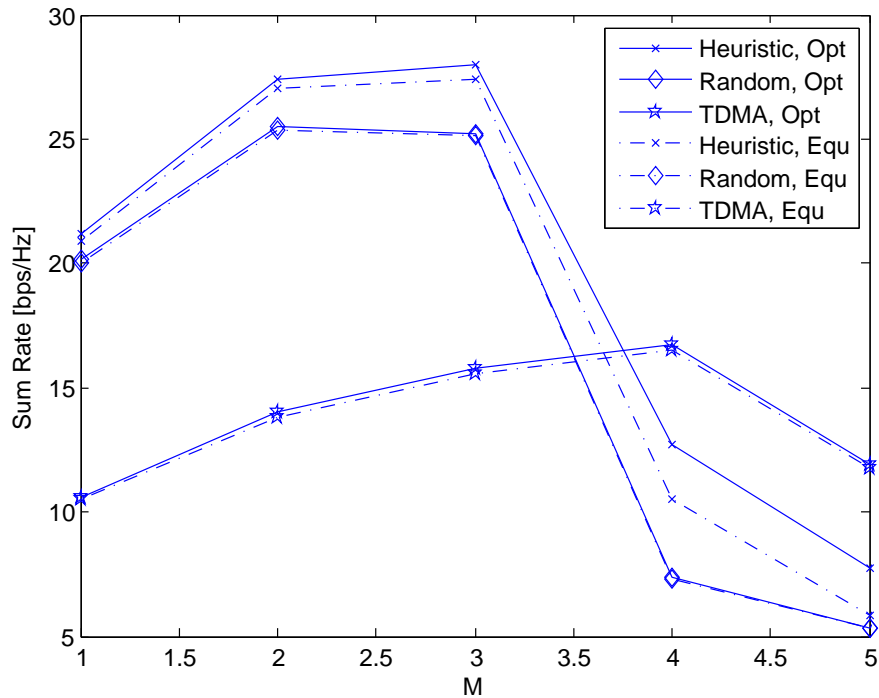
Figure 5.6. Sum rate of two cells for different number of SUs in each cell, M, with $K = 64$ and $L = 5$.

5.5 Discussions

In this section, we will discuss issues about potential extensions of our schemes to multi-cell systems, cooperation between primary and secondary systems, and line-of-sight channels.

5.5.1 Multi-Cell Extension

The extension to a multicell setting is not trivial. Finding a linear precoding method maximizing DOF of the secondary system in general setting is NP-hard [77]. Moreover, as other IA algorithms for the case with multiple user pairs [72, 78, 79, 80, 81, 82, 83, 41], iterative operations may need to fulfill the goal, which may increase information exchange overhead and computational complexity. The extension will be our future work. However, the idea of choosing directions can be used in other systems if perfect IA cannot be achieved due to system limitation. Moreover, our two-cell setting can be treated as a basic block for multi-cell systems where the proposed scheme can be used by two cells that use the same resource while using orthogonal resource allocation, such as TDMA, FDMA, among other cells.

5.5.2 Cooperation between Primary and Secondary Systems

Practically, it is possible that the primary system can assist or even release some of its transmission space to the secondary system as long as its own QoS can be satisfied, e.g., in the spectrum trading system [84]. As proposed in [68], a primary system can set its transmit power on some directions to zero when the assigned power on that direction goes below a given threshold. Through this way, the null space for the secondary system expands while the interference-free transmission can still be guaranteed. In general, the null space releasing can be decided based on the requirement of the primary system only, as in [68], or the requirement of the secondary system can also be considered. After the null space can be used by the secondary system is decided, our proposed design can be used by replacing $\widetilde{\mathbf{H}}_{i,0}$ in (5.23) by the matrix capturing the subspace used by the primary system.

5.5.3 Line-of-Sight Channels

In our analysis, all channel coefficients are assumed to be i.i.d and followed Rayleigh distribution as assumed in most existing work. In reality, *Line-of-Sight* (LoS) may exist and the channel coefficients may be correlated [85]. The ill-conditioned channel may provide opportunities for SUs [86]. If there exists LoS between the PU link, transmit power tends to be allocated more onto it, it is possible to leave more space for the secondary system. In general, if there exists LoS or correlation between SU to the PU link or the SU links, the design may depend on the model and is involving, including both DOF calculation or precoding design [87, 88]. The general design by taking correlation into account is beyond our scope.

5.6 Conclusions

In this chapter, we propose a signal alignment scheme for a two-cell multiple-antenna secondary uplink system by exploiting the nullspace provided by the CP and multiple antennas. The proposed scheme can achieve interference-free transmission to the primary system and within the secondary system. The number of interference-free symbols that can be transmitted by each SU has been derived, which increases with the antennas equipped at the SU and the SBS and the length of CP. Two chordal-distance based precoding matrix design algorithms have been proposed. The proposed scheme can transmit more symbols for each SU simultaneously than TDMA. The proposed ideas can be potentially extended to a secondary system with more than two cells.

CHAPTER 6

OPTIMAL POWER ALLOCATION FOR COGNITIVE RADIO NETWORKS WITH DIRECT AND RELAY-AIDED TRANSMISSIONS

In this chapter, we start our study on spectrum underlay CR systems. We investigate power allocation schemes for CR networks with both direct and relay-aided transmissions. We first formulate an overall rate optimization problem with interference constraints to the PU and peak power constraints at each node and obtain solutions by theoretical analysis. To take the fairness among CR users into consideration, we further investigate the overall rate optimization problem with an additional sum power constraint and achieve fairness between two CR users by adjusting the sum power threshold. Numerical results are provided to show the impact of the relay node and the PU locations on power allocation solutions.

The rest of this chapter is organized as follows. In Section 6.1, we introduce the system model. In Section 6.2, we formulate a power allocation problem and discuss the solution. To take the fairness between CR users into consideration, a power allocation problem with an additional sum power constraint will be discussed in Section 6.3. Numerical results are provided in Section 6.4 to show the impact of different system parameters on the system performance. Finally, Section 6.5 concludes the chapter.

6.1   System Description

We consider an underlay system that a CR network coexists with a PU network, as shown in Fig. 6.1. In the CR network, one CR BS transmits data to two CR users, respectively. CR 2 is served directly by the BS. Due to large path loss, CR 1 receives only a negligible signal power from BS. Thus, we assume the transmission to CR 1 is aided by a relay node. Due to practical constraints, full duplex operation at the relay is very challenging [52]. Therefore, a half-duplex *decode-and-forward* (DF) relay is considered, where it can not transmit and receive simultaneously. Thus, data transmission from the BS to CR 1 will be conducted in
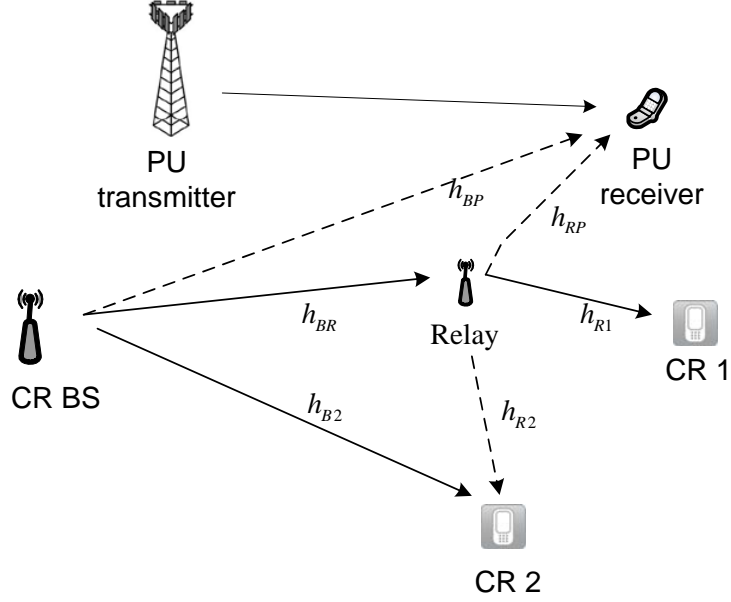
Figure 6.1. The structure of a CR network with direct and relay-aided transmissions.

two phases: the BS first transmits data to the relay and the relay then forwards the data to CR 1.

All channels are modeled as Rayleigh block fading channels, where the channel gains remain constant during two phases. Let h_{BR}, h_{B2}, and h_{BP} denote the channel coefficients between the CR BS to the relay node, to CR 2, and to the PU, respectively. h_{R1}, h_{R2}, and h_{RP} denote the channel coefficients between the relay node to CR 1, to CR 2, and to the PU, respectively. The path gains are with Rayleigh distribution and depend on the distances between the transmitter and the receiver, which can be expressed as

$$|h| = \sqrt{\beta}\phi, \tag{6.1}$$

where ϕ is a unit-variance Raleigh distributed random variable and β is the pathloss, which is inversely proportional to the power of the distance with a path loss exponent, δ, i.e, $\beta = d^{-\delta}$. δ can be obtained to approximate either an analytical or empirical model and is an integer over $[2, 4]$. We assume the system is centralized and the BS has all the channel state information. Transmit power at the relay node is controlled by the BS through control signal.

To improve system performance, the transmission scheme we use in the CR network in Fig. 6.1 is based on a two-phase transmission scheme:

- During phase 1, BS transmits data x_1 for CR 1 to the relay. Meanwhile, CR 2 also receives it.

- During phase 2, the relay node forwards data x_1 to CR 1 while the BS transmits data x_2 for CR 2. CR 2 can use the information obtained in phase 1 about x_1 to cancel the interfering signal from the relay in phase 2, which leads to throughput improvement.

Since the CR network is transparent to the PU network, the interference signal from the PU network can not be controlled and normally be treated as noise. For clarity, we neglect it in the following analysis. The results can be easily extended to the case with PU interference.

During phase 1, the received signals at the relay and CR 2 are

$$y_R[1] \;=\; \sqrt{P_1} h_{BR} x_1 + n_R[1] \tag{6.2}$$

and

$$y_2[1] \;=\; \sqrt{P_1} h_{B2} x_1 + n_2[1], \tag{6.3}$$

respectively. P_1 is the signal power used by the CR BS during phase 1, $n_R[1]$ and $n_2[1]$ are the complex white Gaussian noises at the relay and CR 2 in the first time slot, following the complex white Gaussian distribution, $\mathcal{CN}\left(0, \sigma^2\right)$.

During phase 2, the received signals at CR 1 and CR 2 are

$$y_1[2] \;=\; \sqrt{P_2} h_{R1} x_1 + n_1[2], \tag{6.4}$$

and

$$y_2[2] \;=\; \sqrt{P_3} h_{B2} x_2 + \sqrt{P_2} h_{R2} x_1 + n_2[2], \tag{6.5}$$

respectively, where P_2 and P_3 are the signal powers used by the relay node and the CR BS during phase 2, $n_1[2]$ and $n_2[2]$ are the complex white Gaussian noise variables, following the distribution, $CN\left(0, \sigma^2\right)$, at CR 1 and CR 2, respectively.

According to the cut-set bound theory [89], the rate of transmitting x_1 is

$$R_1\left(P_1, P_2\right) = \min\left\{\frac{1}{2}\log_2\left(1 + \gamma_R\right), \frac{1}{2}\log_2\left(1 + \gamma_1\right)\right\}, \tag{6.6}$$

where

$$\gamma_R = \frac{P_1|h_{BR}|^2}{\sigma^2}, \tag{6.7}$$

and

$$\gamma_1 = \frac{P_2|h_{R1}|^2}{\sigma^2}. \tag{6.8}$$

γ_R is the *signal-to-noise ratio* (SNR) of $y_R[1]$ at the relay node during phase 1 and is calculated from (6.2). γ_1 is the SNR at CR 1 during phase 2 and is obtained from (6.4). Note that $R_1(P_1, P_2)$ depends only on P_1 and P_2 and is independent of P_3.

There are two cases for CR 2. If the BS-to-CR-2 link is better than the BS-to-relay link, i.e., $|h_{B2}| \geq |h_{BR}|$, we call it case I. For this case, CR 2 can decode x_1 successfully if the relay node does. During the second phase, CR 2 can subtract interference signal about x_1 from the relay and then, the SNR for x_2 is expressed as

$$\gamma_2 = \frac{P_3|h_{B2}|^2}{\sigma^2}. \tag{6.9}$$

If the BS-to-CR-2 link is worse than the BS-to-relay link, i.e., $|h_{B2}| < |h_{BR}|$, we call it case II. For this case, the received signals from phases 1 and 2 can form a virtual *multiple-input-multiple-output* (MIMO) system [56] and can be expressed as

$$\begin{bmatrix} y_2[1] \\ y_2[2] \end{bmatrix} = \begin{bmatrix} \sqrt{P_1}h_{B2} \\ \sqrt{P_2}h_{R2} \end{bmatrix} x_1 + \begin{bmatrix} 0 \\ \sqrt{P_3}h_{B2} \end{bmatrix} x_2 + \begin{bmatrix} n_2[1] \\ n_2[2] \end{bmatrix}. \tag{6.10}$$

If the *minimum-mean-square-error* (MMSE) receiver is used, the SNR at CR 2 can be expressed as [71]

$$\gamma_2 = \frac{\left(P_1|h_{B2}|^2 + \sigma^2\right)P_3|h_{B2}|^2}{\sigma^2\left(P_1|h_{B2}|^2 + P_2|h_{R2}|^2\right) + \sigma^4}$$

$$= \frac{P_3|h_{B2}|^2}{\sigma^2 + \frac{\sigma^2 P_2|h_{R2}|^2}{P_1|h_{B2}|^2+\sigma^2}}. \tag{6.11}$$

Since case I is much simpler than case II, and the analysis for case II can be used for solving case I, we focus on case II in the following part. Numerical results including both cases will be shown.

Based on (6.11), the rate of transmitting x_2 is

$$R_2\left(P_1, P_2, P_3\right) = \frac{1}{2}\log_2\left(1 + \gamma_2\right), \tag{6.12}$$

which depends on the powers used at the CR BS during phases 1 and 2, P_1 and P_3, and the power used at the relay node during phase 2, P_2.

The overall data rate of the CR network is the sum rate of both CR users, which depends on the powers used at the CR BS during phases 1 and 2, P_1 and P_3, and the power used at the relay node during phase 2, P_2. It can be expressed as

$$R_a(P_1, P_2, P_3) = R_1(P_1, P_2) + R_2(P_1, P_2, P_3). \tag{6.13}$$

Next, we will investigate the power allocation scheme to optimize the overall data rate of the studied system.

6.2   Overall Rate Optimization

In the studied underlay system, the CR network is allowed to transmit simultaneously with the PU. However, the PU has a priority to use the licensed bands and must be protected. CR transmissions are not allowed to generate unacceptable interference to the PU. Thus, power control in the CR network is important.

To maximize the overall data rate of the CR network while limiting the interference to the PU, we formulate a transmit power control problem by jointly optimizing the transmit

powers at the CR BS during phases 1 and 2, and the transmit power at the relay node during phase 2 under some practical constraints.

By considering the constraints on each node, the optimization problem is formulated as follows

$$\max_{P_1,P_2,P_3} \quad R_a(P_1, P_2, P_3), \tag{6.14a}$$

$$s.t. \quad P_1|h_{BP}|^2 \leq I, \tag{6.14b}$$

$$P_3|h_{BP}|^2 + P_2|h_{RP}|^2 \leq I, \tag{6.14c}$$

$$P_1 \leq P_{BS}, \tag{6.14d}$$

$$P_2 \leq P_R, \tag{6.14e}$$

$$P_3 \leq P_{BS}. \tag{6.14f}$$

Equations (6.14b) and (6.14c) are the interference constraints for phases 1 and 2 to prevent CR network from causing severe interference to the PU, where I is the interference threshold that the PU network can tolerate. Equations (6.14d), (6.14e), and (6.14f) are the peak transmit power constraints at each node due to the equipment capacity.

We consider the signal power of the CR BS during phase 1, P_1, first. From (6.7), the SNR at the relay node, γ_R, is a monotonically increasing function of P_1 while the SNR at CR 1, γ_1, is independent of P_1. Thus, both $R_1(P_1, P_2)$ and $R_2(P_1, P_2, P_3)$ are monotonically increasing functions of P_1. Thus, P_1 should be as large as possible as long as constraints (6.14b) and (6.14d) are satisfied. As a result, the optimal value of P_1 is

$$P_1^* = \min\left\{P_{BS}, \frac{I}{|h_{BP}|^2}\right\}. \tag{6.15}$$

The power used at the CR BS in phase 2, P_3, does not impact $R_1(P_1, P_2)$. From (6.11), $R_2(P_1, P_2, P_3)$ is a monotonically increasing function of P_3 and so is the objective function, which is the sum of $R_1(P_1, P_2)$ and $R_2(P_1, P_2, P_3)$. Thus, the optimal P_3 is

$$P_3^* = \min\left\{P_{BS}, \frac{I - P_2|h_{RP}|^2}{|h_{BP}|^2}\right\}, \tag{6.16}$$

if the power of the relay node, P_2, is given. Since (6.16) is true for all feasible P_2, the optimal solution pair should satisfy it. Thus, only the pairs which satisfy (6.16) will be considered in the rest of the chapter.

Since the rate of transmitting x_1 is determined by both phases, we divide the original problem in two cases.

1) Phase 1 Dominated Case

If $P_2 \geq \frac{P_1^* |h_{BR}|^2}{|h_{R1}|^2}$, the SNR at the relay node can not be larger than the SNR at CR 1, i.e., $\gamma_R \leq \gamma_1$. From (6.6), we have

$$
\begin{aligned}
R_1\left(P_1^*, P_2\right) &= \frac{1}{2} \log_2\left(1 + \gamma_R\right) \\
&= \frac{1}{2} \log_2\left(1 + \frac{P_1^* |h_{BR}|^2}{\sigma^2}\right),
\end{aligned}
\tag{6.17}
$$

which is determined by the first phase. We call it phase 1 dominated case.

From (6.17), $R_1(P_1^*, P_2)$ is independent of P_2. Meanwhile, $R_2(P_1^*, P_2, P_3^*)$ is a decreasing function of P_2. Thus, the overall data rate $R_a(P_1^*, P_2, P_3^*)$ is determined by the second phase and it is a decreasing function of P_2. As a result, P_2 should be as small as possible as long as it satisfies all constraints. In this case, we have

$$
P_2 \geq \frac{P_1^* |h_{BR}|^2}{|h_{R1}|^2}.
\tag{6.18}
$$

Thus, the optimal power at the relay node, P_2, is

$$
\begin{aligned}
P_{2,1}^* &= \frac{|h_{BR}|^2 P_1^*}{|h_{R1}|^2} \\
&= \frac{|h_{BR}|^2 \cdot \min\left\{P_{BS}, \frac{I}{|h_{BP}|^2}\right\}}{|h_{R1}|^2}.
\end{aligned}
\tag{6.19}
$$

2) Phase 2 Dominated Case

If $P_2 \leq \frac{P_1^* |h_{BR}|^2}{|h_{R1}|^2}$, the SNR at the relay node can not be smaller than the SNR at CR 1, i.e., $\gamma_R \geq \gamma_1$. According to (6.6), we have

$$
\begin{aligned}
R_1\left(P_1^*, P_2\right) &= \frac{1}{2} \log_2\left(1 + \gamma_1\right) \\
&= \frac{1}{2} \log_2\left(1 + \frac{P_2 |h_{BR}|^2}{\sigma^2}\right),
\end{aligned}
\tag{6.20}
$$

which is determined by the second phase. Correspondingly, it is called phase 2 dominated case.

From (6.20), both $R_1\left(P_1^*, P_2, P_3^*\right)$ and $R_2\left(P_1^*, P_2\right)$ depend on P_2, which is more complicated than the phase 1 dominated case. According to the signal power at the CR BS during phase 2, P_3, we investigate the problem in two cases.

Case A: When $P_2 \leq \frac{I - P_{BS}|h_{BP}|^2}{|h_{RP}|^2}$, we have

$$P_3^* = P_{BS}. \tag{6.21}$$

From Appendix C.1, the optimal power at the relay node, P_2, for this case is

$$P_{2,2}^* = \min\left\{\frac{P_1^*|h_{BR}|^2}{|h_{R1}|^2}, \frac{I - P_{BS}|h_{BP}|^2}{|h_{RP}|^2}, P_R\right\}, \tag{6.22}$$

when $ad - eac < ec^2$, where $a = P_{BS}|h_{B2}|^2$, $c = \sigma^2$, $d = \frac{\sigma^2|h_{R2}|^2}{P_1^*|h_{B2}|^2+\sigma^2}$, and $e = \frac{|h_{BR}|^2}{\sigma^2}$. Otherwise,

$$P_{2,2}^* = \arg\max_{P_2 \in \mathcal{P}} R_a\left(P_1^*, P_2, P_3^*\right), \tag{6.23}$$

where $\mathcal{P} = \left\{0, \min\{\frac{P_1^*|h_{BR}|^2}{|h_{R1}|^2}, \frac{I - P_{BS}|h_{BP}|^2}{|h_{RP}|^2}, P_R\}\right\}$. Note that if $P_2 = 0$ is the optimal solution, it is better to set $P_1 = 0$ to save energy. This is the extreme case that the channel condition for CR 1 is severe. In the studied overhearing-based transmission scheme, this case seldom occurs.

Case B: When $P_2 \geq \frac{I - P_{BS}|h_{BP}|^2}{|h_{RP}|^2}$, we have

$$P_3^* = \frac{I - P_2^*|h_{RP}|^2}{|h_{BP}|^2}. \tag{6.24}$$

From Appendix C.2, the optimal power at the relay node, P_2, for this case, denoted as $P_{2,3}^*$, can be found following Algorithms C.1 and C.2 for $k > i$ and $k < i$, respectively, where $h = \frac{I}{|h_{BP}|^2}$, $i = \frac{|h_{RP}|^2}{|h_{BP}|^2}$, $j = \sigma^2$, $k = \frac{\sigma^2|h_{R2}|^2}{P_1^*|h_{B2}|^2+\sigma^2}$, and $t = \frac{|h_{BR}|^2}{\sigma^2}$.

In brief, the global optimal transmit power at the CR BS during phase 1 is

$$P_1^* = \min\left\{P_{BS}, \frac{I}{|h_{BP}|^2}\right\}. \tag{6.25}$$

The optimal transmit power at the relay node during phase 2, P_2, is

$$P_2^* = \arg\max_{P_{2,i}^*} R_a(P_1^*, P_{2,i}^*, P_{3,i}^*), i = 1, 2, 3, \tag{6.26}$$

where

$$P_{3,i}^* = \min\left\{P_{BS}, \frac{I - P_{2,i}^*|h_{RP}|^2}{|h_{BP}|^2}\right\}. \tag{6.27}$$

Then, the optimal transmit power for the CR BS during phase 2, P_3, can be obtained by substituting P_2^* into (6.16), which is

$$P_3^* = \min\left\{P_{BS}, \frac{I - P_2^*|h_{RP}|^2}{|h_{BP}|^2}\right\}. \tag{6.28}$$

Note that even though the problem is not convex, the power allocation solution is global optimal since all feasible regions have been taken into consideration.

6.3 Optimization With Total Power Constraint

In the previous section, we consider the power allocation on the CR BS and the relay node. The solution satisfies the interference constraints to the PU network and the peak power constraints on both nodes. However, we ignore the fairness between two CR users. Since the interference constraint considers the sum of the powers from the relay and the BS node during phase 2 while it only considers the power from the BS during phase 1, sum power used for transmitting x_1 is always larger than the power used for transmitting x_2, which is unfair for CR 2. Since the sum power used by CR 2 is constrained by the peak power constraint at the CR BS, we consider restricting the sum power used by CR 1 to solve the problem. Next, we will analyze the power allocation scheme with the sum power constraint.

By considering the fairness of the two CR users, the sum power for transmitting to CR

1 will be limited. Then, the problem is re-formulated as

$$\max_{P_1, P_2, P_3} \quad R_a\left(P_1, P_2, P_3\right), \tag{6.29a}$$

$$s.t. \quad P_1|h_{BP}|^2 \le I, \tag{6.29b}$$

$$P_3|h_{BP}|^2 + P_2|h_{RP}|^2 \le I, \tag{6.29c}$$

$$P_1 \le P_{BS}, \tag{6.29d}$$

$$P_2 \le P_R, \tag{6.29e}$$

$$P_1 + P_2 \le P_t, \tag{6.29f}$$

$$P_3 \le P_{BS}. \tag{6.29g}$$

Equations (6.29b), (6.29c), (6.29d), (6.29e), and (6.29g) are the same as the previous problem without sum power constraint. The sum power constraint for CR 1 is in (6.29f), where P_t is the sum power threshold.

For the system with total power constraint, the objective function keeps the same, which is a monotonically increasing function of the powers at the CR BS during phase 1, P_1, and phase 2, P_3. Thus, if the power of the relay node, P_2, is given, the optimal P_1 and P_3 can be expressed as a function of it, which are

$$P_1^* = \min\left\{P_t - P_2, P_{BS}, \frac{I}{|h_{BP}|^2}\right\} \tag{6.30}$$

and

$$P_3^* = \min\left\{P_{BS}, \frac{I - P_2|h_{RP}|^2}{|h_{BP}|^2}\right\}, \tag{6.31}$$

respectively.

We discuss the problem at two cases: phase 1 and phase 2 dominated cases, respectively.

1) Phase 1 Dominated Case

If $P_2 \ge \frac{P_1^*|h_{BR}|^2}{|h_{R1}|^2}$, the SNR at the relay node can not be larger than the SNR at CR 1, i.e.,

$$P_{2,1}^* = \min\left\{\left\{\left[\left[\max\{(P_t - z), \frac{z|h_{BR}|^2}{|h_{R1}|^2}\}\right]^+, P_R\right] \cup \left[\left[\frac{P_t|h_{BR}|^2}{|h_{R1}|^2 + |h_{BR}|^2}\right]^+, \min\{(P_t - z), P_R\}\right]\right\}\right.$$

$$\left. \cap \left\{\left[\left[\frac{I - P_{BS}|h_{BP}|^2}{|h_{RP}|^2}\right]^+, P_R\right] \cup \left[0, \min\{P_R, \frac{I - P_{BS}|h_{BP}|^2}{|h_{RP}|^2}\}\right]\right\}\right\}. \tag{6.33}$$

$\gamma_R \leq \gamma_1$. Then,

$$\begin{aligned} R_1\left(P_1^*, P_2\right) &= \frac{1}{2}\log_2\left(1 + \gamma_R\right) \\ &= \frac{1}{2}\log_2\left(1 + \frac{P_1^*|h_{BR}|^2}{\sigma^2}\right), \end{aligned} \tag{6.32}$$

which is determined by the first phase, thus we call it phase 1 dominated case. From (6.30), P_1^* is non-increasing with P_2. Since $\log(\cdot)$ is an increasing function, $R_1\left(P_1^*, P_2\right)$ is a non-increasing function of P_2. From (6.31), P_3^* is a non-increasing function of P_2. Then, from (6.12), $R_2\left(P_1^*, P_2, P_3^*\right)$ is non-increasing with P_2 as well.

Both $R_1\left(P_1^*, P_2\right)$ and $R_2\left(P_1^*, P_2, P_3^*\right)$ are non-increasing functions of P_2, and so is the overall rate function, $R_a\left(P_1^*, P_2, P_3^*\right)$. Thus, the optimal P_2 is the minimal value satisfying all the constraints, which can be expressed as in (6.33), where $z = \min\{P_{BS}, \frac{I}{|h_{BP}|^2}\}$ and $[x]^+ = \max\{0, x\}$.

2) Phase 2 Dominated Case

If $P_2 \leq \frac{P_1^*|h_{BR}|^2}{|h_{R1}|^2}$, the SNR at the relay node can not be smaller than the SNR at CR 1, i.e., $\gamma_R \geq \gamma_1$. Then,

$$\begin{aligned} R_1\left(P_1^*, P_2\right) &= \frac{1}{2}\log_2\left(1 + \gamma_1\right) \\ &= \frac{1}{2}\log_2\left(1 + \frac{P_2|h_{BR}|^2}{\sigma^2}\right), \end{aligned} \tag{6.34}$$

which is dominated by phase 2 and we call it phase 2 dominated case. We then investigate the problem in different regions for P_2.

Case A: When $P_2 \leq P_t - z$, the optimal power used at the CR BS during phase 1, P_1^* is

$$P_1^* = z, \tag{6.35}$$

where $z = \min\{P_{BS}, \frac{I}{|h_{BP}|^2}\}$. In this case, P_1^* is not restricted by the sum power constraint. The calculation follows the case without total power constraint. Note that the region of P_2 is different here. The optimal value found for this case is denoted as $P_{2,2}^*$.

Case B: When $P_2 \geq P_t - z$, P_1^* is dominated by the sum rate constraint, which can be expressed as

$$P_1^* = P_t - P_2. \tag{6.36}$$

From Appendix C.3, we can find out optimal P_2 for $P_2 \leq \frac{I - P_{BS}|h_{BP}|^2}{|h_{RP}|^2}$ and $P_2 \geq \frac{I - P_{BS}|h_{BP}|^2}{|h_{RP}|^2}$, denoted as $P_{2,3}^*$ and $P_{2,4}^*$, respectively.

Consequently, we can find the global optimal solution for P_2 as

$$P_2^* = \arg\max_{P_{2,i}^*} R_a(P_{1,i}^*, P_{2,i}^*, P_{3,i}^*), \quad i = 1, 2, 3, 4 \tag{6.37}$$

where

$$P_{1,i}^* = \min\left\{P_t - P_{2,i}^*, P_{BS}, \frac{I}{|h_{BP}|^2}\right\}, \tag{6.38}$$

and

$$P_{3,i}^* = \min\left\{P_{BS}, \frac{I - P_{2,i}^*|h_{RP}|^2}{|h_{BP}|^2}\right\}. \tag{6.39}$$

Then, the optimal solutions for P_1 and P_3 are

$$P_1^* = \min\left\{P_t - P_2^*, P_{BS}, \frac{I}{|h_{BP}|^2}\right\}, \tag{6.40}$$

and

$$P_3^* = \min\left\{P_{BS}, \frac{I - P_2^*|h_{RP}|^2}{|h_{BP}|^2}\right\}, \tag{6.41}$$

respectively.

Again, the problem is not convex, but the solution is global optimal since all feasible regions have been taken into account.

91

We have discussed the power allocation scheme with sum power constraint. To limit the sum power used for transmitting x_1, we can adjust the power used for transmitting x_1 and x_2 on a same level, and thus, a fair power usage scheme for both users can be obtained.

We can also use this scheme to adjust the rate of both users on a same level, leading to rate fairness between them. This is reasonable since the rate is controlled by the transmission power, which is also demonstrated by numerical results in the next section. Moreover, the problem can be extended to a weighted sum rate case, where the objective function is $R_a(P_1, P_2, P_3) = w_1 R_1(P_1, P_2) + w_2 R_2(P_1, P_2, P_3)$, where w_1 and w_2 are the weights for the rate for CR 1 and CR 2, respectively. The weight can potentially provide certain level of priority and/or fairness between two UEs. A similar way as in this chapter can be used to derive the power allocation results for the weighted sum rate problem.

6.4 Numerical Results

In this part, we evaluate the performance of the optimal power allocation. All results take both cases for CR 2 into consideration, where interference cancelation is used when $h_{B2} \geq h_{BR}$ and MMSE receiver is used when $h_{B2} < h_{BR}$. Besides using MMSE, we also provide the results for *zero-forcing* (ZF) receiver. When ZF is used, the SNR at CR 2 [71] is

$$\gamma_2 = \frac{P_1 P_3 |h_{B2}|^4}{(P_2 |h_{R2}|^2 + P_1 |h_{B2}|^2)\sigma^2}. \tag{6.42}$$

Then, the optimal power allocation solution can be obtained through a similar way as the MMSE receiver. We omit the detail here. The results are provided numerically in the following figures. Since this is no related work on power allocation for the studied network, we only compare the results with a simple equal power allocation (EPA) scheme satisfying all the interference constraints, where

$$P_1 = P_2 = P_3 = \min\left\{P_{BS}, P_R, \frac{P_t}{2}, \frac{I}{|h_{BP}|^2 + |h_{RP}|^2}\right\}, \tag{6.43}$$

where $P_t = +\infty$ for the case without the sum power constraint.
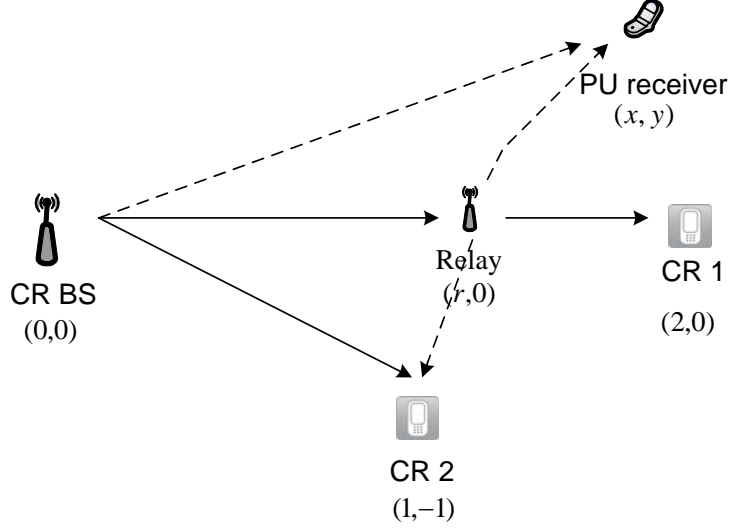
Figure 6.2. The location illustration.

To limit the number of parameters, as in Fig. 6.2, we assume the locations of the CR BS, CR 1 and CR 2 are fixed, which are $(0,0)$, $(2,0)$ and $(1,-1)$. The relay node is placed on the line of the CR BS and CR 1 with location $(r,0)$. The location of the PU is (x,y). All curves in figures are averaged over 50,000 trials. Without loss of generality, we set the peak power constraints as $P_{BS} = P_R = 15$ dB and the noise power on each channel is $\sigma^2 = 1$. The path loss exponent is $\delta = 4$.

6.4.1 Power Allocation Without Sum Power Constraint

In this part, we provide the results for the case without sum power constraint. We will show the impact of the relay and the PU locations on the system performance.

6.4.1.1 The impact of the relay location

Fig. 6.3 shows the impact of the relay location on the power allocation results where the PU location is $(1,2)$. With the increase of r, the relay node moves from the CR BS to CR 1. The distance between the relay node and the PU decreases when r increases from 0 to 1, and increases from 1 to 2. Since the optimal power at the CR BS for phase 1, P_1^*, is only related to the CR-BS-to-PU link and the peak power constraint, it keeps constant for different relay locations for both receivers. Moreover, we can conclude that the behavior
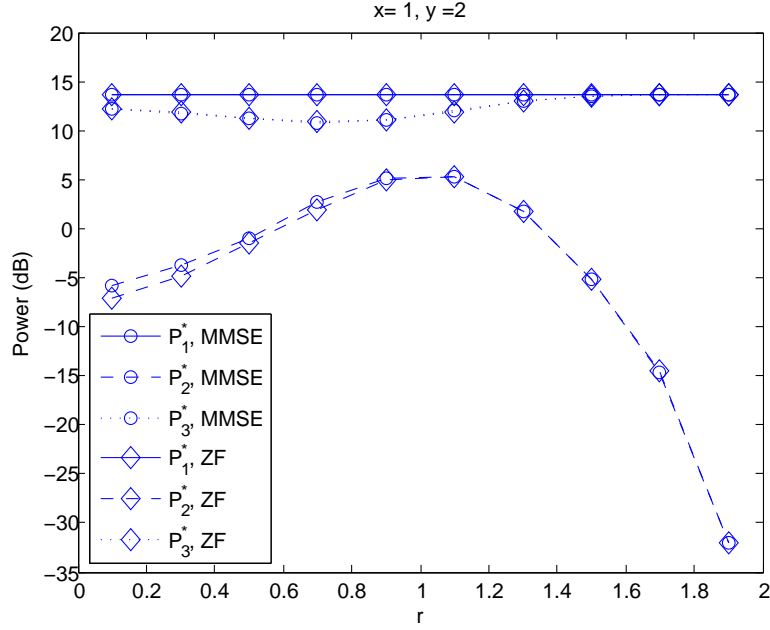
Figure 6.3. Optimized power solution for different relay locations.

of the optimal power used by the relay, P_2^*, and the optimal power used by the BS at the second phase, P_3^*, are dominated by the rate of CR 1 when the relay is close to the BS (when r is small) while it is dominated by the rate of CR 2 when the relay is close to CR 1 (when r is large). The rate of CR 1, $R_1(P_1, P_2)$ is only related to P_1 and P_2. Since P_1 keeps the same for the whole region, $R_1(P_1, P_2)$ is dominated by P_2. When r is small, the BS-to-relay link is always better than the relay-to-CR-1 link and thus, the system is in phase 2 dominated case. For phase 2 dominated case, the rate of CR 1 increases with the increase of P_2. Even though the increase of P_2 will decrease the rate of CR 2, optimal P_2 increases with r. Thus, the behavior of the objective function is dominated by CR 1 when r is small. With the increase of r and P_2, the system will change to phase 1 dominated case. For this case, the increase of P_2 will not lead to the rate increase of CR 1, but it will decrease the rate of CR 2. Thus, optimal P_2 decreases. CR 2 dominates the behavior of the objective function when r is large.

Comparing two different receivers, the optimal power solution at the CR BS, P_1^*, with the MMSE receiver for phase 1 is almost the same as the case with the ZF receiver. During

phase 2, the power at the CR BS, P_3^*, with the MMSE receiver is slightly lower than the case with the ZF receiver while the power at the relay node, P_2^*, with the MMSE receiver is higher than the case with the ZF receiver. Based on the results, the impact of the relay node location on both receivers are the same. Note that, for our simulated case, the impact of σ^2 on the SNR of CR 2 is not significant, and thus, the differences between the absolute optimal transmit powers based on these two receivers are small. For other case, i.e., the transmit power is low, the difference between these two receivers may become large. Since the comparisons between these two receivers are not our focus, we omit the results for other cases here.

Fig. 6.4 shows the overall rates for different relay locations. The overall data rate first increases with r and then decreases. This behavior is the same as the rate of CR 1 while the rate of CR 2 has opposite behavior. Thus, the behavior of the overall data rate is mainly dominated by CR 1. The proposed scheme with the MMSE receiver performs better than with the ZF receiver, however, the difference is pretty small. The reasons for this non-significant performance difference are the follows. First, the impact of σ^2 on our simulated case is not significant. Second, the results are optimized based on each of them. If we use same power allocation results for both of them, the performance difference will become larger. No matter which receiver is used, our proposed schemes have significant perfor-mance gains over EPA. The performance gain is as large as 40% under certain situations. Note that maximal sum rate occurs when the relay node is in the middle of the BS and CR 1, i.e., $r = 1$, when EPA is used while it occurs when the relay is slightly closer to CR 1 when the optimal power allocation scheme is used. When the relay is slightly closer to CR 1, lower power can be used by the relay node and higher power can be used by the BS during phase 2 to increase the rate of CR 2. Even though the rate of CR 1 will decrease under this situation, the rate increase of CR 2 is much more than the rate decrease of CR 1. Optimal power allocation scheme can gain from this condition while EPA can not. When the relay moves towards to CR 1, rate degradation of CR 1 is severe and thus, the sum rate
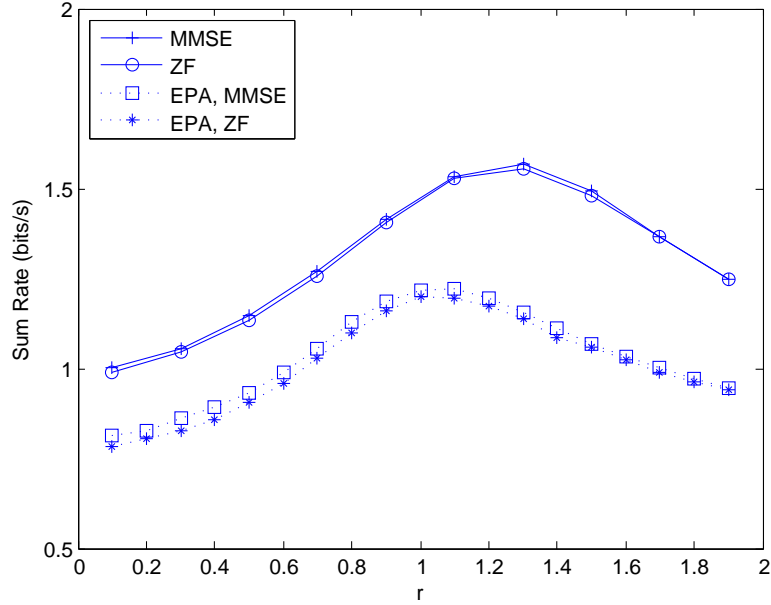
Figure 6.4. Optimized sum rate for different relay locations.

decreases for both schemes.

6.4.1.2 The impact of the PU location

Fig. 6.5 shows the impact of the PU's location on the power allocation results based on the MMSE receiver. Similar results can be obtained for the ZF receiver, which are omitted here. To limit the number of parameters, we move the PU on the *x*-axis for a given *y*. We put the relay node at the middle of the CR BS and CR 1, i.e., at the location $(1, 0)$. The location of the PU node impacts the power allocation solutions through interference constraints. The distances between the PU to the CR BS and the relay node are not large enough when $y = 2$ for different $x \in [-3, 3]$. In this scenario, the interference constraints are active. All three optimal power values first decrease and then increase with *x*, where PU first moves towards the CR BS and the relay node first and then further away from them. The PU is far from the CR BS and the relay node when $y = 5$. The optimal powers at the relay node and the CR BS for phase 2 increase compared to the values for $y = 2$. Moreover, the optimal powers used by each node depend only on the structure of the CR network, and thus, they all keep same for different *x*.
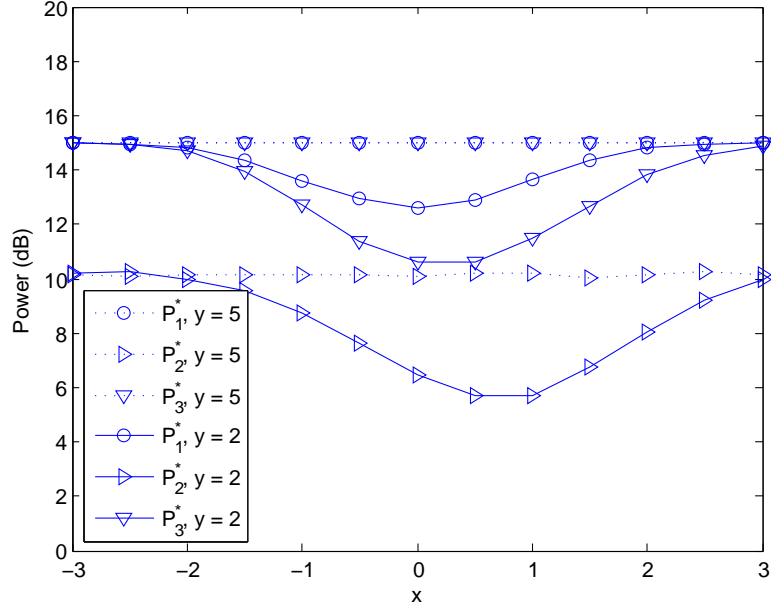
Figure 6.5. Optimized power solution for different PU locations.

The comparisons between the sum rates under optimized power allocation and EPA are shown in Fig. 6.6. Due to the impact of interference constraints, both curves decrease first and then increase with x when $y = 2$. When $y = 5$, the interference constraints are inactive, and thus, both of the curves keep same for different x. Compared to EPA, much more performance gains can be obtained when PU is close to the CR network.

6.4.2 Power Allocation With Sum Power Constraint

Fig. 6.7 shows the sum power results for both CR users for different sum power thresholds: 15 dB and 12 dB, and without total power constraint, i.e., $P_t = +\infty$. The results are based on the MMSE receiver with $r = 1$, $y = 2$. When P_t is large, it is equivalent to the results without sum power constraint. With the decrease of the sum power threshold, P_t, the sum power used by CR 1 decreases while the sum power used by CR 2 increases. Thus, we can adjust the sum power threshold according to the locations of the nodes to make the powers used by both CR users on the same level, leading to fair power allocation results.

Fig. 6.8 shows the optimized power results for different sum power constraints. To show the impact, we put the PU far from the CR network to inactivate the interference
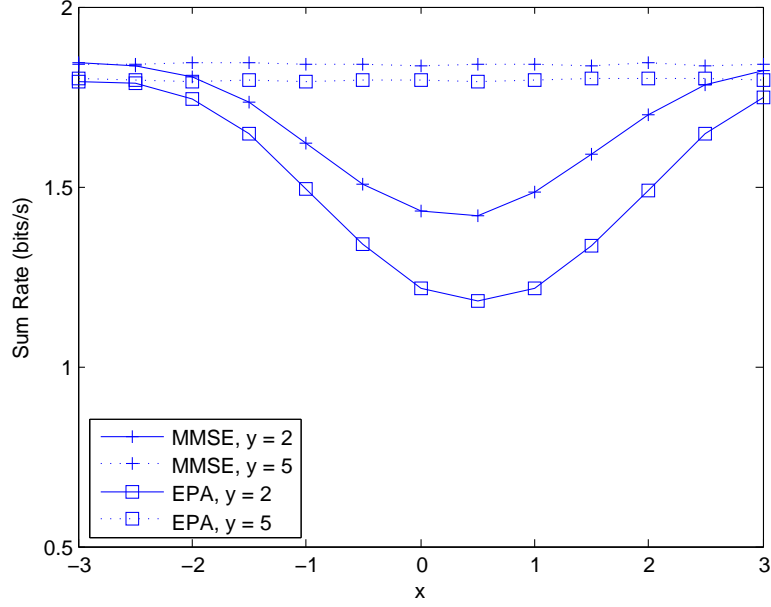
Figure 6.6. Sum rate for different PU locations.

constraint. Moreover, the results are based on the MMSE receiver with $r = 1$. From the figure, we can see that the impact of the sum power constraint is negligible for CR 2, P_3^*, since P_3 is independent of the sum power constraint when the interference constraint is inactive. With active interference constraint, the power used for transmitting data to CR 2, P_3^*, will slightly decrease due to the increase of power used by the relay node during phase 2. For CR 1, powers used during both phases 1 and 2 increase with P_t. The results will converge to the case without sum rate constraint. To show the impact of sum power constraint on the rate for both user, we provide the results in Fig. 6.9. The rate of CR 1 increases with P_t while the rate of CR 2 decreases. Besides adjusting the sum power used by both users, our scheme with sum power constraint can also be used to adjust the rate for both users.

6.5 Conclusions

In this chapter, we investigate an underlay CR network with direct and relay-aided transmissions. We first investigate power allocation to maximize the overall rate performance
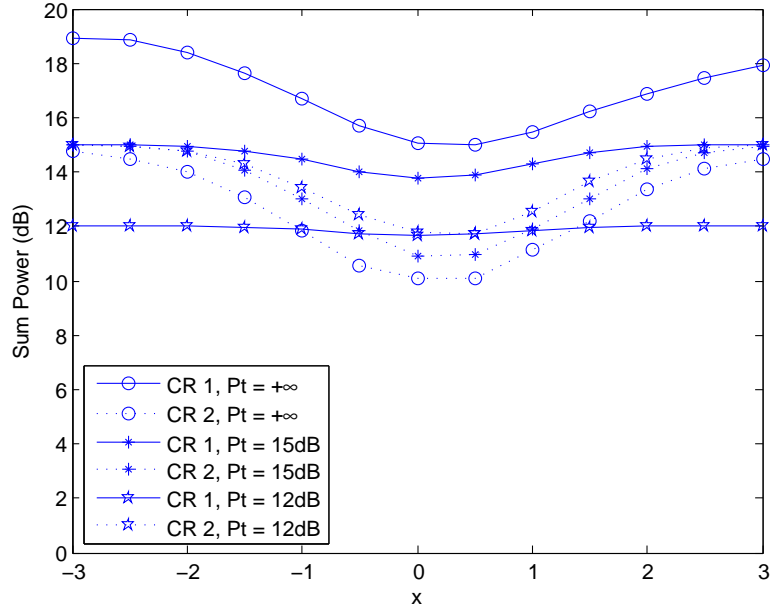
Figure 6.7. Sum power comparison between two CR users for different P_t.

of the CR network while keeping the interference to the PU under a tolerable level. Theoretical analysis has been provided for the optimum results. By taking the fairness between two CR users into consideration, we then address power allocation with an additional sum power constraint. It is shown by numerical results that the locations of different nodes have severe impact on the solution. Without sum power constraint, the relay node can be put slightly closer to the aided user than to the BS to get best system performance. With sum power constraint, fair power allocation between two CR users can be achieved by adjusting sum power threshold. Moreover, rate fairness can be also obtained through adjusting sum power threshold. In a system with multiple relays, our proposed power allocation scheme can be used to choose the best relay. Moreover, the studied network can be treated as a basic block for multi-user systems where we can pair up users first and then allocate power within them.
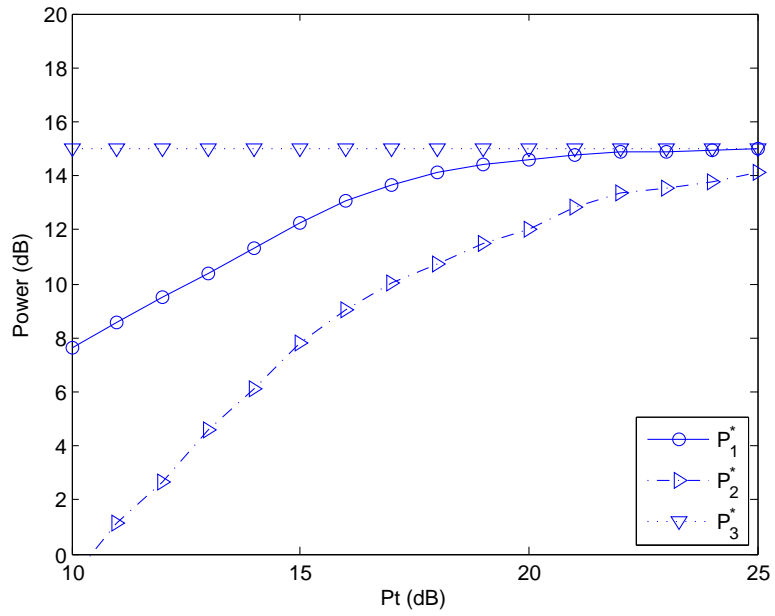
Figure 6.8. Optimized power for different P_t.
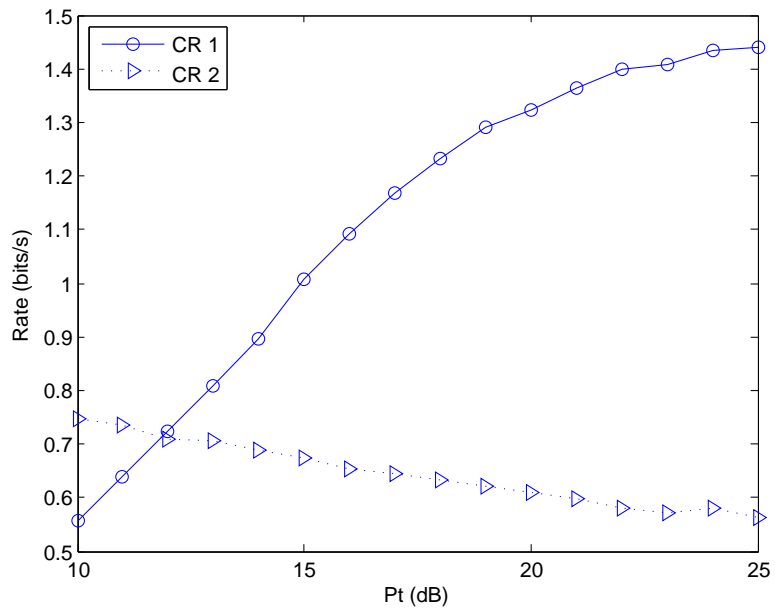
Figure 6.9. Rate comparison between two CR users for different P_t.

CHAPTER 7

GRAPH-BASED ROBUST RESOURCE ALLOCATION FOR COGNITIVE RADIO NETWORKS

In this chapter, stable resource allocation based on graph theory is investigated, which takes all users' preferences into account. Here, we focus on improving robustness of the stable resource allocation. A truncated scheme generating almost stable matchings is first investigated. Based on the properties of the truncated scheme, two types of edge-cutting algorithms, called *direct edge-cutting* (DEC) and *Gale-Shapley based edge-cutting* (GSEC), are developed to improve resource allocation robustness to the channel state information variation. To mitigate the problem that certain SUs may not be able to find suitable resources after edge-cutting, *multi-stage* (MS) algorithms are then proposed. Numerical results show that the proposed algorithms are robust to the channel state information variation.

The rest of this chapter is organized as follows. In Section 7.1, we introduce the system model. In Section 7.2, resource allocation based on stable matching is discussed. In Section 7.3, a truncated algorithm guaranteeing almost stable matching is investigated. Two types of edge-cutting algorithms are proposed in Section 7.4. In Section 7.5, multi-stage algorithms are developed. Numerical results are provided in Section 7.6 to show the impact of different system parameters on the performance of the developed algorithms. Finally, Section 7.7 concludes the chapter.

7.1 System Model

We consider an underlay CR network with multiple channels/bands, where PUs have priorities to use N spectrum channels/bands while M SU pairs want to transmit simultaneously. All channels are modeled as Rayleigh block fading channels. Without loss of generality, we assume the j-th PU uses the j-th spectrum band. As shown in Fig. 7.1, the channel between the i-th SU pair on the j-th spectrum band and the interference channel from the

i-th SU transmitter to the *j*-th PU receiver are denoted as $h_{i,j}$ and $g_{i,j}$, respectively. The transmit power of the *i*-th SU transmitter on the *j*-th spectrum band is $P_{i,j}$. The noise power on all spectrum bands is assumed to be the same, denoted as σ^2. A centralized system is assumed, where the control center with CSI allocates resources. Furthermore, the control center will only assign a frequency band to a SU pair when the corresponding CSI is available, including both CSI between the SU pairs and of the interference channel from the SU transmitter to the PU receiver. Correspondingly, the number of spectrum bands available for the *i*-th SU pair is denoted as $\Delta_{s,i}$ and the number of SU pairs available for the *j*-th spectrum band is denoted as $\Delta_{p,j}$. We consider the scenario that only one SU pair is allowed on each spectrum band and each SU pair can only access at most one spectrum band.

j-th PU receiver

j-th PU transmitter

j-th PU link

$g_{i,j}$ interference channel gain

$I_{j,i}^{p}$ interference power

i-th SU transmitter $h_{i,j}$ SU link channel gain

i-th SU link on the *j*-th band

i-th SU receiver
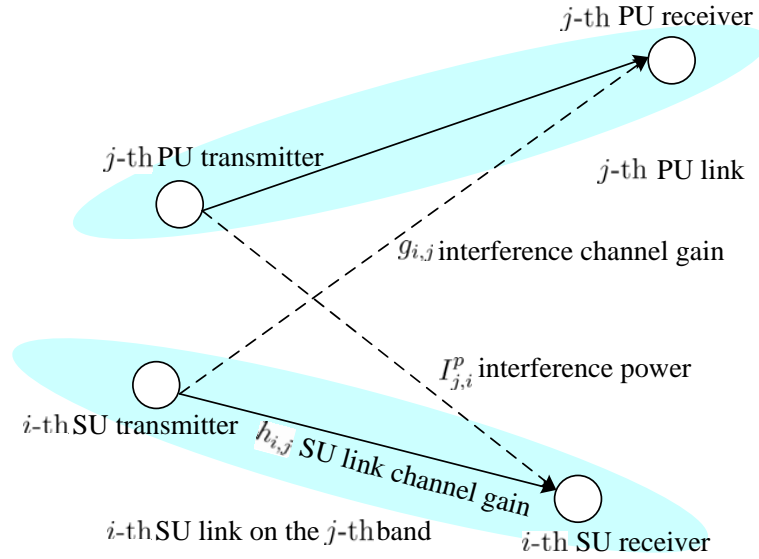
Figure 7.1. Spectrum underlay system model.

To protect the PUs, the interference power generated by the SU pairs on the *j*-th spectrum band should be below a given threshold, that is,

$$I_{i,j} = P_{i,j}|g_{i,j}|^2 \leq I_{th}, \quad \forall i, j, \tag{7.1}$$

where I_{th} is the interference threshold[1]. Moreover, due to the amplifier capacity limit, each

---

[1] Without loss of generality, we assume, for simplicity, that the interference threshold is the same on all

SU transmitter has a peak transmit power constraint, P, that is,

$$P_{i,j} \leq P, \quad \forall i. \tag{7.2}$$

If the i-th SU pair is assigned to the j-th spectrum band, its throughput can be expressed as

$$R_{i,j} = \log_2 \left(1 + \frac{|h_{i,j}|^2 P_{i,j}}{\sigma^2 + I_{j,i}^p} \right), \tag{7.3}$$

where $I_{j,i}^p$ denotes the interference from the j-th PU transmitter to the i-th SU receiver. We assume that the interference powers, $I_{j,i}^p$, are known since the PUs' transmit powers remain the same with or without SU pairs' transmission and, hence, $I_{j,i}^p$ can be estimated in advance.

When performing resource allocation to the SU pairs, we also consider benefits to PUs by incorporating the concept of spectrum trading into the utility function design [84]. PUs will charge more from the SU pairs for providing better service. On the other hand, the performance of PUs will degrade if SU pairs generate strong interference. Therefore, while SU pairs improve their own performance by increasing their transmit powers, they should also get penalties for generating stronger interference. As in [90] and [91], to capture such features of both PUs and SU pairs, if the i-th SU pair uses the j-th spectrum band, the utility can be defined as a linear combination of the throughput of the i-th SU pair, $R_{i,j}$, and the interference generated to the j-th PU, $I_{i,j}$, expressed as

$$w_{i,j}(P_{i,j}) = c_s R_{i,j} - c_p I_{i,j}, \tag{7.4}$$

c_s and c_p are weight factors.

The transmit power, $P_{i,j}$, can be optimized to maximize the utility function in (7.4) subject to constraints (7.1) and (7.2). Since the utility function in (7.4) is a concave function of $P_{i,j}$, the optimal transmit power, $P_{i,j}^*$, is

$$P_{i,j}^* = \left(\min \left\{ \frac{c_s}{c_p |g_{i,j}|^2} - \frac{\sigma^2 + I_{j,i}^p}{|h_{i,j}|^2}, P, \frac{I_{th}}{|g_{i,j}|^2} \right\} \right)^+, \tag{7.5}$$

---

the spectrum bands . The results can be directly extended to the system with different interference thresholds on different spectrum bands.

where $(x)^+ = \max\{0, x\}$. Then, if the i-th SU pair is allocated on the j-th spectrum band to transmit, the utility value of the i-th SU pair and the j-th PU can be expressed as $w_{i,j}(P_{i,j}^*)$.

Even though (7.4) is used for resource allocation in this chapter, the approaches developed here can easily be adapted for other utility functions.

7.2   Resource Allocation Based on Stable Matching

As indicated before, we will focus on resource allocation based on graph theory by taking preferences of both PUs and SU pairs into account. We first describe our resource allocation scheme based on stable matching [92] and then discuss its properties.

Stable matching based resource allocation can be described with the help of a *bipartite* graph, say G, with bipartition, V_1, V_2. See Fig. 7.2, where nodes in V_1 represent SU pairs and nodes in V_2 represent spectrum bands/PUs. As in Section 7.1, the sizes of V_1, V_2 are denoted as M, N, respectively. An edge is put between the i-th SU pair in V_1 and the j-th PU in V_2 if the CSI of the i-th SU pair on the j-th spectrum band is known at the control center. Then, the common utility value of the i-th SU pair and the j-th PU, $w_{i,j}(P_{i,j}^*)$, is assigned to the corresponding edge.
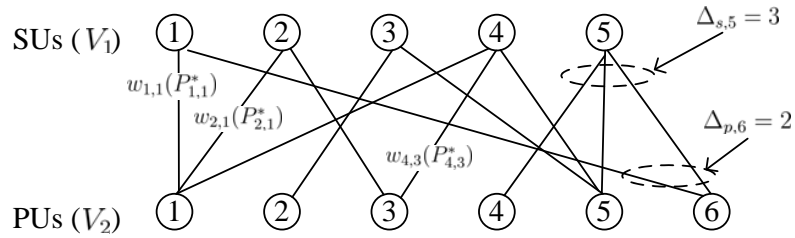
Figure 7.2. Bipartite graph illustration with $M = 5$ and $N = 6$.

To define the preference lists for all SU pairs and PUs, we can regard G as a *complete* bipartite graph, i.e., every node in V_1 is connected to every node in V_2, by setting $w_{i,j}(P_{i,j}^*) = -\infty$ if the CSI of the i-th SU pair on the j-th spectrum band is not available. Furthermore, we assume that the numbers of spectrum bands/PUs and SU pairs are equal, i.e., $M = N$. If the number of SU pairs exceeds the number of spectrum bands, i.e., $M > N$, we can add $(M - N)$ virtual spectrum bands/PUs and edges between all these virtual PUs and all the

SU pairs, and set the weights on these new edges to $-\infty$. Similar operation can be done when the number of spectrum bands exceeds the number of SU pairs.

The preference list for the i-th SU pair is defined as

$$\mathcal{L}_i^s = [j_1, ..., j_N], \tag{7.6}$$

where $j_1, ..., j_N$ is a permutation of $1, ..., N$ satisfying

$$w_{i,j_1}(P_{i,j_1}^*) \leq ... \leq w_{i,j_N}(P_{i,j_N}^*). \tag{7.7}$$

Similarly, the preference list for the j-th PU is defined as

$$\mathcal{L}_j^p = [i_1, ..., i_M], \tag{7.8}$$

where $i_1, ..., i_M$ is a permutation of $1, ..., M$ satisfying

$$w_{i_1,j}(P_{i_1,j}^*) \leq ... \leq w_{i_M,j}(P_{i_M,j}^*). \tag{7.9}$$

Our resource allocation procedure will depend on the preference lists of both SU pairs and PUs. To exploit stable matching from graph theory for resource allocation, more definitions are needed. A *matching* in a bipartite graph is a set of pairwise non-adjacent edges. Given a matching in a bipartite graph with partition sets V_1 and V_2, with V_1 (respectively, V_2) consisting of nodes represent SU pairs (respectively, PUs), if an SU pair is matched with a band/PU, we may allocate that band/PU to that SU pair. Hence, a matching in such a bipartite graph naturally gives a resource allocation in which each spectrum band has at most one SU pair and each SU pair accesses at most one spectrum band. We call a matching in a graph *perfect* if all the nodes in the graph are matched.

An edge in the bipartite graph, G, between the i-th SU pair and the j-th PU, denoted as (s_i, p_j), where s_i and p_j denote the i-th SU pair and the j-th PU, respectively, is said to be *unstable* relative to a matching $\mathcal{M}$ in G, if

1. $(s_i, p_j) \notin \mathcal{M}$,

Table 7.1. The Gale-Shapley Preference-based Channel Allocation Algorithm

 1: Initialize all the SU pairs and PUs to be free.
 2: Each PU asks its most preferred SU pair which has not rejected it yet.
 3: **if** Each SU pair receives exactly one request from the PUs. **then**
 4:   Stop and output the results as the channel allocation result.
 5: **else**
 6:   Every SU pair receiving more than one requests chooses the PU that is highest on its preference list and rejects the other PUs.
 7: **end if**
 8: **if** All PUs have proposed to all SU pairs. **then**
 9:   Stop and output the results as the channel allocation result.
10: **else**
11:   Goto Step 2.
12: **end if**

2. s_i is unmatched by $\mathcal{M}$, or prefers p_j over its current match in $\mathcal{M}$, and

3. p_j is unmatched by $\mathcal{M}$, or prefers s_i over its current match in $\mathcal{M}$.

If there is no unstable edges relative to the matching, $\mathcal{M}$, then it is called *stable*.

Based on the above definition, it is desirable to find a resource allocation that corresponds to a stable matching. This can be done by using the GS algorithm [57]. In Table 7.1, we give a version of the GS algorithm in which PUs propose to SU pairs (see Step 2). However, the roles of PUs and SU pairs can be exchanged. So the GS algorithm can be presented in which SU pairs propose to PUs. Here, we focus on the PU-proposing version of the GS algorithm as shown in Table 7.1.

By applying the PU-proposing version of the GS algorithm in Table 7.1, we have the following result (see [57]).

Lemma 7.1 *For the complete bipartite graph in which the number of SU nodes equals the number of PU nodes, the PU-proposing version of the GS algorithm generates a perfect stable matching. Moreover, for this matching, each PU is matched to the best possibility among all stable matchings, and each SU pair is matched to the worst possibility among all stable matchings.*

According to Lemma 7.1, we know that, if we apply the version of the GS algorithm in Table 7.1, each PU will be matched to the best possibility among all stable matchings. That means, the weight in the resulting stable matching for each PU is maximum among all the stable matchings. Thus, the sum or average weight of the matching must be the maximum among all the stable matchings [57].

Theorem 7.1 *Let G be a complete bipartite graph with partition sets V_1, V_2 such that V_1 (respectively, V_2) consists of SU (respectively, PU) nodes. Define the weight on edges according to (7.4) and (7.5), and define preference lists of nodes according to (7.6) – (7.9). Then, the GS algorithm in Table 7.1 produces a stable resource allocation that has maximum sum or average weight among all possible stable resource allocations.*

As we pointed out before, there are two versions of GS algorithms, the PU- and the SU-proposing ones. In general, the PU- and SU-proposing versions may provide different matching results. Next, we show that, for our studied scenario, the stable matching produced by the version in Table 7.1 is unique, regardless of PU- or SU-proposing algorithm is used. By Lemma 7.1, SU pairs are matched to the worst possibility among all stable matchings after applying the PU-proposing version of the GS algorithm. On the other hand, if we apply the SU-proposing version of the GS algorithm, SU pairs will be matched to the best possibility among all stable matchings [57]. Since the weights on the edges are the same for both SU-proposing and PU-proposing versions, the maximum sum weight among all possible stable matchings is uniquely determined no matter which version of the GS algorithm we use. Hence, the best possibility and the worst possibility for each SU pair among all stable matchings are the same. Thus, we have

Theorem 7.2 *The stable matching produced in the Theorem 7.1 is unique.*

The conclusion on uniqueness in Theorem 7.2 is the same as in [93]; but the procedure used there is different from the above. Note that, for our scenario, this uniqueness conclusion implies that the same allocation results are obtained regardless of which version of GS

algorithm is applied.

Note that Theorem 7.2 holds if (7.4) is replaced by a different utility function, as long as the preference lists of SU pairs and PUs are calculated from the weight function on the edges.

7.3   Almost Stable Resource Allocation

In the previous section, we proposed a stable resource allocation scheme based on the GS algorithm and discussed some of its properties. However, the stable matching results need not be robust to CSI variation. In fact, CSI variation of one channel may lead to a totally different stable matching result, which is not desirable in practice, especially when the number of nodes in the system is large. To measure the system robustness, we use the amount of variation of the resource allocation after CSI variation as a metric. Based on our definition, with CSI variation, the larger the resource allocation variation is, the less robust the system is to the CSI variation and vice versa.

To improve the robustness of the resource allocation scheme with respect to CSI variation, we consider a truncated GS algorithm. Instead of executing the GS algorithm fully to get a stable resource allocation, the truncated GS algorithm outputs a resource allocation result after executing a fixed number of rounds in the GS algorithm. Note that the GS algorithm, as in Table 7.1, consists of a number of asking-accepting/rejecting rounds; during each round the PUs propose to the SU pairs and the SU pairs answer the proposals. Denote by T the number of rounds we execute the algorithm. From [94], based on the truncated GS algorithm, a change of CSI of one node will only affect the part of resource allocation within distance $2T$ from the node of the change. Comparing to the stable resource allocation, where a change of CSI of one node may affect all nodes in the system, allocation based on the truncated GS algorithm should be much more robust to the CSI variation.

The resulting resource allocation from the truncated GS algorithm may be unstable. To measure the stability of such resource allocation, we introduce the concept of ϵ-stable (or

almost stable) matching. Let $\epsilon > 0$ be given. The matching, $\mathcal{M}$, in the graph, G, is said to be ϵ-*stable* if the number of unstable edges in G is at most $\epsilon|\mathcal{M}|$, where $|\mathcal{M}|$ is size of $\mathcal{M}$. Let Δ be the maximum degree of nodes (i.e., $\Delta = \max\{\Delta_{s,i}, \Delta_{p,j}\}$, $\forall i, j$, where $\Delta_{s,i}, \Delta_{p,j}$ are the numbers of edges at the i-th SU pair and the j-th PU, respectively). For the ϵ-stable matching, we have the following theorem from [94]:

Theorem 7.3 *By executing at most $2 + \Delta^2/\epsilon$ rounds of the GS algorithm, we can find an ϵ-stable resource allocation.*

The detailed proof for Theorem 7.3 can be found in [94]. Based on the procedure in [94], we can further bound the number of execution rounds by using $\Delta_s = \max\{\Delta_{s,i}\}$, the maximum degree among the nodes representing SU pairs only.

Theorem 7.4 *By executing at most $2 + \Delta_s^2/\epsilon$ rounds of the GS algorithm, we can find an ϵ-stable resource allocation.*

Our proof of Theorem 7.4 follows the same procedure as that of Theorem 7.3 by using the maximum degree among nodes for SU paris, Δ_s, instead of the maximum degree of all nodes, Δ. It is clear that $\Delta_s \leq \Delta$. Hence, in practical scenarios, the bound in Theorem 7.4 is tighter than the bound in Theorem 7.3 from [94].

Besides the stability property, we also concern about the utility of resource allocation. Given one resource allocation, $\mathcal{M}$, its utility, denoted as $w_{\mathcal{M}}$, is defined as the sum utilities of PUs/SU pairs in $\mathcal{M}$. Let $\mathcal{S}$ denote the stable resource allocation produced by the GS algorithm, with $w_{\mathcal{S}}$ as the corresponding utility. A resource allocation, $\mathcal{M}$, is a $(1 + \epsilon)$-*approximation* of the maximum-weight stable matching if its utility, $w_{\mathcal{M}}$, satisfies $(1 + \epsilon)w_{\mathcal{M}} \geq w_{\mathcal{S}}$. For the truncated GS algorithm, we have the following conclusion regarding its utility and the detailed proof is in the Appendix D.1.

Theorem 7.5 *By executing at most $2 + \Delta_s/\epsilon$ rounds of the GS algorithm, we can find a $(1 + \epsilon)$-approximation of the maximum-weight stable resource allocation.*

In [94], the result based on the truncated GS algorithm is compared with the maximum-weight resource allocation (instead of stable resource allocation). For the scenario studied by us, it is more reasonable to compare the result from truncation with other stable resource allocation.

The robustness of the resource allocation from the truncated GS algorithm is affected by T, the number of rounds the GS algorithm is executed. A change in the bipartite graph only affects the result in the radius-$2T$ neighbourhood of the changing point, instead of the whole resource allocation result [94]. Theorems 7.4 and 7.5 provide upper bounds on T to achieve ϵ-stability and $(1 + \epsilon)$-approximation of the maximum-weight stable resource allocation, respectively. Both bounds depend only on ϵ and Δ_s. Given ϵ, decreasing Δ_s is expected to help decrease the required number of executing rounds, T. From these observations, several algorithms for decreasing Δ_s are developed in the next section in order to achieve robust designs.

7.4 Edge-Cutting for Robust Design

Based on our discussion in the previous section, the robustness of resource allocation obtained from the truncated GS algorithm depends on the number of rounds, say T, of the GS algorithm that we execute. Smaller T leads to higher robustness. Since the smallest T to achieve ϵ-stability or $(1 + \epsilon)$-approximation depends on the instantaneous CSI, we instead focus on reducing the upper bounds on T.

From Theorems 7.4 and 7.5, the upper bounds on T to achieve ϵ-stability or $(1 + \epsilon)$-approximation are related to Δ_s, the maximum number of available bands of any SU pair. Both bounds can be decreased by decreasing Δ_s. Thus, to improve robustness of resource allocation, a small Δ_s is preferable. It is possible that SU pairs only access CSI of a small number of PU bands, and Δ_s is small naturally. However, PUs, in order to improve their own utilities, may be willing to share their information to attract more SU pairs, as in the spectrum trading scenario [84]. In this case, the maximum number of bands available at

SU pairs, Δ_s, may be large. Note that, the number of available bands for the i-th SU pair is the number of edges connected to it in the constructed bipartite graph.

For robust design, we propose edge-cutting algorithms to decrease the maximum number of edges connected to SU pairs, Δ_s. In other words, if the number of available bands at the i-th SU pair, $\Delta_{s,i}$, is larger than a given threshold, denoted as Δ_c^{max}, it will be asked to give up some bands before performing resource allocation. In the following, two different types of edge-cutting algorithms will be developed: *direct edge-cutting* (DEC) that cuts edges based on the preference lists, and *GS-Based Edge-Cutting* (GSEC) that cuts edges based on the GS algorithm.

7.4.1 Direct Edge-Cutting (DEC)

In this part, we propose ways to delete edges according to the preference lists of SU pairs and/or PUs. We will first describe a general approach that depends on a parameter $p \in [0, 1]$, and we get two special approaches by letting $p = 0$ or 1.

For the edge, (s_i, p_j), between the i-th SU pair s_i and the j-th PU p_j, let $t_{i,j}^p = k$ if s_i is the k-th element on p_j's preference list, and $t_{i,j}^s = l$ if p_j is the l-th element in s_i's preference list. We set a preference value on the edge (s_i, p_j) as a convex combination of $t_{i,j}^p$ and $t_{i,j}^s$, which can be expressed as $t_{i,j} = pt_{i,j}^s + (1-p)t_{i,j}^p$, where $0 \le p \le 1$. We let each SU pair keep Δ_c^{max} (a fixed constant) edges that have the highest preference values. So in the resulting graph, each SU pair is incident with precisely Δ_c^{max} edges. We call this process *SP-preferred DEC* (SP-DEC) algorithm, as it can be based on the preference lists of both SUs and PUs. The weight factors can be adjusted according to the priorities in the preference lists of SU pairs and PUs. We consider two extreme cases: $p = 1$ and 0.

When $p = 1$, then SP-DEC keeps Δ_c^{max} edges at each SU pair that is at the top of its preference list; this approach is called *SU-preferred DEC* (S-DEC) as it only takes SU's preference lists into consideration.

When $p = 0$, then SP-DEC keeps Δ_c^{max} edges at each SU pair with the highest preference values (we can randomly choose the edges that have same preference value), and those

edges occur at the top of PUs' preference lists; this approach is called *PU-preferred DEC* (P-DEC) as it takes PUs' preference lists into consideration.

7.4.2 GS-based Edge-Cutting (GSEC)

The DEC procedures described above reduce the maximum number of edges connected to the SU pairs, and are easy to implement. However, they do not take the original GS matching process into account. Hence, the resource allocation results obtained from the GS algorithm after the DEC procedures may be quite different from the result obtained by applying the GS algorithm on the original graph. Moreover, it is possible that certain SU pairs with similar preference lists will compete with each other, so there is a chance that some of them are not allocated any resource.

For instance, consider a system with two PUs, p_1 and p_2, and two SU pairs, s_1 and s_2, where both p_1 and p_2 prefer s_1 to s_2, and both s_1 and s_2 prefer p_1 to p_2. Applying the GS algorithm in Table 7.1, s_1 is assigned to p_1, and s_2 is assigned to p_2. However, the result can be different if we apply the GS algorithm after a DEC procedure. Set $\Delta_c^{max} = 1$, so that the maximum number of edges connected to each SU pair is one. Applying S-DEC, we obtain a graph in which both s_1 and s_2 are connected to p_1, but not to p_2. Then applying the GS algorithm to the new graph, s_1 is allocated to the channel of p_1, but s_2 cannot transmit.

In order to use DEC to obtain a resource allocation result closer to the result obtained by applying the GS algorithm, we propose an edge-cutting algorithm based on the GS algorithm (GSEC algorithm). In general, the edges involved in the first few rounds of the GS algorithm will be kept. However, minor changes are made to satisfy the requirement on the maximum number of edges connected to each node representing an SU pair. In order to make sure the maximum number of edges connected to each SU pair is Δ_c^{max}, each SU pair can reject at most $\Delta_c^{max} - 1$ edges during the GS process. We now describe the GSEC algorithm. See Table 7.2.

First, a vector $\mathbf{d} \in \mathbb{N}^M$ is used in which the ith coordinate, d_i, records the number of edges rejected by the ith SU pair, s_i. Initially $d_i = 0$ for all i, and all SU pairs are involved.

During each round of the GS algorithm in Table 7.1, each PU asks its most preferred SU pair. At the end of a round, increase d_i by the number of edges/PUs rejected by s_i during this round, and update $\mathcal{P}_i$, the set of the indices of the PUs who have asked s_i during this round. There are three cases after executing a particular round of the GS algorithm: $d_i < \Delta_c^{max} - 1$, $d_i = \Delta_c^{max} - 1$, and $d_i > \Delta_c^{max} - 1$.

If $d_i < \Delta_c^{max} - 1$, then the number of PUs rejected by s_i has not reached the limit; in this case, keep all edges between s_i and the PUs with indices in $\mathcal{P}_i$, and s_i remains in the process for the next round.

If $d_i = \Delta_c^{max} - 1$ then the number of PUs rejected by s_i reaches the limit; keep all edges between s_i and the PUs with indices in $\mathcal{P}_i$, but s_i is removed from the process.

Now assume $d_i > \Delta_c^{max} - 1$. Then the number of PUs rejected by s_i exceeds the limit. So s_i will be removed from the process. To meet the requirement that $d_i \leq \Delta_s - 1$, we remove $d_i - (\Delta_c^{max} - 1)$ PUs with indices in $\mathcal{P}_i$. There are different ways to remove PUs with indices in $\mathcal{P}_i$. A natural way is to remove those $d_i - (\Delta_c^{max} - 1)$ PUs with the lowest ranks in the preference list of s_i. Thus, the process keeps the PUs on the top of s_i's preference list, and it is independent of other PUs and SU pairs.

The GSEC process stops when all SU pairs are removed from the process or when the GS algorithm stops. It is possible that the GS algorithm stops before all SU pairs are removed. In this case, all PUs and SU pairs are matched. If this case occurs, $\Delta_c^{max} - 1 - d_i$ edges can be added for each s_i that is still in the process.

Therefore, when the GSEC process stops, each SU pair will have Δ_c^{max} edges. The detailed algorithm is given in Table 7.2. Note that, during the process of the GSEC, a matching will be generated as well. This matching will be the same as the one if we execute the GS algorithm on the bipartite graph from the GSEC. Thus, we can use the matching generated from the GSEC directly for resource allocation without running the GS algorithm again.

To illustrate the difference between GSEC and DEC, we apply GSEC algorithm to the

Table 7.2. Gale Shapley based Edge-Cutting Algorithm

1: Initialize all SUs and PUs to be free. Define a vector $\mathbf{d} \in \mathbb{N}^M$ as an indicator with the i-th coordinate d_i recording the number of PUs rejected by s_i, the i-th SU pair. Set $d_i = 0$ for $i = 1, ..., M$. Define a vector $\mathbf{m} \in \mathbb{N}^M$ with the i-th element $m(s_i)$ recording the indices of the PUs connected to s_i. Initialize $m(s_i) = 0$ for $i = 1, ..., M$. Let $\mathcal{A}$ denote the indices of SU pairs which are available and initialize $\mathcal{A} = \{1, ..., M\}$. Define $\mathbf{E} \in \mathbb{N}^{M \times N}$ to record the edges that remain after edge-cutting. Set $e_{i,j} = 1$ if the edge between s_i and the j-th PU is kept. Initialize $\mathbf{E}$ to be a zero matrix.

2: Each PU asks its most preferred SU with indices in $\mathcal{A}$ that has not rejected it.

3: **for** $i \in \mathcal{A}$ **do**

4:     Let $\mathcal{P}_i$ denote the set of the indices of those PUs which have proposed to s_i during this round.

5:     **if** s_i is not proposed, $\mathcal{P}_i = \emptyset$ **then**

6:         Do nothing.

7:     **else if** s_i is only proposed by one PU, say the j-th PU and $m(s_i) = 0$ **then**

8:         Accept the j-the PU and set $e_{i,j} = 1$.

9:     **else**

10:         **if** $m(s_i) \neq 0$ **then**

11:             $\mathcal{P}_i = \mathcal{P}_i \cup m(s_i)$

12:         **end if**

13:         Accept the PU in $\mathcal{P}_i$ that is highest on s_i's preference list.

$$m(s_i) = \arg \max_{j \in \mathcal{P}_i} w_{i,j}(P^*_{i,j}).$$

        Increase d_i by the number of PUs rejected by s_i during this round, that is $d_i = d_i + |\mathcal{P}_i| - 1$, where $|\mathcal{P}_i|$ denotes the number of elements in $\mathcal{P}_i$.

14:         **if** $d_i \geq \Delta_c^{max} - 1$ **then**

15:             $\mathcal{A} = \mathcal{A} - \{i\}$

16:             **if** $d_i = \Delta_c^{max} - 1$ **then**

17:                 $e_{i,j} = 1$, for $j \in \mathcal{P}_i$.

18:             **else**

19:                 Delete $d_i - (\Delta_c^{max} - 1)$ elements from $\mathcal{P}_i$ that are lowest on s_i's preference list. Then, set $e_{i,j} = 1$, for $j \in \mathcal{P}_i$.

20:             **end if**

21:         **end if**

22:     **end if**

23: **end for**

24: **if** $\mathcal{A} = \emptyset$ **then**

25:     Stop.

26: **else if** All PUs are matched or they have already proposed to all SUs in $\mathcal{A}$ **then**

27:     For $i \in \mathcal{A}$, add $\Delta_c^{max} - 1 - d_i$ edges between s_i and those PUs at the top of s_i's preference list and then stop.

28: **else**

29:     Go to step 3.

30: **end if**

example at the beginning of this subsection. Both PUs, p_1 and p_2, ask the first SU pair, s_1, during the first round. Since the s_1 can only keep $\Delta_c^{max} = 1$ edge and it prefers p_1 over p_2, it keeps only the edge (s_1, p_1), and s_1 leaves the process. In the second round, the second PU, p_2, asks the second SU, s_2, and keeps the edge (s_2, p_2). The GS algorithm stops. (Since both s_1 and s_2 have $\Delta_c^{max} = 1$ edges, no extra edges need to be added.) Based on the graph after GSEC, s_1 will be allocated to the channel of p_1 while s_2 will be on the channel of p_2. This resource allocation result is the same as the original GS algorithm while the maximum number of edges connected to each SU pair is one after the GSEC. Therefore, resource allocation based on the GSEC process might give a result that is closer to the original GS algorithm while reducing the maximum number of edges connected to individual SU pairs.

Remark 1 *Essentially, both DEC and GSEC shorten the preference lists of SU pairs and PUs. Any change on the deleted edges has no impact on the resource allocation results. This also explains why the edge-cutting algorithms improve robustness of the resource allocation.*

Remark 2 *After edge-cutting, some of SU pairs may not be able to find suitable channels. Consider the example at the beginning of Section 7.4.2, only the first SU pair can transmit after DEC while both of them can transmit without edge-cutting. In the next section, a multi-stage edge-cutting algorithm will be proposed to mitigate this problem.*

Remark 3 *In addition to improving the robustness of resource allocation, edge-cutting also reduces the computational complexity.*

7.5   Multi-Stage Edge-Cutting

In the previous section, we proposed two different types of edge-cutting algorithms (DEC and GSEC) to reduce the maximum number of channels available at individual SU pairs after edge-cutting, Δ_c^{max}, to improve the robustness of resource allocation with respect to

the CSI variation. We expect that resource allocation results are more robust when Δ_c^{max} is made smaller. However, if Δ_c^{max} is too small (so the number of channels available at each SU pair is small), some SU pairs may not be able to find suitable channels to transmit. To mitigate this problem, we propose a *multi-stage* (MS) edge-cutting algorithm.

The basic idea of the MS algorithm is to operate the GS algorithm after DEC or GSEC algorithms several times and to adjust the edge-cutting result during the procedure to increase the number of SU pairs that are allocated channels to transmit. The procedure is called MS algorithm, briefly described as follows. First, the DEC or the GSEC algorithm is operated on the original graph and then the GS algorithm. (This is the same as the procedure in Section 7.4.) We then output the corresponding edge-cutting result only for the SU pairs who have been assigned channels. Remove the matched SU pairs, the corresponding matched PU nodes, and the edges among them from the procedure. Denote the sets of remaining SU pairs and PUs as $\mathcal{S}_r$ and $\mathcal{P}_r$, respectively. Note that no SU pair in $\mathcal{S}_r$ was asked by any PUs in the previous stage since if one SU pair was asked, it was assigned a channel and would not be in $\mathcal{S}_r$. Thus, the nodes in $\mathcal{S}_r$ has no impact on the previous stage. Then, we can ignore all previous procedures related to nodes in $\mathcal{S}_r$ and conduct the edge-cutting and the resource allocation again based on the subgraph of the original graph constituting of all nodes in $\mathcal{S}_r \bigcup \mathcal{P}_r$, and corresponding edges. Through this way, the maximum number of edges connected to each SU pair involving in the MS algorithm is still Δ_c^{max}. Repeat the procedure until all nodes are removed. The detailed procedure is given in Table 7.3.

Moreover, like the GSEC algorithm, the MS algorithm will generate a matching during the process. This matching will be the same as the one if we execute the GS algorithm on the output bipartite graph from the MS algorithm and thus, can be used directly for resource allocation.

In general, by using the MS algorithm, the number of SU pairs which can transmit increases while the maximum number of edges connected to each SU pair kept in the graph is still Δ_c^{max}.

Table 7.3. Multi-stage Edge-Cutting Algorithm

1: Initialize the input graph (V_1^i, V_2^i, E^i) as $V_1^i \leftarrow V_1$, $V_2^i \leftarrow V_2$ and $E^i \leftarrow E$, where V_1, V_2, and E denote all SU pairs, PUs, and all edges among them, respectively, from the original graph. Initialize the output graph (V_1^o, V_2^o, E^o) to be empty.

2: The DEC or GSEC algorithm is conducted on (V_1^i, V_2^i, E^i) to reduce the number of edges connected to individual SU pairs. The resulting graph is denoted as (V_1^e, V_2^e, E^e), where V_1^e, V_2^e, and E^e denote the SU pairs, PUs and the remaining edges among SU pairs and PUs after edge-cutting on (V_1^i, V_2^i, E^i), respectively.

3: The GS algorithm is operated on (V_1^e, V_2^e, E^e).

4: **if** Each SU pair is allocated a channel for transmission, **then**

5:     Stop the algorithm and set the output graph (V_1^o, V_2^o, E^o) as $V_1^o \leftarrow V_1^o \cup V_1^e$, $V_2^o \leftarrow V_2^o \cup V_2^e$, and $E^o \leftarrow E^o \cup E^e$

6: **else**

7:     Let $\mathcal{S}_r$ denote the set of indices of those SU pairs which are not yet assigned a channel, and $\mathcal{P}_r$ denote the set of indices of those PUs which have no matched SU pair. Update $V_1^o \leftarrow V_1^o \cup (V_1^e - \mathcal{S}_r)$, $V_2^o \leftarrow V_2^o \cup (V_2^e - \mathcal{P}_r)$, and add edges among $V_1^e - \mathcal{S}_r$ and $V_2^e - \mathcal{P}_r$ in E^e to E^o.

8:     Update $V_1^i \leftarrow \mathcal{S}_r$, $V_2^i \leftarrow \mathcal{P}_r$, and E^i as the edges among $\mathcal{S}_r$ and $\mathcal{P}_r$ based on the original graph (V_1, V_2, E). The preference list of each member of $V_1^i \cup V_2^i$ will simply be the restriction of the original preference list to $V_1^i \cup V_2^i$.

9:     **if** All nodes have empty preference list, **then**

10:       Stop the algorithm.

11:     **else**

12:       Go to item 2.

13:     **end if**

14: **end if**

7.6 Numerical Results

In this section, numerical results are presented to show the performance of the proposed algorithms in the application scenario where the number of users is large and the number of channels with CSI variation is small. Here, we consider the case with 200 SU pairs and 200 PUs, i.e., $M = N = 200$ and assume all CSI is known. Results are averaged after 20,000 trials. For each trial, algorithms are executed once based on the original CSI and then, conducted second time by changing CSI of 5 SU pairs. The utility gap shown in Figs. 7.3(b), 7.4(b), and 7.5(b) is defined as $(w_S - w)/w_S$, where w_S is the sum utility based on the GS algorithm and w is the utility based on the proposed algorithm. The SU allocation variation is defined as the number of SU pairs with different allocation results after CSI change. The SU allocation variation saving in Figs. 7.3(a), 7.4(a), and 7.5(a) is the relative value compared to the GS algorithm. We also show the allocation difference between each proposed algorithm and the GS algorithm, which is defined as the number of SU pairs with different allocation results between a proposed algorithm and the GS algorithm. For a resource allocation scheme, smaller resource allocation variation means higher robustness to the CSI variation. For all results, we set the *signal-to-noise ratios* (SNRs) between any SU pair and any interference channel from SU transmitter to the PU receiver as $0dB$ and $-10dB$, respectively. Interference threshold is $-10dB$ and the maximum transmit power is $10dB$.

7.6.1 Single-Stage Truncation or Edge-Cutting

Figs. 7.3(a) and 7.3(b) show the impact of the maximum number of available bands for each SU pair, Δ_c^{max}, on allocation variation saving and utility, where $\epsilon = 0.1$. Fig. 7.3(a) shows that the reduction in Δ_c^{max} increases the robustness of resource allocation for all edge-cutting algorithms. Even though smaller Δ_c^{max} leads to a larger utility gap from the GS algorithm as shown in Fig. 7.3(b), the saving on SU allocation variation is significant compared to that of the utility gap.

Next, let us compare the performance of the truncated GS algorithm and the edge-cutting algorithms. Fig. 7.3(a) shows that when Δ_c^{max} is small, the edge-cutting algorithms may provide higher resource allocation robustness than the truncated GS algorithm. When Δ_c^{max} is large, the truncated GS algorithm can provide more robust results. For the utility gap in Fig. 7.3(b), except for the GSEC before CSI change, it is larger for edge-cutting algorithms than for the truncated GS algorithm when Δ_c^{max} is small, and the other way around when Δ_c^{max} is large. Executing the GSEC algorithm before CSI change can provide a negligible performance gap from the GS algorithm. This is due to the fact the edges kept by the GSEC algorithm are based on the GS algorithm, and almost all edges involved in the GS algorithm are kept. The advantage cannot be maintained after CSI changes. But, the GSEC algorithm still provides smaller utility gap than DEC algorithms. Different DEC algorithms have similar performance.

As we discussed in Section 7.4.2, it is expected that resource allocation results from GSEC are closer to those from the GS algorithm than those from DEC, which is illustrated in Fig. 7.3(c). GSEC provides the same resource allocation result as the GS algorithm even when the maximum available channels allowed at each SU pair is only 10% of all channels, i.e., $\Delta_c^{max} = 20$. However, the DEC algorithms always provide resource allocation results that are different from those from the GS algorithm. This advantage of GSEC is only significant for the case before CSI change. After CSI change, the performance gap becomes smaller since GSEC is operated based on the CSI before change. Comparing the results in Fig. 7.3(a), GSEC loses certain level of robustness in order to get resource allocation results closer to those from the GS algorithm. This is the case because the more the algorithm depends on the original graph, the more sensitive it is to change on the graph (i.e., the CSI variations).

7.6.2 Single-Stage Truncation and Edge-Cutting

Besides operating truncation or edge-cutting separately, these operations can be combined. For example, we can fist apply edge-cutting algorithms on the original graph. We then run
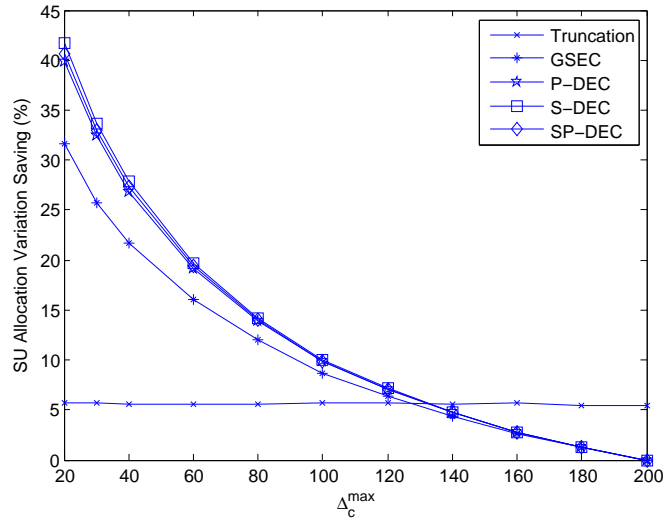
(a) SU allocation variation saving.
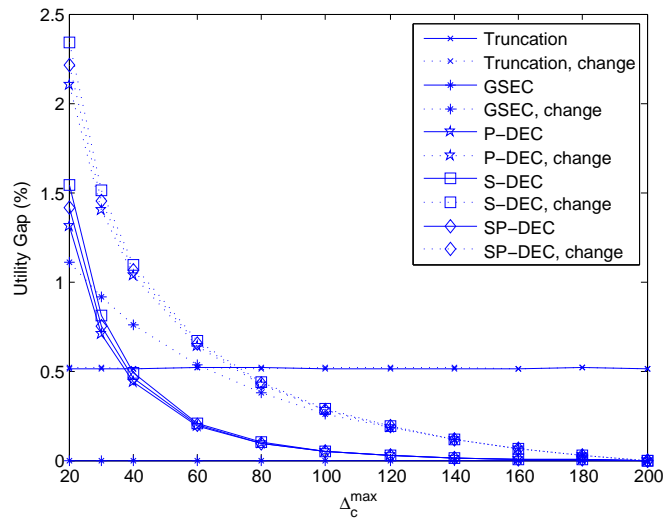
(b) Utility gap.
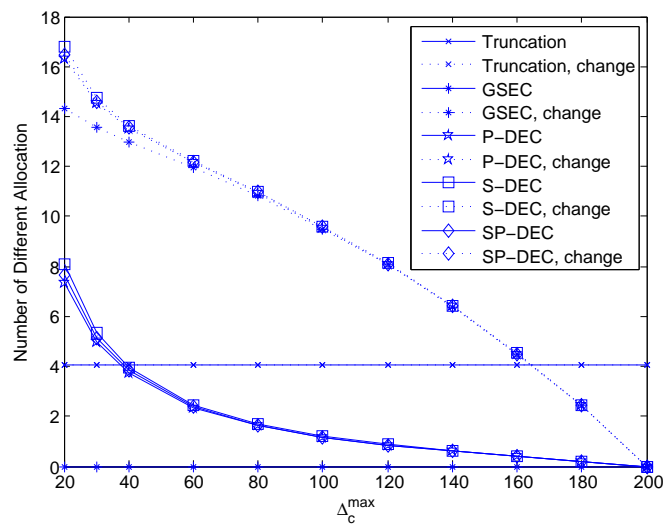
(c) Resource allocation difference.

Figure 7.3. Performance for algorithms with truncated or edge-cutting.

120

the GS algorithm on the new graph, and stop when we obtain a resource allocation that is ϵ-stable or is an $(1 + \epsilon)$-approximation compared with the results on the original graph. Figs. 7.4(a) and 7.4(b) show the SU allocation variation saving and utility performance, respectively. The results based on truncation only are also provided for comparison reason. Moreover, all three DEC algorithms have similar performance, and only results based on S-DEC are provided here. As Δ_c^{max} increases, the performance curves of algorithms with edge-cutting and truncation converge to that of the truncated only algorithm, instead of to that of the original GS algorithm. Compared with the results in Figs. 7.3(a) and 7.3(b), utilizing both edge-cutting and truncation can result in higher SU allocation variation saving accompanied a larger utility gap. The resource allocation difference is shown in Fig. 7.4(c). For all edge-cutting algorithms with truncation, the number of different resource allocations is larger compared to that from the edge-cutting only case and the performance curve converges to the truncation only case as Δ_c^{max} increases.

7.6.3 Multi-Stage Truncation and Edge-Cutting

In this part, the performance of the MS algorithm is presented. Figs. 7.5(a) and 7.5(b) show the utility gap and SU allocation variation saving, respectively. With the help of the MS algorithm, the utility gap between the MS algorithm and the original GS algorithm is significantly reduced compared with the single-stage algorithm. The gap based on the CSI before the change is negligible while there is a small gap, less than 0.5%, after the CSI change. However, the SU allocation variation saving is smaller compared with the corresponding single-stage algorithms. Comparing results based on different edge-cutting algorithms, the utility gap for MS GSEC is slightly larger than the MS DEC algorithms while it can have higher SU allocation variation saving. This is different from the single-stage case. For MS GSEC, it can allocate more SU pairs in the first stage and the impact of the latter stages is smaller compared to the other DEC algorithms. Thus, it can keep higher SU allocation variation saving than the single-stage algorithm while the utility gap is larger as well.
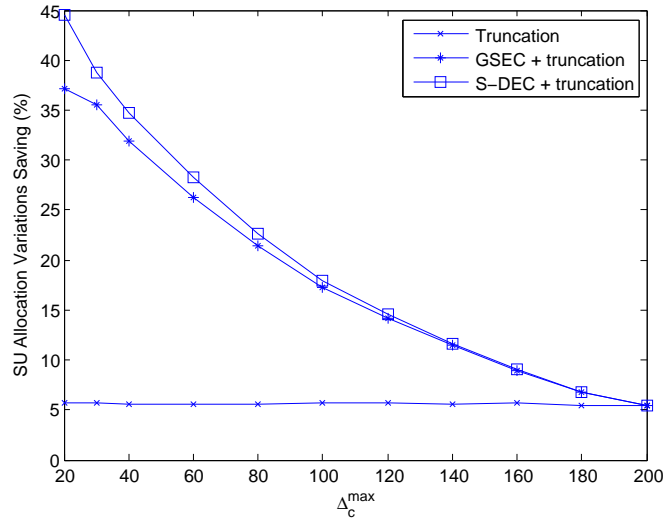
(a) SU allocation variation saving.
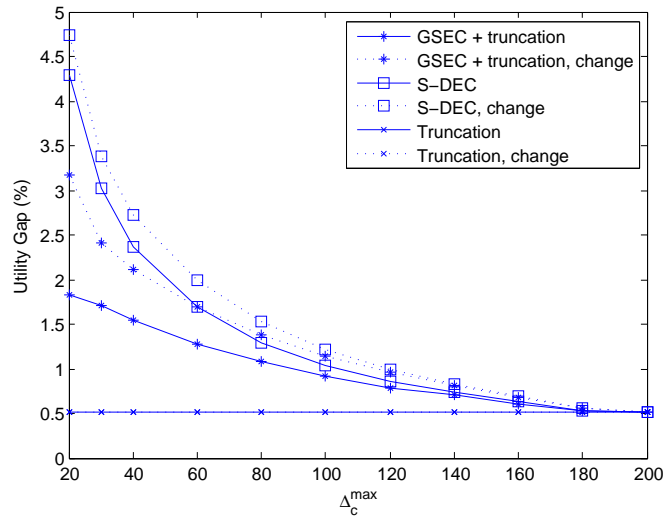
(b) Utility gap.
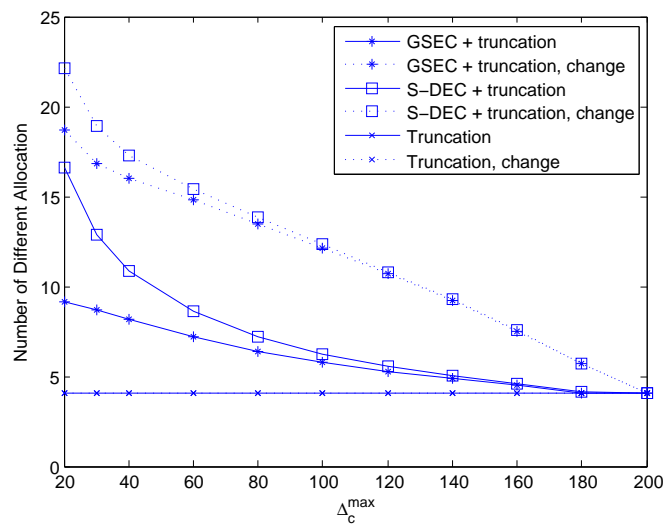
(c) Resource allocation difference.

Figure 7.4. Performance for algorithms with truncation and edge-cutting.

Moreover, Fig. 7.5(c) shows the allocation difference between the MS algorithm and the original GS algorithm. Comparing with the results in Fig. 7.4(c), the number of allocation difference based on the MS algorithms is smaller than the one from the single-stage algorithm.

7.7 Conclusions

In this chapter, we have studied robust resource allocation for CR networks. First, we develop a resource allocation scheme based on stable matching, which takes both SU pairs' and PUs' preferences into account. We then discuss the properties of almost stable resource allocation, which is robust to the CSI variation compared with stable resource allocation. Based on the properties of almost stable resource allocation, we propose the DEC and GSEC algorithms to further improve the robustness of the resource allocation scheme. The MS algorithms are then discussed to compensate for possible losses from the DEC and GSEC algorithms. Numerical results show that our proposed schemes are robust to the CSI variations.
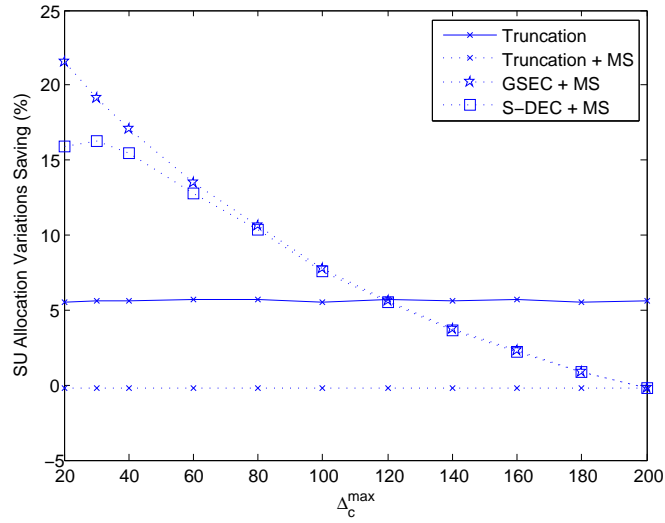
(a) SU allocation variation saving.
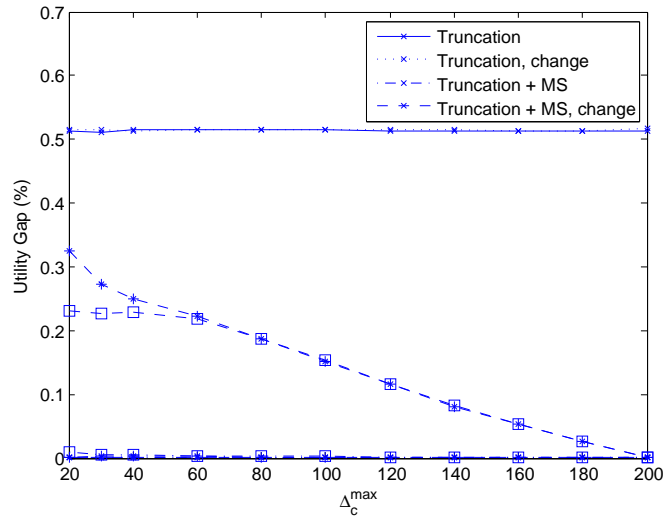
(b) Utility gap.
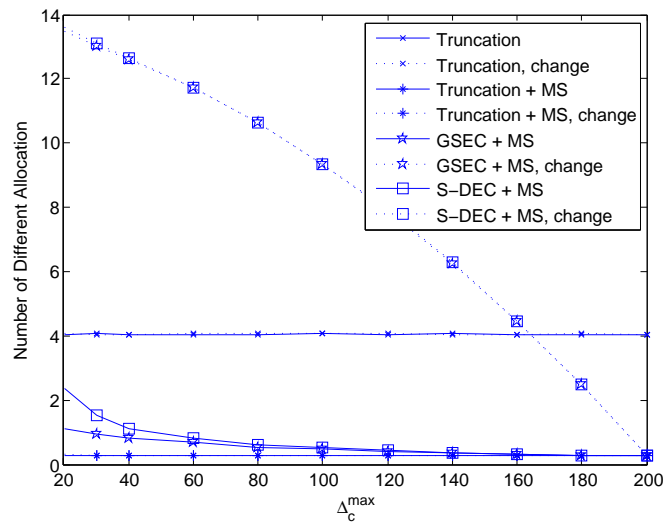
(c) Resource allocation difference.

Figure 7.5. Performance for different multi-stage algorithms.

CHAPTER 8

CONCLUSIONS

In this dissertation, we focus on improving spectral efficiency of wireless communications networks by studying efficient spectrum sensing and spectrum access strategies. The main contributions are summarized as follows.

We have first studied spectrum sensing techniques. We have investigated the optimal design of SD for CR networks. We have formulated a throughput optimization problem of the SU system given the target detection probability and the interference constraint to the PU system. A unique optimal false-alarm probability has been found for the studied problem. Then, we have investigated the optimal spectrum sensing length design for a general PU on-off model. We have formulated a throughput optimization problem of the CR network given the target interference constraint to the PU system, the detection and the false-alarm probabilities. Exhaustive search has been used to find out the optimal sensing block length after simplifying the problem as a one-parameter problem.

We then studied the transmission design for the spectrum overlay systems. We have focused on a MIMO-OFDM primary system. We have discussed a scenario allowing the primary link to release some of its own freedom to the secondary link without violating its own QoS requirement to improve the performance of the secondary link. A throughput maximization problem is formulated to find out the optimal subspace that can be released by the primary link to the secondary link. We then have extended our study to a multi-cell multiple-antenna secondary uplink system. The number of interference-free symbols that can be transmitted by each SU has been derived, which increases with the antennas equipped at the SU and the SBS and the length of CP. Two chordal-distance based precoding matrix design algorithms have been proposed. The proposed scheme can transmit more symbols for each SU simultaneously than TDMA.

We have also studied the design for the spectrum underlay systems. We have investigated an underlay CR network with direct and relay-aided transmissions. We have first investigated power allocation to maximize the overall rate performance of the CR network while keeping the interference to the PU under a tolerable level. By taking the fairness between two CR users into consideration, we then have addressed power allocation with an additional sum power constraint. We also have developed a resource allocation scheme based on stable matching, which takes both SU pairs' and PUs' preferences into account. We have discussed the properties of almost stable resource allocation, which is robust to the CSI variation compared with stable resource allocation. Based on the properties of almost stable resource allocation, we have proposed the DEC and GSEC algorithms to further improve the robustness of the resource allocation scheme. The MS algorithms have then been discussed to compensate for possible losses from the DEC and GSEC algorithms.

APPENDIX A

PROOF FOR CHAPTER 2

A.1 Proof of Property 2.1

Take the derivative of $\bar{n}_I$ with P_f, we have

$$
\begin{aligned}
\frac{d\bar{n}_I}{dP_f} &= -(1 - P_d)\frac{dE_{\mathcal{H}_1}[N]}{dP_f} \\
&= -\frac{1 - P_d}{E_{\mathcal{H}_1}(LLR_i)}\left(\frac{1 - P_d}{1 - P_f} - \frac{P_d}{P_f}\right).
\end{aligned}
\tag{A.1}
$$

From (2.7), we have

$$
E_{\mathcal{H}_1}(LLR_i) = -\log(1 + \gamma) + \gamma > 0
\tag{A.2}
$$

In CR networks, we normally have $P_d > 0.5$ and $P_f < 0.5$. Thus,

$$
\frac{1 - P_d}{1 - P_f} - \frac{P_d}{P_f} < 0.
\tag{A.3}
$$

Then,

$$
\frac{d\bar{n}_I}{dP_f} > 0.
\tag{A.4}
$$

Therefore, the average number of samples that are interfered by the SU, $\bar{n}_I$, is a monotonically increasing function of the false-alarm probability, P_f.

A.2 Proof of Property 2.2

To show the concavity of the function, we derive the second derivative of $\bar{n}_T$ with P_f.

We have

$$
\frac{d^2\bar{n}_T}{dP_f^2} = \frac{P(\mathcal{H}_0)}{E_{\mathcal{H}_0}(LLR_i)}\left(2\log\frac{P_d}{1 - P_d} + 2\log\frac{1 - P_f}{P_f} + \frac{1}{P_f}\right).
\tag{A.5}
$$

From (2.7), we have

$$
E_{\mathcal{H}_0}(LLR_i) = -\log(1 + \gamma) + \frac{\gamma}{1 + \gamma} < 0.
\tag{A.6}
$$

Moreover, when $P_f < 0.5$ and $P_d > 0.5$, we have

$$2\log\frac{P_d}{1-P_d} > 0, \quad 2\log\frac{1-P_f}{P_f} > 0, \quad \frac{1}{P_f} > 0. \tag{A.7}$$

Thus, we have

$$\frac{\mathrm{d}^2\bar{n}_T}{\mathrm{d}P_f^2} < 0. \tag{A.8}$$

Therefore, the number of data samples transmitted effectively, $\bar{n}_T$, is a concave function of the false-alarm probability, P_f. And we can find out a unique optimal solution to (2.13).

APPENDIX B

PROOF FOR CHAPTER 3

B.1 Distribution analysis

Here, we analyze the distributions of the statistics for all four cases. We use the notation B to denote the statistic, i.e., $B = \sum_{i=1}^{M} |r_i|^2$. There are only two hypotheses for r_i where both s_i and n_i follow Gaussian distributions. Thus, B follows a generalized chi-square distribution. B can be expressed as the linear combination of two chi-square random variables, i.e., $B = \sum_{m=1}^{2} \sigma_m^2 B_m$, where $\sigma_1^2 = \sigma_n^2$, $B_1 \sim \chi^2(2k)$ and $\sigma_2^2 = \sigma_s^2 + \sigma_n^2$, $B_2 \sim \chi^2(2(M-k))$, in which k equals to the number of samples that $r_i = n_i$. To simplify the expression, we use central limit theorem to approximate B. Then, B is approximated as

$$B \sim N\left(\mu, \sigma^2\right), \tag{B.1}$$

where $\mu = [2M(\gamma+1) - 2k\gamma]\sigma_n^2$ and $\sigma^2 = [4k + 4(M-k)(\gamma+1)^2]\sigma_n^4$.

APPENDIX C

PROOF FOR CHAPTER 6

C.1 Optimal relay power for case A

According to P_3^*, we investigate the problem in two cases. When $P_2 \leq \frac{I - P_{BS}|h_{BP}|^2}{|h_{RP}|^2}$, we have $P_{BS} \leq \frac{I - P_2|h_{RP}|^2}{|h_{BP}|^2}$. Thus,

$$P_3^* = P_{BS}. \tag{C.1}$$

Differentiate the objective function, (6.14a), with respective to P_2, we have

$$
\begin{aligned}
f(P_2) &= \frac{\partial R_a\left(P_1^*,\ P_2,\ P_3^*\right)}{\partial P_2} \\
&= \frac{\partial R_1\left(P_1^*,\ P_2,\ P_3^*\right)}{\partial P_2} + \frac{\partial R_2\left(P_1^*,\ P_2,\ P_3^*\right)}{\partial P_2} \\
&= \frac{ed^2\left((P_2 + \frac{c}{d})^2 + \frac{eac - ad}{ed^2}\right)}{2(1 + eP_2)((c + dP_2)^2 + a(c + dP_2))},
\end{aligned} \tag{C.2}
$$

where $a = P_{BS}|h_{B2}|^2$, $c = \sigma^2$, $d = \frac{\sigma^2|h_{R2}|^2}{P_1^*|h_{B2}|^2 + \sigma^2}$, and $e = \frac{|h_{BR}|^2}{\sigma^2}$. It is obvious that the denominator is positive, i.e., $2(1 + eP_2)((c + dP_2)^2 + a(c + dP_2)) > 0$. For the numerator, we have $(P_2 + \frac{c}{d})^2 + \frac{eac - ad}{ed^2} > \frac{ec^2 + eac - ad}{ed^2}$. Thus, $f(P_2) > 0$ when $ad - eac < ec^2$. For this case, the overall rate monotonically increasing with P_2. Thus, the optimal P_2 for this case is

$$P_{2,2}^* = \min\left\{\frac{P_1^*|h_{BR}|^2}{|h_{R1}|^2}, \frac{I - P_{BS}|h_{BP}|^2}{|h_{RP}|^2}, P_R\right\}. \tag{C.3}$$

When $ad - eac > ec^2$, we have

$$
f(P_2)
\begin{cases}
< 0, & P_2 < \sqrt{\frac{ad - eac}{ed^2}} - \frac{c}{d}, \\
> 0, & P_2 > \sqrt{\frac{ad - eac}{ed^2}} - \frac{c}{d}.
\end{cases} \tag{C.4}
$$

Correspondingly, the overall rate decreases when

$$P_2 \in \left[0,\ \sqrt{\frac{ad - eac}{ed^2}} - \frac{c}{d}\right] \tag{C.5}$$

and increases when

$$P_2 \in \left[\sqrt{\frac{ad - eac}{ed^2}} - \frac{c}{d},\ \min\{\frac{P_1^*|h_{BR}|^2}{|h_{R1}|^2}, \frac{I - P_{BS}|h_{BP}|^2}{|h_{RP}|^2}, P_R\}\right]. \tag{C.6}$$

130

$$
\begin{aligned}
f(P_2) &= \frac{\partial R_a\left(P_1^*, P_2, P_3^*\right)}{\partial P_2} = \frac{\partial R_1\left(P_1^*, P_2, P_3^*\right)}{\partial P_2} + \frac{\partial R_2\left(P_1^*, P_2, P_3^*\right)}{\partial P_2} \\
&= \frac{tk(k-i)(P_2 + \frac{j}{k})^2 + (tj^2 + thj - ij - kh) - \frac{tj^2(k-i)^2}{k}}{2(1 + tP_2)\left[k(k-i)\left(P_2 + \frac{2jk - ij + hk}{2k(k-i)}\right)^2 + j^2 + hj - \frac{(2jk - ij + hk)^2}{4k(k-i)}\right]},
\end{aligned}
\tag{C.9}
$$

Thus,

$$
P_{2,2}^* = \arg \max_{P_2 \in \mathcal{P}} R_a\left(P_1^*, P_2, P_3^*\right),
\tag{C.7}
$$

where $\mathcal{P} = \left\{0, \min\{\frac{P_1^*|h_{BR}|^2}{|h_{R1}|^2}, \frac{I - P_{BS}|h_{BP}|^2}{|h_{RP}|^2}, P_R\}\right\}$.

C.2   Optimal relay power for case B

When $P_2 \geq \frac{I - P_{BS}|h_{BP}|^2}{|h_{RP}|^2}$, we have $P_{BS} \geq \frac{I - P_2|h_{RP}|^2}{|h_{BP}|^2}$. Thus,

$$
P_3^* = \frac{I - P_2^*|h_{RP}|^2}{|h_{BP}|^2}.
\tag{C.8}
$$

For this case, we take the first derivative of the objective function, and get (C.9), where

$h = \frac{I}{|h_{BP}|^2}$, $i = \frac{|h_{RP}|^2}{|h_{BP}|^2}$, $j = \sigma^2$, $k = \frac{\sigma^2|h_{R2}|^2}{P_1^*|h_{B2}|^2 + \sigma^2}$, and $t = \frac{|h_{BR}|^2}{\sigma^2}$.

Let $P_L = \frac{I - P_{BS}|h_{BP}|^2}{|h_{RP}|^2}$ and $P_U = \min\left\{\frac{P_1^*|h_{BR}|^2}{|h_{R1}|^2}, P_R, \frac{I}{|h_{RP}|^2}\right\}$. From (C.9), we define the numerator and denominator functions $N(P_2)$ and $D(P_2)$ as

$$
N(P_2) = tk(k-i)(P_2 + \frac{j}{k})^2 + (tj^2 + thj - ij - kh) - \frac{tj^2(k-i)^2}{k},
\tag{C.10}
$$

and

$$
D(P_2) = k(k-i)\left(P_2 + \frac{2jk - ij + hk}{2k(k-i)}\right)^2 + j^2 + hj - \frac{(2jk - ij + hk)^2}{4k(k-i)},
\tag{C.11}
$$

respectively, where $h = \frac{I}{|h_{BP}|^2}$, $i = \frac{|h_{RP}|^2}{|h_{BP}|^2}$, $j = \sigma^2$, $k = \frac{\sigma^2|h_{R2}|^2}{P_1^*|h_{B2}|^2 + \sigma^2}$, and $t = \frac{|h_{BR}|^2}{\sigma^2}$. To simplify the notations, we set $b' = \frac{2jk - ij + hk}{2k(k-i)}$, $c' = (tj^2 + thj - ij - kh) - \frac{tj^2(k-i)^2}{k}$, and $d' = j^2 + hj - \frac{(2jk - ij + hk)^2}{4k(k-i)}$. We investigate the property of the functions for different cases.

Case 1: $k > i$

We investigate the numerator first. If $tk(k-i)(P_L + \frac{j}{k})^2 + c' > 0$, we have $N(P_2) > 0$ for all $P_2 \in [P_L, P_U]$. If $tk(k-i)(P_L + \frac{j}{k})^2 + c' < 0$, $N(P_2) < 0$ when $P_2 \in \left[P_L, \sqrt{\frac{-c'}{tk(k-i)}} - \frac{j}{k}\right]$ and $N(P_2) > 0$ when $P_2 \in \left[\sqrt{\frac{-c'}{tk(k-i)}} - \frac{j}{k}, P_U\right]$.

For the denominator, we consider the cases when $P_L \geq -b'$ or $P_L < -b'$, respectively.

When $P_L \geq -b'$, $D(P_2) > 0$ if $k(k-i)(P_L + b')^2 + d' > 0$. If $k(k-i)(P_L + b')^2 + d' < 0$, $D(P_2) < 0$ when $P_2 \in \left[P_L, \sqrt{\frac{-d'}{k(k-i)}} - b'\right]$ and $D(P_2) > 0$ when $P_2 \in \left[\sqrt{\frac{-d'}{k(k-i)}} - b', P_U\right]$. When $P_L < -b'$, we have $D(P_2) > 0$ for $P_2 \in [P_L, P_U]$ if $d' > 0$. If $d' < 0$, $D(P_2) < 0$ for $P_2 \in \left[-\sqrt{\frac{-d'}{k(k-i)}} - b', \sqrt{\frac{-d'}{k(k-i)}} - b'\right]$ and $D(P_2) > 0$ for $P_2 \in \left[P_L, -\sqrt{\frac{-d'}{k(k-i)}} - b'\right] \cup \left[\sqrt{\frac{-d'}{k(k-i)}} - b', P_U\right]$.

Case 2: $k < i$

For the numerator, $N(P_2) < 0$ for $P_2 \in [P_L, P_U]$ when $tk(k-i)(P_L + \frac{j}{k})^2 + c' < 0$. When $tk(k-i)(P_L + \frac{j}{k})^2 + c' > 0$, $N(P_2) > 0$ when $P_2 \in \left[P_L, \sqrt{\frac{-c'}{tk(k-i)}} - \frac{j}{k}\right]$ and $N(P_2) < 0$ when $P_2 \in \left[\sqrt{\frac{-c'}{tk(k-i)}} - \frac{j}{k}, P_U\right]$.

For the denominator, we still consider two cases, i.e., $P_L > -b'$ and $P_L < -b'$. When $P_L > -b'$, $D(P_2) < 0$ for $P_2 \in [P_L, P_U]$ if $k(k-i)(P_L+b')^2+d' < 0$. If $k(k-i)(P_L+b')^2+d' > 0$, $D(P_2) > 0$ when $P_2 \in \left[P_L, \sqrt{\frac{-d'}{k(k-i)}} - b'\right]$ and $D(P_2) < 0$ when $P_2 \in \left[\sqrt{\frac{-d'}{k(k-i)}} - b', P_U\right]$. When $P_L < -b'$ $D(P_2) < 0$ for $P_2 \in [P_L, P_U]$ when $d' < 0$. If $d' > 0$, $D(P_2) > 0$ for $P_2 \in \left[-\sqrt{\frac{-d'}{k(k-i)}} - b', \sqrt{\frac{-d'}{k(k-i)}} - b'\right]$ and $D(P_2) < 0$ for $P_2 \in \left[P_L, -\sqrt{\frac{-d'}{k(k-i)}} - b'\right] \cup \left[\sqrt{\frac{-d'}{k(k-i)}} - b', P_U\right]$.

Thus, we can find out the positive and negative regions of $f(P_2)$. If $f(P_2) > 0$, the objective function is a monotonically increasing function in that specific region. If $f(P_2) < 0$, the corresponding objective function is a monotonically decreasing function. Then, the optimal P_2, denoted as $P_{2,3}^*$, can be found following Algorithm C.1 and C.2 for $k > i$ and $k < i$, respectively.

C.3 Optimal relay power for case A: with total power constraint

We discuss the case when $P_2 > P_t - z$. According to the value of P_3^*, we further divide the region into two parts.

$$f(P_2) \quad = \quad \frac{a_3 P_2^3 + a_2 P_2^2 + a_1 P_2 + a_0}{(1 + eP_2)(j(t - P_2) + k)(j(t - P_2) + k + (i - P_2)(t - P_2))}, \quad \text{(C.15)}$$

When $P_2 \leq \frac{I - P_{BS}|h_{BP}|^2}{|h_{RP}|^2}$, we have

$$P_3^* = P_{BS}. \tag{C.12}$$

Calculate the first derivative of the objective function with respective to P_2, we have

$$
\begin{aligned}
f(P_2) &= \frac{\partial R_1\left(P_1^*, \, P_2, \, P_3^*\right)}{\partial P_2} + \frac{\partial R_2\left(P_1^*, \, P_2, \, P_3^*\right)}{\partial P_2} \\
&= \frac{ea^2 P_2^2 - (2a^2be + 2ac + d - dce)P_2 + e(ab + c)^2 - dc}{2(1 + eP_2)\left[a^2 P_2^2 - (2a^2b + 2ac + d)P_2 + (ab + c)^2\right]}
\end{aligned}
\tag{C.13}
$$

where $a = \sigma^2 - \frac{\sigma^2 |h_{R2}|^2}{|h_{B2}|^2}$, $b = P_t + \frac{\sigma^2}{|h_{B2}|^2}$, $c = \frac{\sigma^2 |h_{R2}|^2 (P_t |h_{B2}|^2 + \sigma^2)}{|h_{B2}|^4}$ and $e = \frac{|h_{R1}|^2}{\sigma^2}$.

From (C.13), the numerator and denominator functions have the same structure as the corresponding functions in (C.9), respectively. Thus, we can find out the positive and negative regions of $f(P_2)$ and then the optimal P_2 for this case will be obtained, denoted as $P_{2,3}^*$.

When $P_2 \geq \frac{I - P_{BS}|h_{BP}|^2}{|h_{RP}|^2}$, we have

$$P_3^* = \frac{I - P_2^*|h_{RP}|^2}{|h_{BP}|^2}. \tag{C.14}$$

Then, differentiate the objective function with respective to P_2, we can get (C.15), where $i = \frac{I}{|h_{RP}|^2}$, $j = \frac{\sigma^2(|h_{B2}|^2 - |h_{R2}|^2)|h_{BP}|^2}{|h_{RP}|^2 |h_{B2}|^2}$, $k = \frac{\sigma^2 |h_{R2}|^2 |h_{BP}|^2 (P_t|h_{B2}|^2 + \sigma^2)}{|h_{RP}|^2 |h_{B2}|^4}$, $t = P_t + \frac{\sigma^2}{|h_{B2}|^2}$ and $e = \frac{|h_{R1}|^2}{\sigma^2}$. And $a_3 = -2ej$, $a_2 = -j + 3(jt + k)e + ej(j + i + t)$, $a_1 = (jt + k)(2 - e(j + i + t)) - e(jt^2 + kt + ki + j^2t + jk + jit)$, and $a_0 = -jt^2 - kt - ki + e(jt + k)(jt + k + it)$.

We can see that both the numerator and denominator functions are still polynomial functions. Based on the properties of the polynomial functions, same as other cases, we can find out the positive and negative regions of $f(P_2)$. Then, the optimal P_2 for this case can be obtained, denoted as $P_{2,4}^*$. Due the space limit, we omit the detail here. The results will be shown numerically.

Table C.1. For the case when $k > i$

---

if $k > i$ **then**

  if $tk(k-i)(P_L + \frac{j}{k})^2 + c' > 0$ **then**

    if $P_L \geq -b'$ **then**

      if $k(k-i)(P_L + b')^2 + d' > 0$ **then**

        $P_{2,3}^* = P_U$

      else

        $P_{2,3}^* = \arg\max\limits_{P_2 \in \{P_L, P_U\}} R_a(P_1^*, P_2, P_3^*)$

      end if

    else

      if $d' > 0$ **then**

        $P_{2,3}^* = P_U$

      else

        $P_{2,3}^* = \arg\max\limits_{P_2 \in \{-\sqrt{\frac{-d'}{k(k-i)}} - b', P_U\}} R_a(P_1^*, P_2, P_3^*)$

      end if

    end if

  else

    if $P_L \geq -b'$ **then**

      if $k(k-i)(P_L + b')^2 + d' > 0$ **then**

        $P_{2,3}^* = \arg\max\limits_{P_2 \in \{P_L, P_U\}} R_a(P_1^*, P_2, P_3^*)$

      else

        $P_{2,3}^* = \arg\max\limits_{P_2 \in \mathcal{P}} R_a(P_1^*, P_2, P_3^*)$, where $\mathcal{P} = \{\min\{\sqrt{\frac{-d'}{k(k-i)}} - b', \sqrt{\frac{-c'}{tk(k-i)}} - \frac{j}{k}\}, P_U\}$

      end if

    else

      if $d' > 0$ **then**

        $P_{2,3}^* = \arg\max\limits_{P_2 \in \{P_L, P_U\}} R_a(P_1^*, P_2, P_3^*)$

      else

        $P_{2,3}^* = \arg\max\limits_{P_2 \in \mathcal{P}} R_a(P_1^*, P_2, P_3^*)$, where $\mathcal{P} = \left\{ P_L, \min\left\{ c_m, \sqrt{\frac{-d'}{k(k-i)}} - b' \right\}, P_U \right\}$,

        where $c_m = \max\left\{ \sqrt{\frac{-c'}{tk(k-i)}} - \frac{j}{k}, -\sqrt{\frac{-d'}{k(k-i)}} - b' \right\}$.

      end if

    end if

  end if

end if

Table C.2. For the case when $k < i$

if $k < i$ **then**

    if $tk(k - i)(P_L + \frac{j}{k})^2 + c' > 0$ **then**

        if $P_L \geq -b'$ **then**

            if $k(k - i)(P_L + b')^2 + d' > 0$ **then**

$$P_{2,3}^* = \arg \max_{P_2 \in \mathcal{P}} R_a(P_1^*, P_2, P_3^*), \text{ where } \mathcal{P} = \left\{ \min\left\{ \sqrt{\tfrac{-d'}{k(k-i)}} - b', \sqrt{\tfrac{-c'}{tk(k-i)}} - \tfrac{j}{k} \right\}, P_U \right\}$$

            else

$$P_{2,3}^* = \arg \max_{P_2 \in \{P_L, P_U\}} R_a(P_1^*, P_2, P_3^*)$$

            end if

        else

            if $d' > 0$ **then**

$$P_{2,3}^* = \arg \max_{P_2 \in \mathcal{P}} R_a(P_1^*, P_2, P_3^*), \text{ where } \mathcal{P} = \left\{ P_L, \min\left\{ c_m, \sqrt{\tfrac{-d'}{k(k-i)}} - b' \right\}, P_U \right\},$$

$$\text{where } c_m = \max\left\{ \sqrt{\tfrac{-c'}{tk(k-i)}} - \tfrac{j}{k}, -\sqrt{\tfrac{-d'}{k(k-i)}} - b' \right\}.$$

            else

$$P_{2,3}^* = \arg \max_{P_2 \in \{P_L, P_U\}} R_a(P_1^*, P_2, P_3^*)$$

            end if

        end if

    else

        if $P_L \geq -b'$ **then**

            if $k(k - i)(P_L + b')^2 + d' > 0$ **then**

$$P_{2,3}^* = \arg \max_{P_2 \in \{P_L, P_U\}} R_a(P_1^*, P_2, P_3^*)$$

            else

$$P_{2,3}^* = P_U$$

            end if

        else

            if $d' > 0$ **then**

$$P_{2,3}^* = \arg \max_{P_2 \in \{-\sqrt{\frac{-d'}{k(k-i)}} - b', P_U\}} R_a(P_1^*, P_2, P_3^*)$$

            else

$$P_{2,3}^* = P_U$$

            end if

        end if

    end if

end if

APPENDIX D

PROOF FOR CHAPTER 7

D.1 Proof of Theorem 7.5

The proof of Theorem 7.5 follows an argument in [94]. Let T denote the number of rounds we execute the GS algorithm. For $0 \leq n \leq T$, let $\mathcal{M}_n$ denote the matching at the end of n-th round. The i-th SU pair is denoted as s_i, and the j-th PU is denoted by p_j. Define w as a weight function on edge. So $w_{s_i,p_j}(P^*_{i,j})$ is the weight of edge between s_i and p_j. If s_i is matched at the end of the n-th round, we use $m_n(s_i)$ to denote the PU matched to s_i. Let $C_n(p_j)$ denote the set of those SU pairs which have not rejected p_j at the end of n-th round (which is called the candidate set of p_j).

During any round, each PU removes at most one SU node from its candidate set, since each PU proposes to at most one SU pair during any round. The edge (s_i, p_j) is called *lost* if s_i is removed from the candidate set of p_j. We use L_n to denote the set of the lost edges by the end of the n-th round. For $\mathcal{M}_n$, the matching at the end of the n-th round, we define the weight of s_i as $w_n(s_i) = w_{s_i,m_n(s_i)}$ (if s_i is matched in $\mathcal{M}_n$) and $w_n(s_i) = 0$ (if s_i is unmatched in $\mathcal{M}_n$), where $w_{s_i,m_n(s_i)} := w_{s_i,m_n(s_i)}(P^*_{s_i,m_n(s_i)})$, see (7.4) and (7.5). Then, the total weight of the matching $\mathcal{M}_n$ can be expressed as

$$w_{\mathcal{M}_n} = \sum_{s_i \in V_1} w_n(s_i), \tag{D.1}$$

where V_1 denotes the set of SU nodes. Moreover, the total weight of the edges in L_n, denoted as w_{L_n}, is defined as the sum of weights of the edges in L_n.

We define the potential of p_j, denoted as $f_n(p_j)$, as follows. If p_j is matched in $\mathcal{M}_n$ or $C_n(p_j) = \emptyset$ then set $f_n(p_j) = 0$. Otherwise, set

$$f_n(p_j) = \max_{s_i \in C_n(p_j)} w_{s_i,p_j}, \tag{D.2}$$

which is the maximum weight of edges connecting p_j to the SU pairs in $C_n(p_j)$. The total potential of the matching $\mathcal{M}_n$ at the end of n-th round is the sum of the potentials of all

PUs, that is,

$$f_{\mathcal{M}_n} = \sum_{p_j \in V_2} f_n(p_j), \qquad (D.3)$$

where V_2 denotes the set of PU nodes.

Lemma D.1 *For $n \geq 2$, $f_{\mathcal{M}_n} \leq w_{L_n} - w_{L_{n-1}}$.*

Proof: Let p_j denote the j-th PU node. If $f_n(p_j) > 0$ then p_j is not matched by $\mathcal{M}_n$ and $C_n(p_j) \neq \emptyset$. Thus, during the n-th round, p_j is rejected by some SU pair, say s_k (the k-th SU node), and the edge (s_k, p_j) is lost. So $(s_k, p_j) \in L_n - L_{n-1}$. Note that p_j prefers s_k over other SU pairs in $C_n(p_j)$, which means, $f_n(p_j) \leq w_{s_k, p_j}$. Hence,

$$f_{\mathcal{M}_n} = \sum_{p_j \in V_2} f_n(p_j) \leq \sum_{p_j \in V_2} w_{s_k, p_j} \leq w_{L_n} - w_{L_{n-1}}, \qquad (D.4)$$

and the lemma is proved.

Lemma D.2 *For $n \geq 2$, $f_{\mathcal{M}_n} \leq f_{\mathcal{M}_{n-1}}$.*

Proof: Since $f_{\mathcal{M}_n} = \sum_{p_j \in V_2} f_n(p_j)$ and $f_{\mathcal{M}_{n-1}} = \sum_{p_j \in V_2} f_{n-1}(p_j)$, we compare $f_n(p_j)$ and $f_{n-1}(p_j)$ for each $p_j \in V_2$.

If p_j is matched in both $\mathcal{M}_{n-1}$ and $\mathcal{M}_n$, then by definition, $f_n(p_j) = f_{n-1}(p_j) = 0$.

If p_j is matched in $\mathcal{M}_n$, but not in $\mathcal{M}_{n-1}$, then by definition, $f_n(p_j) \leq f_{n-1}(p_j)$.

Now assume that p_j is matched to some $s_i \in V_1$ in $\mathcal{M}_{n-1}$ but p_j is not matched in $\mathcal{M}_n$. Then $f_{n-1}(p_j) = 0$ and $f_n(p_j) = w_{s_k, p_j}$, where s_k is such that $w_{s_k, p_j} = \max_{s_t \in C_n(p_j)} w_{s_t, p_j}$. Moreover, since in the n-th round, s_i must reject p_j and accept another PU, say $p_{j'}$ with $j \neq j'$, we have $f_{n-1}(p_{j'}) = w_{s_i, p_{j'}}$ and $f_n(p_{j'}) = 0$. Thus,

$$f_n(p_j) - f_{n-1}(p_j) = w_{s_k, p_j} \leq w_{s_i, p_j} \leq w_{s_i, p_{j'}} = f_{n-1}(p_{j'}) - f_n(p_{j'}), \qquad (D.5)$$

which is equivalent to

$$f_n(p_j) + f_n(p_{j'}) \leq f_{n-1}(p_j) + f_{n-1}(p_{j'}). \qquad (D.6)$$

By summing up over all PUs, we have $f_{\mathcal{M}_n} \leq f_{\mathcal{M}_{n-1}}$.

Lemma D.3 *For $n \geq 2$, $w_{L_n} \geq (n-1)f_{M_n}$.*

Proof: By Lemmas D.1 and D.2, $w_{L_n} = \sum_{t=2}^{n}(w_{L_t} - w_{L_{t-1}}) \geq \sum_{t=2}^{n} f_{M_t} \geq (n-1)f_{M_n}$.

Lemma D.4 *For all $n \geq 2$, $w_{L_n} \leq (\Delta_s - 1)w_{M_n}$.*

Proof: Let s_i denote the i-th SU pair and p_j denote the j-th PU. If $(s_i, p_j) \in L_n$ (i.e., lost by the end of the n-th round), then s_i is matched to a better choice, $m_n(s_i)$, by the end of the n-th round. That is, $w_{s_i,p_j} < w_{s_i,m_n(s_i)}$. Since s_i can lose at most $\Delta_s - 1$ edges, the total weight of all lost edges adjacent to s_i is at most $(\Delta_s - 1) \cdot w_{s_i,m_n(s_i)}$. Hence, by summing over all SU pairs, we obtain $w_{L_n} \leq (\Delta_s - 1)w_{M_n}$.

By Lemmas D.3 and D.4, we have

Lemma D.5 *For any real $\gamma > 0$ and integer $n \geq 1 + (\Delta_s - 1)/\gamma$, $f_{M_n} \leq \gamma w_{M_n}$.*

Next, we present the proof of Theorem 7.5.

Proof: Let $\mathcal{S}$ be the unique stable matching produced by the GS algorithm. We use s_i to denote the i-th SU pair and p_j to denote the j-th PU. Suppose $(s_i, p_j) \in \mathcal{S}$.

Note that when p_j is matched to s_k in $\mathcal{M}_n$ for some k (possibly $k = i$), p_j prefers s_k over s_i and $w_{s_i,p_j} \leq w_{s_k,p_j} = w_n(p_j)$. Also note that when p_j is not matched in $\mathcal{M}_n$, then p_j has not asked s_i, $s_i \in C_n(p_j)$, and $w_{s_i,p_j} \leq f_n(p_j)$.

Hence,

$$w_{s_i,p_j} \leq f_n(p_j) + w_n(p_j) \tag{D.7}$$

and therefore

$$w_{\mathcal{S}} = \sum_{(s_i,p_j) \in \mathcal{S}} w_{s_i,p_j} \tag{D.8}$$

$$\leq \sum_{p_j \in V_2} (f_n(p_j) + w_n(p_j)) \tag{D.9}$$

$$= f_{M_n} + w_{M_n}. \tag{D.10}$$

From Lemma D.5, we conclude that

$$w_{\mathcal{S}} \leq (1 + \epsilon) w_{M_n} \tag{D.11}$$

whenever $n \geq 1 + (\Delta_s - 1)/\epsilon$.

Thus, Theorem 7.5 follows by choosing $T = \lfloor 2 + \Delta_s/\epsilon \rfloor$.

REFERENCES

[1] *Spectrum Policy Task Force report*, FCC ET Docket 02-155, Nov. 2002.

[2] J. Mitola, "Software radios: survey, critical evaluation and future directions," *IEEE Aerosp. Electron. Syst. Mag.*, vol. 8, no. 4, pp. 25–31, Apr. 1993.

[3] J. Mitola and G. Q. Maguire, "Cognitive radio: making software radios more personal," *IEEE Personal Commun.*, vol. 6, no. 4, p. 13, Aug. 1999.

[4] S. Haykin, "Cognitive radio: Brain-empowered wireless communication," *IEEE J. Sel. Areas Commun.*, vol. 23, pp. 201–220, Feb. 2005.

[5] F. K. Jondral, "Software-defined radiobasics and evolution to cognitive radio," *EURASIP J. Wireless Commun. and Networking*, vol. 2005, pp. 275–283, Mar. 2005.

[6] I. F. Akyildiz, W.-Y. Lee, and S. Mohanty, "Next generation/dynamic spectrum access/cognitive radio wireless networks: A survey," *Comput. Netw.*, vol. 50, pp. 2127–2159, May 2006.

[7] L. Lu, X. Zhou, U. Onunkwo, and G. Y. Li, "Ten years of research in spectrum sensing and sharing in cognitive radio," *Eurasip J. Wireless Commun. and Networking*, vol. 28, Jan. 2012. [Online]. Available: http://jwcn.eurasipjournals.com/content/2012/1/28.

[8] C. Stevenson, G. Chouinard, Z. Lei, W. H. Shellhammer, and W. S. Caldwell, "IEEE 802.22: The first cognitive radio wireless regional area network standard," *IEEE Commun. Mag.*, vol. 47, no. 1, p. 130, May 2009.

[9] J. Ma, G. Y. Li, and B. H. Juang, "Signal processing in cognitive radio," *Proc. IEEE*, vol. 97, no. 5, pp. 805–823, May 2010.

[10] S. Haykin, D. J. Thomson, and J. H. Reed, "Spectrum sensing for cognitive radio," *Proc. IEEE*, vol. 97, no. 5, pp. 849–877, May 2010.

[11] A. Sahai, N. Hoven, and R. Tandra, "Some fundamental limits in cognitive radio," in *Proc. Allerton Conf. on Commun., Control and Comput.*, Oct. 2004.

[12] J. Thukral and H. Bolcskei, "Interference alignment with limited feedback," in *IEEE Int. Symp. Inf. Theory (ISIT)*, June 2009, pp. 1759 – 1763.

[13] K. Gomadam, V. Cadambe, and S. Jafar, "Approaching the capacity of wireless networks through distributed interference alignment," in *Proc. IEEE Global Commun. Conf. (GLOBECOM)*, New Orleans, LO, Dec. 2008.

[14] R. Zhang, F. Gao, and Y.-C. Liang, "Cognitive beamforming made practical: Effective interference channel and learning-throughput tradeoff," *IEEE Trans. Commun.*, vol. 58, pp. 706–718, Feb. 2010.

[15] Q. Zhao and B. Sadler, "A survey of dynamic spectrum access," *IEEE Signal Processing Mag.*, vol. 24, no. 3, pp. 79–89, May 2007.

[16] T. Clancy, "Achievable capacity under the interference temperature model," in *Proc. 26th IEEE Int. Conf. Comput. Commun. (INFOCOM)*, May 2007.

[17] Y. H. Vivek Ashok Bohara, See Ho Ting and A. Pandharipande, "Interference-free overlay cognitive radio network based on cooperative space time coding," in *Proc. 5th Int. Conf. on Cognitive Radio Oriented Wireless Netw. and Commun.*, 2010.

[18] A. Sonnenschein and P. M. Fishman, "Radiometric detection of spread-spectrum signals in noise of uncertain power," *IEEE J. Sel. Topics Signal Process.*, vol. 2, no. 1, pp. 4–17, Feb. 2008.

[19] R. Tandra and A. Sahai, "SNR walls for signal detection," *IEEE J. Sel. Topics Signal Process.*, vol. 2, no. 1, pp. 4–17, Feb. 2008.

[20] W. Jouini, "Energy detection limits under log-normal approximated noise uncertainty," *IEEE Signal Process. Lett.*, vol. 18, no. 7, pp. 423–426, July 2011.

[21] M. Ghozzi, F. Marx, M. Dohler, and J. Palicot, "Cyclostatilonarilty-based test for detection of vacant frequency bands," in *Proc. 2nd Int. Conf. on Cognitive Radio Oriented Wireless Netw. and Commun.*, June 2006.

[22] P. D. Sutton, K. E. Nolan, and L. E. Doyle, "Cyclostationary signature in practial cognitive radio applications," *IEEE J. Sel. Areas Commun.*, vol. 26, pp. 13–24, Jan. 2008.

[23] W. Y. Lee and I. F. Akyildiz, "Optimal spectrum sensing framework for cognitive radio networks," *IEEE Trans. Wireless Commun.*, vol. 7, no. 10, pp. 3845–3857, Oct. 2008.

[24] A. Ghasemi and E. S. Sousa, "Optimization of spectrum sensing for oppotunistic spectrum access in cognitive radio networks," in *Proc. IEEE Consumer Commun. Netw. Conf.*, Jan. 2007, pp. 1022–1026.

[25] X. Zhou, J. Ma, G. Y. Li, Y. H. Kwon, and A. C. K. Soong, "Probability-based optimization of inter-sensing duration and power control in cognitive radio," *IEEE Trans. Wireless Commun.*, vol. 8, no. 10, pp. 4922–4027, Oct. 2009.

[26] Y. Pei, A. T. Hoang, and Y. C. Liang, "Sensing-throughput tradeoff in cognitive radio networks: how frequently should spectrum sensing be carried out," in *Proc. IEEE Int. Symp. Personal, Indoor Mobile Raido Commun.*, Spet. 2007.

[27] J. Ma, X. Zhou, and G. Y. Li, "Probability-based periodic spectrum sensing during secondary communication," *IEEE Trans. Commun.*, vol. 58, pp. 1291–13–1, Apr. 2010.

[28] M. Xu, H. Li, and X. Gan, "Energy efficient sequential sensing for wideband multi-channel cognitive network," in *Proc. IEEE Int. Conf. Commun.*, June 2011.

[29] T. Shu and M. Krunz, "Throughput-efficient sequential channel sensing and probing in cognitive radio networks under sensing errors," in *Proc. ACM MobiCom'09*, Spet. 2009.

[30] Y. Pei, Y. Liang, K. C. Teh, and K. H. Li, "Energy-efficient design of sequential channel sensing in cognitive radio networks: optimal sensing strategy," *IEEE J. Sel. Areas Commun.*, no. 8, pp. 1648–1659, Sept. 2011.

[31] A. Wald, *Sequential Analysis*, John Wiley & Sons Inc., 1947.

[32] N. Kundargi and A. Tewfik, "A performance study of novel sequential energy detection methods for spectrum sensing," in *Proc. IEEE Int. Conf. Acoust., Speech, and Signal Process.*, Mar. 2010.

[33] A. G. Tartakovsky, S. R. Li, and G. Yaralov, "Sequential detection of targets in multi-channel systems," *IEEE Trans. Inf. Theory*, vol. 49, no. 2, pp. 425–445, Feb. 2003.

[34] K. Haghighi, A. Svensson, and E. Agrell, "Wideband sequential spectrum sensing with varying thresholds," in *Proc. IEEE Global Telecommun. Conf.*, Dec. 2010.

[35] X. Yan, H. Zhang, and S. Rangarajan, "Ssct: a simple sequential spectrum sensing scheme for cognitive radio," in *Proc. IEEE Global Telecommun. Conf.*, Dec. 2009.

[36] A. Jayaprakasam and V. Sharma, "Sequential detection based cooperative spectrum sensing algorithms in cognitive radio," in *First UK-India International Workshop on Cognitive Wireless Systems*, Dec. 2009.

[37] K. S. Jithin, V. Sharma, and R. Gopalarathnam, "Cooperative distributed sequential spectrum sensing," in *National Conf. Commun.*, Jan. 2011.

[38] G. Feng, W. Chen, and Z. Cao, "A joint PHY-MAC spectrum sensing algorithm exploiting sequential detection," *IEEE Signal Process. Lett.*, vol. 17, no. 8, pp. 703–706, Aug. 2010.

[39] S. M. Perlaza, N. Fawaz, S. Lasaulce, and M. Debbah, "From spectrum pooling to space pooling: Opportunistic interference alignment in MIMO cognitive networks," *IEEE Trans. Signal Process.*, vol. 58, no. 7, pp. 3728–3741, July 2010.

[40] K. Hamdi, W. Zhang, and K. B. Letaief, "Opportunistic spectrum sharing in cognitive MIMO wireless networks," *IEEE Trans. Wireless Commun.*, vol. 8, no. 8, pp. 4098–4109, Aug. 2009.

[41] M. Amir, A. El-Keyi, and M. Nafie, "Constrained interference alignment and the spatial degrees of freedom of MIMO cognitive networks," *IEEE Trans. Inform. Theory*, vol. 57, no. 5, pp. 2994–3004, May 2011.

[42] L. S. Cardoso, M. Kobayashi, F. Rodrigo, P. Cavalcanti, and M. Debbah, "Vandermonde-subspace frequency division multiplexing for two-tiered cognitive radio networks," *IEEE Trans. Commun.*, vol. 61, no. 6, pp. 2212–2220, June 2013.

[43] M. Maso, M. Debbah, and L. Vangelista, "A distributed approach to interference alignment in OFDM-based two-tiered networks," *IEEE Trans. Veh. Technol.*, vol. 62, no. 5, pp. 1935–1949, 2013.

[44] R. Zhang and Y.-C. Liang, "Exploiting multi-antennas for opportunstic spectrum sharing in cognitive raio networks," *IEEE J. Sel. Topics Signal Process.*, vol. 2, no. 1, pp. 88–102, Feb. 2008.

[45] Z. Xiong, K. Cumanan, and S. Lambotharan, "Robust SINR balancing technique for a cognitive radio network using probability based interference constraints," in *Proc. IEEE Int. Symp. on New Frontier in Dynamic Spectrum Access Networks (DySPAN)*, 2010.

[46] X. Kang, Y.-C. Liang, A. Nallanathan, H. K. Garg, and R. Zhang, "Optimal power allocation for fading channels in cognitive radio networks: Ergodic capacity and outage capacity," *IEEE Trans. Wireless Commun.*, vol. 8, pp. 940–950, Feb. 2009.

[47] J. Wang, G. Scutari, and D. P. Palomar, "Robust MIMO cognitive radio via game theory," *IEEE Trans. Signal Process.*, vol. 59, no. 3, pp. 1183–1201, Mar. 2011.

[48] Y. J. A. Zhang and A. M.-C. So, "Optimal spectrum sharing in MIMO cognitive radio networks via semidefinite programming," *IEEE J. Sel. Areas Commun.*, vol. 29, pp. 362–373, Feb. 2011.

[49] G. Kramer, M. Gastpar, and P. Gupta, "Cooperative strategies and capacity theorems for relay networks," *IEEE Trans. Inform. Theory*, vol. 51, pp. 3037–3063, Sept. 2005.

[50] J. Mietzner, L. Lampe, and R. Schober, "Distributed transmit power allocation for multihop cognitive radio systems," *IEEE Trans. Wireless Commun.*, vol. 8, pp. 5187–5201, Oct. 2009.

[51] G. Zhao, C. Yang, G. Y. Li, D. Li, and A. Soong, "Power and channel allocation for cooperative relay in cognitive radio networks," *IEEE J. Sel. Topics Signal Process.*, vol. 15, no. 1, pp. 151–159, Feb. 2011.

[52] D. M. Pozar, *Microwave Engineering*. John Wiley & Sons, 1998.

[53] L. Li, X. Zhou, H. Xu, G. Y. Li, D. Wang, and A. Soong, "Simplified relay selection and power allocation in cooperative cognitive radio systems," *IEEE Trans. Wireless Commun.*, vol. 10, pp. 33–36, Jan. 2011.

[54] B. Bandemer, Q. Li, X. E. Lin, and A. Paulrag, "Overhearing-based interference cancellation for relay networks," in *Proc. IEEE Veh. Technol. Conf.*, Sept. 2009, pp. 1–5.

[55] C. Thai and P. Popovski, "Coordinated direct and relay transmission with interference cancelation in wireless systems," *IEEE Commun. Lett.*, vol. 15, no. 4, pp. 416–418, Apr. 2011.

[56] C. D. T. Thai and P. Popovski, "Rate regions for coordination of decode-and-forward relays and direct users," in *Proc. IEEE Int. Conf. Commun. (ICC)*, 2012.

[57] D. B. West, *Introduction to Graph Theory*, 2nd ed.   Prentice Hall, 2001.

[58] D. Feng, L. Lu, Y. Yuan-Wu, G. Y. Li, G. Feng, and S. Li, "Device-to-device communications underlaying cellular networks," *IEEE Trans. Commun.*, vol. 61, no. 8, pp. 3541–3551, Aug. 2013.

[59] E. A. Jorswieck, "Stable matchings for resource allocation in wireless networks," in *Proc. IEEE Int. Conf. Digital Signal Process. (DSP)*, Corfu, July 2011.

[60] B. Holfeld, R. Mochaourab, and T. Wirth, "Stable matching for adaptive cross-layer scheduling in the LTE downlink," in *Proc. IEEE Veh. Technol. Conf. (VTC)*, Dresden, June 2013.

[61] A. Leshem, E. Zehavi, and Y. Yaffe, "Multichannel opportunistic carrier sensing for stable channel access control in cognitive radio systems," *IEEE J. Sel. Area Commun.*, vol. 30, no. 1, pp. 82–95, Jan. 2012.

[62] S. Bayat, R. H. Y. Louie, B. Vucetic, and Y. Li, "Dynamic decentralised algorithms for cognitive radio relay networks with multiple primary and secondary users utilising matching theory," *Trans. Emerging Tel. Tech.*, vol. 24, pp. 486–502, May 2013.

[63] H. Kim and K. G. Shin, "Efficient discovery of spectrum opportunities with MAC-layer sensing in cognitive radio networks," *IEEE Trans. Mobile Comput.*, vol. 7, pp. 533–545, May 2008.

[64] G. L. Stuber, J. R. Barry, S. W. Mclaughlin, G. Y. Li, M. A. Ingram, and T. G. Pratt, "Broadband MIMO-OFDM wireless communications," *Proceeding of the IEEE*, vol. 92, no. 2, pp. 271–294, Feb. 2004.

[65] L. Lu, G. Y. Li, and A. Maaref, "Spatial-frequency signal alignment for opportunistic transmission," *IEEE Trans. Signal Process.*, vol. 62, no. 6, pp. 1561–1575, Mar. 2014.

[66] L. S. Cardoso, M. Kobayashi, O. Ryan, and M. Debbah, "Vandermonde-subspace frequency division multiplexing for cognitive radio," in *Proc. IEEE Workshop Signal Process. Advances Wireless Commun.*, 2008, pp. 421–425.

[67] I. Krikidis, "Space alignment for cognitive transmission in MIMO uplink channels," *EURASIP journal on Wireless Commu. and Networking*, 2010.

[68] ——, "Space alignment based on primary transmission-outage for cognitive transmission," *IEEE Electronics Lett.*, vol. 48, no. 19, pp. 1213–1214, Sept. 2012.

[69] S. M. Perlaza, M. Debbah, S. Lasaulce, and J. M. Chaufray, "Opportunistic interference alignment in MIMO interference channel," in *Proc. IEEE Int. Symp. Personal, Indoor Mobile Raido Commun.*, Spet. 2008.

[70] L. S. Cardoso, F. R. P. Cavalcanti, M. Kobayashi, and M. Debbah, "Vandermonde-subspace frequency division multiplexing receiver analysis," in *Proc. IEEE Int. Symp. Personal, Indoor Mobile Raido Commun.*, Spet. 2010.

[71] D. Tse and P. Viswanath, *Fundamentals of Wireless Communication*. Cambridge University Press, September 2005.

[72] V. Cadambe and S. Jafar, "Interference alignment and degress of freedom of the *k*-user interference channel," *IEEE Trans. Inform. Theory*, vol. 54, no. 8, pp. 3425–3441, 2008.

[73] N. Lee, J.-B. Lim, and J. Chun, "Degrees of freedom of the MIMO Y channel: Signal space alignment for network coding," *IEEE Trans. Inform. Theory*, vol. 56, no. 7, pp. 3332–3342, July 2010.

[74] T. Gou, T. Koike-Akino, and P. Orlik, "Improved and opportunistic interference alignment schemes for multi-cell interference channels," in *Proc. IEEE Veh. Technol. Conf.*, May 2012, pp. 1–5.

[75] K. Ko and J. Lee, "Multiuser MIMO user selection based on chordal distance," *IEEE Trans. Commun.*, vol. 60, no. 3, pp. 646–654, Mar. 2012.

[76] W. A. Adkins and S. H. Weintraub, *Algebra: An Approach via Module Theory*. Springer-Verlag, 1992.

[77] M. Razaviyayn, M. Boroujeni, and Z.-Q. Luo, "Linear transceiver design for interference alignment: Complexity and computation," *IEEE Trans. Inf. Theory*, vol. 58, no. 5, pp. 2896–2910, May 2012.

[78] M. Razaviyayn, G. Lyubeznik, and Z.-Q. Luo, "On the degrees of freedom achievable through interference alignment in a mimo interference channel," *IEEE Trans. Signal Process.*, vol. 60, pp. 812–821, Feb. 2012.

[79] C. M. Yetis, T. Gou, S. A. Jafar, and A. H. Kayran, "On feasibility of interference alignment in MIMO interference networks," *IEEE Trans. Signal Process.*, vol. 58, no. 9, pp. 4771–4782, Sept. 2010.

[80] M. Hong and Z.-Q. Luo, "Signal processing and optimal resource allocation for the interference channel," *EURASIP E-Reference Signal Process.*, 2013. [Online]. Available: http://arxiv.org/pdf/1206.5144v1.pdf.

[81] I. Santamaria, O. Gonzalez, R. W. H. Jr., and S. W. Peters, "Maximum sum-rate inter-ference alignment algorithms for MIMO channels," in *Proc. IEEE Global Commun. Conf. (GLOBECOM)*, Miami, FL, Dec. 2010.

[82] H. Yu and Y. Sung, "Least squares approach to joint beam design for interference alignment in multiuser multi-input multi-output interference channels," *IEEE Trans. Signal Process.*, vol. 58, no. 9, pp. 4960–4966, Sept. 2010.

[83] K. Gomadam, V. R. Cadambe, and S. A. Jafar, "A distributed numerical approach to interference alignment and applications to wireless interference networks," *IEEE Trans. Inf. Theory*, vol. 57, no. 10, pp. 3309–3322, June 2011.

[84] C. Xiong, G. Y. Li, L. Lu, D. Feng, Z. Ding, and H. Mitchell, "Spectrum trading for efficient spectrum utilization," *EAI Trans. Wireless Spectrum*, 2014. [Online]. Available: eudl.eu/pdf/10.4108/ws.1.1.e1

[85] M. Matthaiou, P. Kerret, G. K. Karagiannidis, and J. A. Nossek, "Mutual information statistics and beamforming performance analysis of optimized LoS MIMO systems," *IEEE Trans. Commun.*, vol. 58, no. 11, pp. 3316–3329, Nov. 2010.

[86] C. Shen and M. P. Fitz, "Opportunistic spatial orthogonalization and its application in fading cognitive radio networks," *IEEE J. Sel. Topics Signal Process.*, vol. 5, no. 1, pp. 182–188, Feb. 2011.

[87] K. Kobayashi, T. Ohtsuki, and T. Kaneko, "Precoding for MIMO systems in line-of-sight (LOS) environment," in *Proc. IEEE Global Commun. Conf. (GLOBECOM)*, Nov. 2007.

[88] W. Wang, G. Shen, S. Jin, D. Wang, and J. Chen, "Approximate minimum SER pre-coding for spatial multiplexing ovre Ricean channels," in *Proc. IEEE Int. Symp. Per-sonal, Indoor Mobile Raido Commun.*, Spet. 2009, pp. 2360–2364.

[89] M. Yu, J. Li, and H. Sadjadpour, "Amplify-forward and decode-forward: the impact of location and capacity contour," in *Proc. IEEE Military Commun. Conf.*, Oct. 2005, pp. 1609–1615.

[90] M. Xiao, N. B. Shroff, and E. K. P. Chong, "A utility-based power-control scheme in wireless cellular systems," *IEEE/ACM Trans. Networking*, vol. 11, no. 2, pp. 210–221, Apr. 2003.

[91] T. Alpcan, T. Basar, and R. Srikant, "CDMA uplink power control as a noncooperative game," *Wireless Networks*, vol. 8, no. 6, pp. 659–670, Nov. 2002.

[92] L. Lu, D. He, X. Yu, and G. Y. Li, "Energy efficient resource allocation for cogni-tive radio networks," in *Proc. IEEE Global Telecommun. Conf. (GLOBECOM'13)*, Atlanta, Dec. 2013.

[93] Y. Y. A. Leshem and E. Zehavi, "Stable matching for channel access control in cognitive radio systems," in *Proc. Int. Workshop Cognitive Inf. Processing (CIP)*, Elba, June 2010, pp. 470–475.

[94] P. Floreen, P. Kaski, V. Polishchuk, and J. Suomela, "Almost stable matchings by truncating the gale-shapley algorithm," *Algorithmica*, vol. 28, no. 1, pp. 102–118, 2010.